Technische Universität München
Lehrstuhl für Medizintechnik

Surface Microstructuring for controlled Drug Release in coronary Stents

Michael Stöver

Vollständiger Abdruck der von der Fakultät für Maschinenwesen der Technischen Universität München zur Erlangung des akademischen Grades eines

Doktor-Ingenieur (Dr.-Ing.)

genehmigten Dissertation

Vorsitzender: Univ.-Prof. Dr.-Ing. Horst Baier

Prüfer der Dissertation:

1. Univ.-Prof. Dr. med., Dr.-Ing. habil Erich Wintermantel
2. Univ.-Prof. Dr. Sannakaisa Virtanen,
   Friedrich-Alexander-Universität Erlangen-Nürnberg

Die Dissertation wurde am 13.09.2006 bei der Technischen Universität München eingereicht und durch die Fakultät für Maschinenwesen am 21.11.2006 angenommen.

Abstract

This thesis introduces a novel type of electrochemical microstructuring for 316L stainless steel. The microstructuring methods were developed as a basis for a drug eluting coronary stent system. Coronary stents are used in order to dilate narrowed arteries. In order to prevent inflammation reactions, which lead to an excessive proliferation of cells and thus to a renarrowing of the artery, the new generation of stents are coated with drugs. The aim of this thesis was to create three dimensional microstructures on the surface as a basis for drug coatings. The microstructures are supposed to provide a protection for the drug during the implantation process and, moreover, control the release of the drug by providing microdepots retaining a certain amount of the drug. It was found that suitable microstructures can be generated by a combined etching method comprising a first electrochemical grain boundary etching step followed by an isotropic etching step. The first step is performed with nitric acid and creates a microgrid of narrow grain boundary furrows. These furrows are hollowed out by a second etching step, carried out either with phosphoric acid, hydrochloric acid or oxalic acid. The generated structures were found to be superior or equal in terms of corrosion properties and cell proliferation behavior compared to conventional grit blasted stents. It was shown that the in vitro release behavior could be substantially decelerated, with up to three times more drug retention after the first week of release in comparison to grit blasted stents.

Zusammenfassung

Es wurde ein neues Verfahren zur Oberflächenmodifikation von biokompatiblem Edelstahl entwickelt, mit dem durch elektrochemische Ätzung Mikrostrukturen im Mikrometerbereich aus den intrinsischen Materialstrukturen erzeugt werden können. Das Verfahren dient als Basis für eine Medikamentenbeschichtung von Stützen für verengte Herzkranzgefässe (Stents). Ein großes Problem bei dieser Behandlung ist eine hohe Wiederverschlussrate, die durch Entzündungsreaktionen verursacht wird. Diese kann durch eine Beschichtung des Stents mit entzündungshemmenden Medikamenten verhindert werden. Mit Hilfe des Verfahrens werden in einem zweistufigen Ätzprozess Mikrokavitäten erzeugt, die in der Lage sind, eine gewisse Menge an Medikament aufzunehmen und verzögert freizusetzen. Es wurde nachgewiesen, dass die erzeugten Oberflächen in Hinblick auf in vitro Korrosions- und Zellbesiedelungseigenschaften besser oder gleichwertig zu konventionellen sandgestrahlten Oberflächen sind. Der in vitro Medikamenten Release konnte erheblich verzögert werden, die erzeugten Oberflächen wiesen nach einer Woche Release noch eine im Vergleich zu sandgestrahlten Stents bis zu drei mal höhere Menge an gespeichertem Medikament auf.

Acknowledgements

Contents

1 Introduction

1.1 Surface Modification of Implants

A plurality of substances has been established for the purpose of substituting or supporting organic functions of the human body, ranging from metals to ceramics to polymers. Almost all materials currently used are still being optimized in terms of composition and processing. In recent times, parallel to the development in other fields, the focus has been aiming more and more at the surface properties of the material. Since body tissue normally interacts only with the upmost few micrometers of an implanted material, the chemical and topographic properties often decide over the success or failure of an implantation process. Depending on the intended use of an implant, various topographies may be required. The desired surface may be very smooth as in the case of implants directly in contact with the blood flow (e.g. artificial heart valves), a structured surface with very high roughness as in the case of permanent implants where good adhesion and quick cell ingrowth are important (e.g. shafts of hip implants) or surface structures with intermediate roughness. An example for the requirement of intermediate roughness are temporary implants like screws and nails where a sufficient adhesion is required, with the possibility of a subsequent removal of the implant. Another example where the surface properties have to be adjusted carefully are permanent bone implants near sensitive areas like the brain. In this case a high surface roughness may be beneficial to promote cell ingrowth, however if this process is overdrawn the result may be an abound ingrowth of the implant into the sensitive areas [1, 2, 3].

Commonly used techniques in order to modify surfaces include chemical treatments, laser structuring as well as mechanical surface treatments. Most of these techniques are conventional techniques which have been adapted for use in biomedical engineering. A simple, widespread surface modification technique, with which an increase in surface roughness can be achieved, is grit blasting. An increased roughness may provide both improved adhesion properties and a favored basis for cell growth [4, 5]. Accordingly, grit blasting is applied for permanent implants which require a consol-

1

idated ingrowth, e.g. shafts of hip implants, dental implants [6, 5]. The technique is comparatively easy to perform and applicable for large quantities. However, for grit blasted implants it is known that a risk of remaining particles exists [7, 8]. Another limitation results from the fact that mechanical stresses are imposed on the material. When applied to sensitive structures, grit blasting carries the risk of deformations and may lead to considerable scrap rates.

For titanium implants also chemical and plasmachemical surface modifications are subject of current research with promising results [9, 10, 11]. In this case highly reactive, mostly fluorine containing chemicals are used in order to etch the surfaces. Similar to grit blasting, with this methods the surface roughness can be increased, resulting in promoted cell ingrowth.

Another microstructuring method is offered by laser ablation. With this method three dimensional structures can be created. These structures may be used to promote cell ingrowth, however an even more important feature offered by these structures is the possibility to load the surface with therapeutic substances. This way drugs can be applicated directly into the affected location, resulting in a high therapeutic efficacy at small amounts of drugs needed. Examples for drug coatings are antibiotics, antithrombotic agents as well as cell growth stimulants (e.g. [12, 13]).

Other microstructuring techniques that give the possibility to create three dimensional structures originate mainly from the field of microchip fabrication. Photo- and laser-lithographic techniques are employed by depositing a protection layer of lacquer on the substrate. Subsequently the microstructures are etched electrochemically into the material. With multi step etchings it is possible to generate three dimensional structures as well as undercuts [10, 14, 15]. The technique is time-consuming and very difficult to apply for complex geometries.

In this thesis a novel microstructuring technique for stainless steel materials is introduced, which combines the advantages of a selective three dimensional structuring with the convenience of a mere chemical method. The technique bases on electrochemical etching, in a way that intrinsic material structures are used in order to form three dimensional structures out of the material. The technique was developed for coronary stents as a basis for an on-site drug coating system without the use of protective polymers. The basic requirement was the development of a microstructuring method which is economical and applicable on mechanically sensitive structures.

The microstructures should offer sufficient adhesion for a drug coating and, after elution of the drug, serve as a favored surface for cell ingrowth. It was found that, beyond, with a combination of special electrochemical etching techniques microdepots can be generated within the surface, which offer the possibility to store drugs within the surface. With this combination technique microdepots of different size and different shapes can be generated, which allows to tailor the depot properties according to the respective use.

1.2 Stents as a Treatment of Coronary Heart Disease

Coronary stents are employed to dilate narrowed coronary arteries in order to ensure a sufficient blood flow. They consist of a cylindrical wire-mesh of biocompatible material which is placed into the artery and is dilated by means of a balloon catheter (fig. 1.1). Afterward the stent remains permanently in the artery, acting as a mechanical scaffold which keeps the vessel open. The indication for a use of stents is the occurrence of coronary heart disease as a consequence of atherosclerosis. Symptoms of this disease are heart insufficiency, angina pectoris as well as pending or suffered cardiac infarction[16, 17].

1.2.1 Pathology of Atherosclerosis

Atherosclerosis describes a degeneration process of arterial blood vessels which leads to a reduced or, in the worst case, an interrupted blood flow. Athero sclerosis translated from Greek means as much as gruel-like rigidification. Atherosclerosis is caused by intra-arterial deposits, originated by conglomeration of lipids, complex carbohydrates, blood and connective tissue as well as calcium deposits [18]. The process normally starts with the generation of a lipid enriched area underneath the intima. The artery consists of three layers of which the intima is the innermost layer of the artery. It consists of a monolayer of endothelial cells. The middle layer, the media, consists of circumferrentially orientated smooth muscle cells and collagen fibers. The outer layer, the adventitia, comprises connective tissue made up of fibroblasts and associated collagen fibers [19]. Within the lipid enriched area beneath the intima

Figure 1.1: *Schematic illustration of coronary stenting (with permission of the Medical University of South Carolina). The stent is placed into the narrowed area on a balloon catheter. After dilatation of the stent the catheter is removed, while the stent remains permanently within the vessel, preventing a renarrowing of the vessel.*

defense cells differentiate into so called foam cells through incorporation of lipid enriched material [20]. Although excessive research has been performed over decades, the exact cause for this process is not yet fully understood. As early as 1976 it was suggested that the origin is an inflammatory process which starts with minor injuries of the endothelial layer. These microinjuries, which may be caused by morphologic damages, biochemical impairments, bacterial toxins etc., enable the permeation of defense cells through the endothelial layer [21, 22]. In connection with the presence of a special protein (oxidized low density lipoprotein, LDL), which is assumed to play the decisive role in the development of atherosclerosis, these cells are able to differentiate into foam cells. Subsequently a migration of smooth muscle cells from the media into the intima connected with an increase of extracellular fibrils can be observed. The result is a capsular type structure of connective tissue with an adipoid core (plaque) [23] (s. fig. 1.2).

In the progress of the disease the altering of the vessels can lead to a sever impairment of the blood flow. This can be caused either by a gradual narrowing of the artery or by a rupture of the plaque [24]. The result are the typical consequences of the coronary heart disease like angina pectoris, formation of thrombuses and finally heart attack.

4
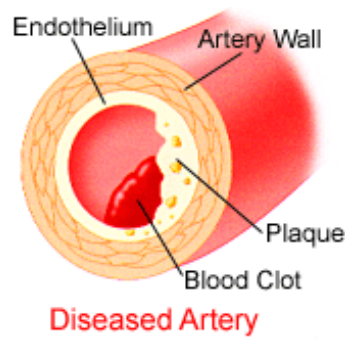
Figure 1.2: *Section through an artery affected by atherosclerosis (Source: www.tmc.edu/thi/cad1.gif). Intra-arterial deposits consisting of lipids, complex carbohydrates, blood and connective tissue as well as calcium deposits lead to the formation of plaque beneath the endothelium. The final result is an impairment of the blood flow.*

1.2.2 Coronary Stenting

Associated with the tendency toward minimal invasive interventions and the steady improvement of the technique, coronary stenting has become the method of choice for the treatment of coronary heart disease symptoms. The stenting procedure is carried out by placing a stent crimped on a balloon catheter into the narrowed artery. The catheter is normally inserted through the femoral artery, occasionally through the carotid artery. At the site of the stenosis the stent is dilated with up to 16 atms using Ringers solution for the dilatation process.

The preferred stent material is medical grade stainless steel because of its mechanical properties and its good machinability combined with fair X-ray visibility. To a lesser extent Nitinol stents and stents made of cobalt alloys are used, while Nitinol allows to fabric self expandable stents because of its superelastic behavior. The majority of stents are meanwhile fabricated out of small tubes by means of laser cutting. This technique mostly replaced older methods using wire meshes or spirally wound wires. Typical dimensions of coronary stents are one to two millimeters diameter (before dilatation) and 8 to 25 mm length. The thickness and width of the single struts are in the range of 100 μm.

1.2.3 Pathology of Restenosis and Strategies for its Prevention

The main problem occurring with the use of stents is a renarrowing of the artery through proliferating tissue (e.g. [25]). This proliferation is to be regarded as an inflammatory response against the introduced foreign body as well as the microinjuries at the arterial wall that are caused by the dilatation process. In the first stage an activation of circulating thrombocytes can be observed [26]. The implantation of a stent results in a complete destruction of the endothelial layer within the area of implantation [27]. As a result a thin thrombus is formed between the stent surface and the vessel. In the first weeks this thrombus works as a border between the stent material and the vessel wall. In order to prevent the risk of thrombus formation within the vessel high doses of acetylsalicylic acid are given during this stage. Another process that is induced within the first weeks is a proliferation of smooth muscle cells. This effect is enhanced by the shear stresses induced into the arterial wall that stimulate the growth of smooth muscle cells [28]. If this proliferation persists it leads to a considerable lumen loss which is referred to as restenosis. Parallel to the phase of proliferation of smooth muscle cells expanding endothelial cell clusters develop which finally escalate to a coherent cell layer. Since endothelial cells work as a regulator for smooth muscle cells, the generation of an endothelial cell layer is the main criteria for the prevention of an excessive proliferation of smooth muscle cells [29, 30, 28]. Grewe et al. state a time interval of about three month for this based on their experiments on human arteries [31]. The propagation of endothelial cells depend on the chemical as well as the topographical properties of the stent surface. The propagation is favored by surface structures in the range of 15-20 μm that promote adhesion and ingrowth of the cells [32, 33].

As the most effective means against restenosis drugs are used that inhibit the proliferation of smooth muscle cells and/ or promote quick reendothelization. A plurality of substances have been investigated for this purpose which can be divided into four classes. The first class are anti-inflammatory drugs that intervene with the immune response. Amongst this kind of substances is the well proven immuno-suppressant Rapamycin [34, 35] as well as the widespread anti-inflammatory dexamethasone [36]. The second class are the directly anti-proliferative substances that inhibit the progeny of smooth muscle cells. Paclitaxel as another commonly used stent coating drug is an example for this class [37, 38]. Less commonly used are selective migration inhibitors (e.g. Baltimastat) and drugs that support healing and reendothelization

(e.g. growth factors or the hormone estrogen) [39].

In order to guaranty a sufficiently high drug concentration and to minimize side effects, it is sensible to deliver the drug locally instead of a systemic delivery. Therefore a coating of the stents is necessary. Two main problems occur with the use of drug coated stents in terms of surface properties. The first problem are stresses imposed on the coating during the implantation process which can lead to flaking of the coating, accompanied by a considerable drug loss. The second problem is to provide a decelerated release kinetic in order to guaranty a sufficient efficacy of the drug. Currently most drug eluting stents are covered with a polymer in order to prevent flaking and to be able to controll the release kinetics [40, 41, 42]. Due to better mechanical properties, mostly non degradable polymers are used. However recent data indicate that the use of non degradable polymers can lead to substantial long term side effects like late restenosis [43] and thrombotic stent occlusions [44]. These long term side effects are attributed to a chronic inflammation effect, expressed by a local accumulation of defence cells [45]. Moreover it would be beneficial to individually choose type and concentration of the drug, according to the history and the disease pattern of the patient [46]. This is not possible for the currently used polymer coatings since the stents are coated directly after the fabrication process. Due to the complexity of the process this step normally cannot be performed directly before implantation. Since different geometries are employed for each patient it is also not possible to store coated stents with different drug concentrations.

In recent time coating systems have been developed with which stents can be coated within the catheter laboratory immediately before implantation, preferably without the use of a polymer. In this case high demands are set on the surface properties. The main requirement is good adhesion of the drug which is realized by increasing the surface roughness of the stent. For this purpose grit blasting is used, which is the only surface modification method, known to the author, which is commercially used for stents without polymer coatings. Besides functional benefits, stents with increased surface roughness might offer another advantage. In 2005 a randomized study on humans (n = 200) was performed by Dibra et al. comparing uncoated grit blasted and electropolished stents [47]. In this study no significant difference could be observed between the two surfaces. Nevertheless it was found that the rough surfaces tent to yield slightly lower restenosis rates than smooth surfaces without having negative side effects. The result is attributed to a better endothelialization of the surface. The effect of controlled cell promotion can also be achieved very

efficiently by creating defined microstructures on the surface [48].

An even more important requirement that has to be provided by the topography of the surface is the achievement of a delayed release kinetic. Without the use of an additional polymer most of the drug (Rapamycin) on a grit blasted stent is removed within a few days after implantation. In internal studies the peak of the Rapamycin concentration in the surrounding tissue was found on the third day after implantation. At the sixth day the concentration had dropped to one third of the peak value. A sufficient time period for Rapamycin and Paclitaxel to effectively reduce restenosis, however, is assumed to be in the range of weeks (e.g. [49, 43, 50, 51, 52]). In this context Duda et al. state for Rapamycin [52]: *"It is not clear how long the drug needs to remain in the area, but it appears that 4–6 weeks is sufficient based on the clinical data generated to date "*. An interesting fact in this context is described by Parry et al. [53] who found in in vitro experiments that *"the effects of sirolimus on smooth muscle cell proliferation were reversible since cells resumed proliferation several days after washout of sirolimus "*.

A different approach is offered by laser ablation techniques. With short laser pulses small slots can be cut into surfaces [54], that can be used as drug depots. This method brings about the limitation that only rather large depots can be generated so that a drug coating is distributed inhomogeneously and the release kinetics are only slightly improved. Furthermore the adhesion properties are not improved to a large degree, so that an additional polymer coating is still needed. A perspective application for this method could be a multi-layer coating, for example a release of an immunosuppressant which is followed by an endothelial cell growth stimulator.

1.2.4 Drug Delivery Stent Systems

Different drug releasing stent systems are currently used, the most common being polymer coated Rapamycin (BX Velocity stent, Cypher©) or Paclitaxel eluting stents (NIRx stent, Boston Scientific). The Taxus stent comprises a non degradable polymer (on a hydrocarbon basis) coating containing Paclitaxel in two modifications, a slow and a fast release. The slow release type features 1 μg paclitaxel per mm^2 with a release time of 28 days, the fast release 2 μg paclitaxel per mm^2) with a 24-hour release time [55]. The Cypher© stent coating consists of a non degradable polymer on a metacrylate basis that contains Rapamycin in a concentration of 140

μm/cm^2 and a top layer as diffusion barrier. The stent releases 80% of the amount of Rapamycin within the first month [52, 49]. Alternatively surface roughened stents with Rapamycin coating are used without the use of a polymer (Yukon©). This stent uses a pure Rapamycin coating, applied via spray coating of an ethanolic Rapamycin solution. A commercially used pure Paclitaxel coating is not known to the author, however Duda et al. state that *it is even possible to apply paclitaxel as a simple coating without the necessity of a polymer.* [55].

A significant reduction of the restenosis rate could be proved for all three stents. The SIRIUS Trial showed a reduction from 35.4% to 3.2% for the Cypher© stent, in the TAXUS IV Trial a reduction from 24.4% to 5.5% could be achieved with the Paclitaxel stent [56]. The restenosis reduction of the Yukon© stent is sligthly lower than that of the Cypher© with a restenosis rate of 14,7 % compared to 25,9 % for the bare metal stents [57]. The restenosis rates of these stents, however, are still considerable when risk factors like diabetes (17.6%) or the stenting of a bifurcated vessel (28.0%) are present [58].

2 Working Hypothesis and Proceeding

This thesis aims at the development of microstructured surfaces on coronary stainless steel stents by means of electrochemical etching. The surfaces are designed in a way to enable a coating of the stent with therapeutic drugs, preferably without the use of an additional polymer. The procedure of stenting with drug eluting stents can be separated into three stages, with each one having different requirements on the surface properties.

The first stage addresses the implantation of the stent. During the implantation process the drug coating is subjected to friction forces due to contact with the arteries, mechanical stresses due to stent deformations at turnings and shear stresses induced by the blood flow. The basic requirement in order to assure a protection of the drug during this phase is a sufficient adhesion of the drug. This can be realized by a high surface microroughness and by a mechanical interlocking of the drug layer and the stent surface.

Once the stent is placed within the stenosed artery the phase of the drug release begins. In this stage a controlled, gradual release is required in order to assure a maximum efficiency of the drug. The idea followed in this thesis is to create evenly distributed microdepots on the stent surface, that store part of the drug coating, in order to achieve a controlled release without an additional barrier layer. The microdepots are created on the three outer sides of the stent (s. fig 2.1), which will immediately be in contact with the tissue after dilatation. Until now little is known about the ideal size and shape of such microdepots. Small and deep depots will retain a small amount of drug for a long time, while broad shallow depots will store a larger amount of drug for a short time. In this thesis the microstructures were designed in a way to yield a depth to width ratio in the range of 1 to 2, in order to have a suitable compromise between a sufficient retaining capacity and a sufficient amount of stored drug. The depth of the microdepots is limited due to mechanical

10

aspects, since the microdepots act as notches and thus weaken the integrity of the material. When assuming depots with a rounded base, a depot of 10 μm depth and 5 μm width, would have a notch radius of 2.5 μm and a ratio of depth to notch radius of 4. Intern studies showed that conventionally approved (e.g. grit blasted) stents may have notch numbers as high as 10, so that this notch numbers are considered uncritical by the author. The effective load bearing area in this case will be diminished by not more than 20 μm which can be leveled out by an adaptation of the stent design.

The third stage of the stenting procedure is the bare stent phase. After release of the drug, which previously formed a barrier between stent and tissue, the stent is in direct contact with the tissue. In order to assure a long term fixation of the stent within the tissue and to prevent chronic inflammation processes, an optimal surface has to be biocompatible after release of the drug and should provide a suitable basis for cell ingrowth. The latter can be achieved by microstructures which support the ingrowth of cells. In this context it was shown by Palmaz and by Fuss that structures in the range of the size of cells (about 10-20 μm) can promote coordinated cell growth [32, 33].

Preliminary experiments with etchants like aqua regia showed that it was not possible to generate suitable surfaces with conventional etching methods. These experiments yielded surfaces with moderately increased roughness, however the other requirements could not be met. The decisive idea that is followed up in this thesis origins from metallographic practices. The approach was to aggravate the selectivity of etchings, that are used in the field of metallography in order to visualize grain patterns, by electric current in a way that three dimensional structures are worked out of the intrinsic structures of the material. Two electrochemical etching techniques have been developed, with which it is possible to generate evenly distributed microstructures of several micrometers depth on medical grade stainless steel. The first one is based on hydrochloric acid etching and renders an evenly faceted surface. This etching method yields a high surface roughness, however without providing depots. Due to bad reproductivity and unexpected bad adhesion behavior this method was found not to be suitable as a basis for drug coating of stents. The second method is based on nitric acid etching and produces a fine grid of furrows on the surface. The furrows created with nitric acid can have different shapes when contemplating the cross sectional view. Depending on the selectivity of the etching process the forms can range from rather broad V-shapes to narrow, crevice like furrows. Basing on
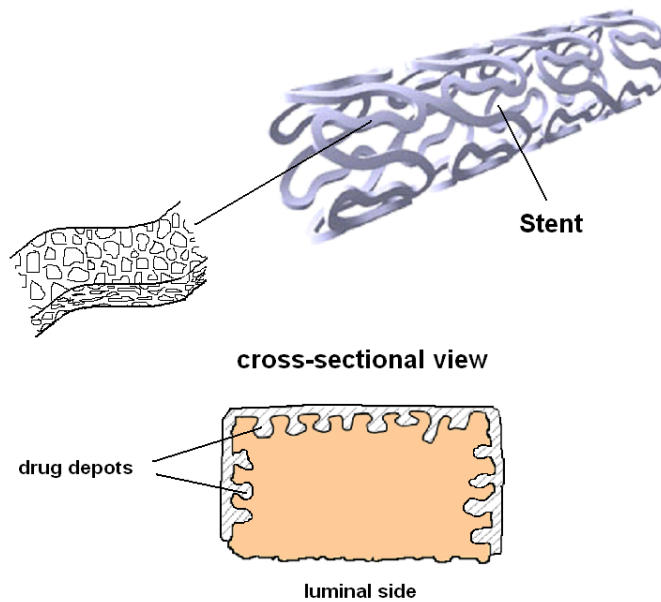
Figure 2.1: *Schematic illustration of a microstructured stent strut. The cross sectional view below illustrates the distribution of the depots. The inner (luminal) side of the stent does not have drug depots, since this side is subjected to the blood flow after implantation, so that a drug would be washed out quickly.*

this observation a mathematical model was established in order to predict the shape and size of the furrows. Independent of the shape variations, the microstructures generated with nitric acid have sharp tips and relatively low depot volume, making them unsuitable as a one step etching method.

However, it was found that especially the narrower crevices are well suited as a basis for two step etching methods as described in chapter 7. The two step etching method comprises the creation of narrow furrows with nitric acid, which are hollowed out by a second, isotropic etching step. Three acid solutions were investigate in terms of suitability for this second etching step, phosphoric acid, hydrochloric acid and oxalic acid. The generated topographies were analyzed by scanning electron microscopy as well as by software analysis of cross sectional micrographs. For the software analysis a polygon line was generated around the stent simulating the boarder line between the artery tissue and the stent. Using this model the average depot volume, the average depot depth as well as the distribution of the depots of the generated structures were calculated.

Furthermore it is tested if an electropolishing step as a normally obligatory pretreat-

ment can be waived when using electrochemical etch treatments. The fabrication of stents by laser cutting leads to sharp edges and burrs that require an after-treatment. For conventional stents a first pickling step with a hydrofluoric acid containing solution is performed directly after cutting in order to remove burrs. Subsequently an electropolishing treatment is necessary to round edges and smooth the surface. When applying the combined electrochemical etchings, the second step produces a smoothing effect, therefore the pickling step might be spared.

Another welcome side effect of electrochemical treatments is, that the surface is cleaned and chemically activated by the etching process, so that the adhesion properties might be further improved. An implementation of this principle can be found in the preparation of surfaces for bonding processes [59, 60]. However, the etching process might influence the surface properties in both a negative or a positive way in respect to corrosion properties. Most authors found an increased chemical resistance of 316L after etching treatments with various acids such as nitric, phosphoric and hydrochloric acids [61, 62, 63]. In contrary, sometimes also negative effects from nitric acid etchings are reported, like an increased susceptibility against crevice corrosion [64]. Therefore chemical and electrochemical analysis of the modified surfaces was performed in order to evaluate the corrosion behavior and possible changes of the surface composition of the stents.

In order to assess the efficacy of the surfaces, drug quantifications were performed and the release kinetics were analyzed in comparison to grit blasted stents. The mechanical performance of the modified stents was evaluated by static strength and dynamic fatigue tests. Finally cell seeding tests were performed to contemplate biocompatibility aspects of the surface modifications. Fibroblasts, which are relatively robust, versatile cells, were used in order to assess the general biocompatibility properties. In addition the surfaces were seeded with endothelial cells and with smooth muscle cells. The intention of these experiments was to obtain information about the possibility of influencing cells individually by the microstructures.

1. Creation of microstructured surfaces
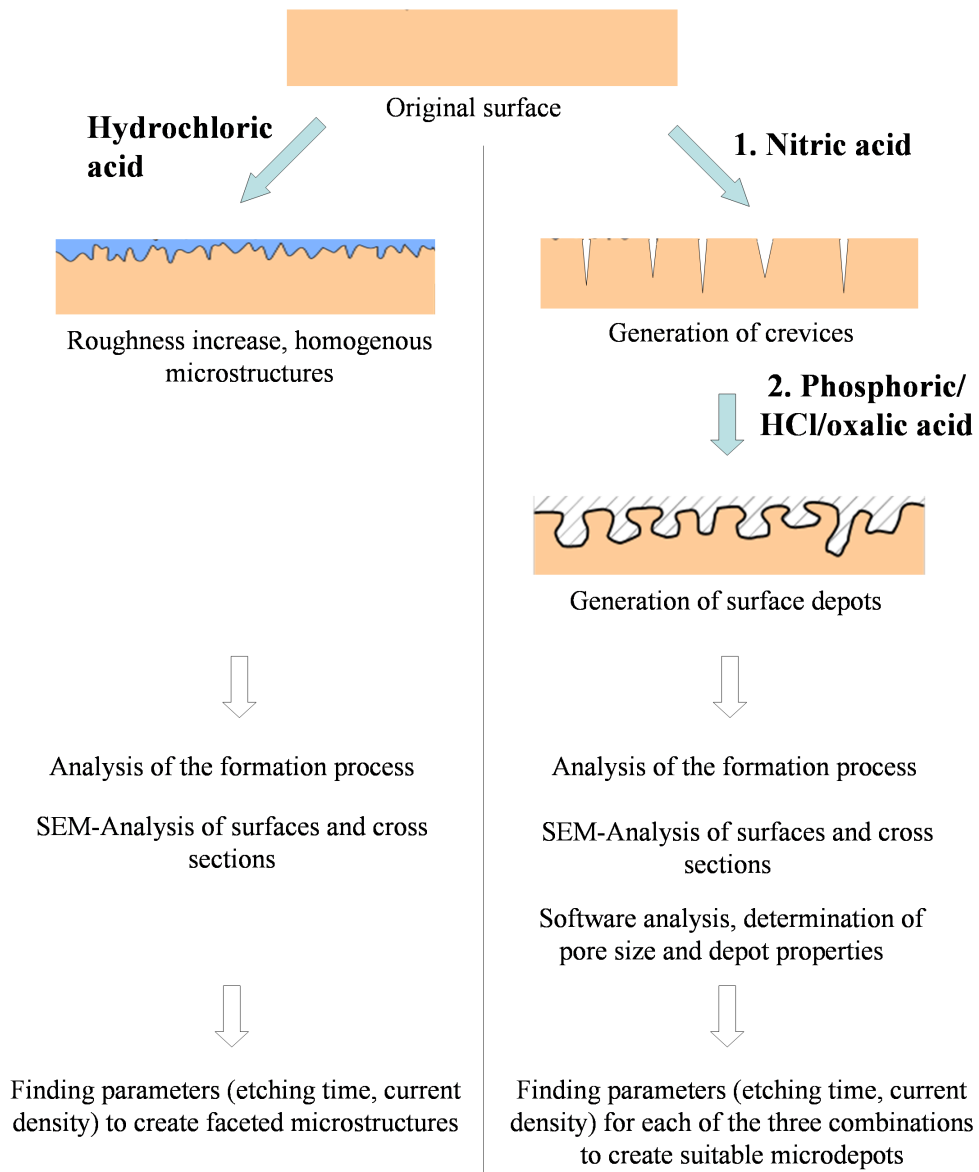
Figure 2.2: *Survey of Proceeding I, Creation of the surfaces.*

2. Analysis of the surfaces

Surface with faceted microstructures (hydrochloric acid etching)	Surfaces with suitable microdepots (Phosphoric, hydrochloric and oxalic acid combination)
⬇ (If reproducible)	⬇ (If reproducible)
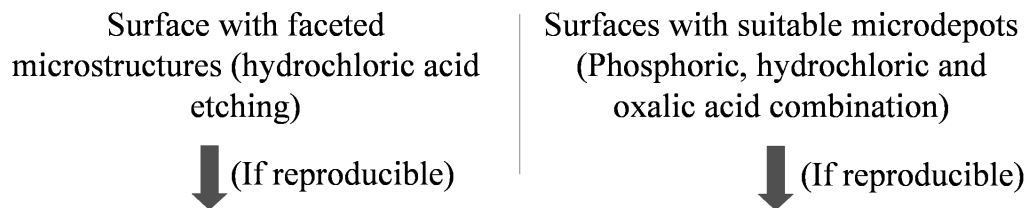
**● Chemical Analysis
(Corrosion Behavior)**

Cyclic voltammetry: Determination of passivity area and rest potentials

Long term ion release of Ni and Cr

EPS, AES: Composition of surface

● Biological Tests

Cell seeding: Proliferation of fibroblasts, smooth muscle cells and endothelial cells on the surfaces

● Mechanical Tests

Evaluation of notch effects

Radial strength tests

Fatigue tests, simulation of 10 years in vivo use

● Assessment of Effectivity

Coating behavior and adhesion properties

Determination of in vitro release kinetics (30 days), comparison to grit blasted stents

Figure 2.3: Survey of Proceeding II, Analysis of the surfaces.

3 Electrochemical Theory

3.1 Basics

Electrochemical etching is a well established method for different uses in the area of metal processing and analysis. The main applications are spark erosion processing as well as the visualization of grain structures for metallographic analysis. The fundamentals of electrolytic etching will be explained in the following section.

For the following contemplations two metal electrodes are assumed which are surrounded by a liquid electrolyte. Miscellaneous solvents (e.g. water, methanol) with mobile charge carriers (e.g. NaCl, HNO_3) can be used as electrolytes. The larger the solvent molecules, the larger is the solvate covering around the ions and thus the lower is the mobility of the ions. The conductivity of an electrolyte is a function of the number of solved charge carriers, their charge as well as their mobility:

- At lower concentrations the conductivity increases with increasing concentrations because of an increasing number of charge carriers. At further increased concentrations, however, the mobility of ions decreases due to mutual interference and an increasing formation of neutral ion pairs is the result, which do not contribute to the conductivity (incomplete dissociation). Thus at high concentrations the conductivity of the electrolyte normally decreases again.

- An increase of temperature causes a higher mobility of ions and thus a higher conductivity.

- If acids or bases are used as electrolytes the charge movement takes place mainly via a special migration mechanism of protons and hydroxide ions. This type of charge movement is considerably quicker than the direct transport by ions, so an especially well conductivity is present.

The processes at the boundary layer between electrode and electrolyte are described by the Helmholtz layer model.
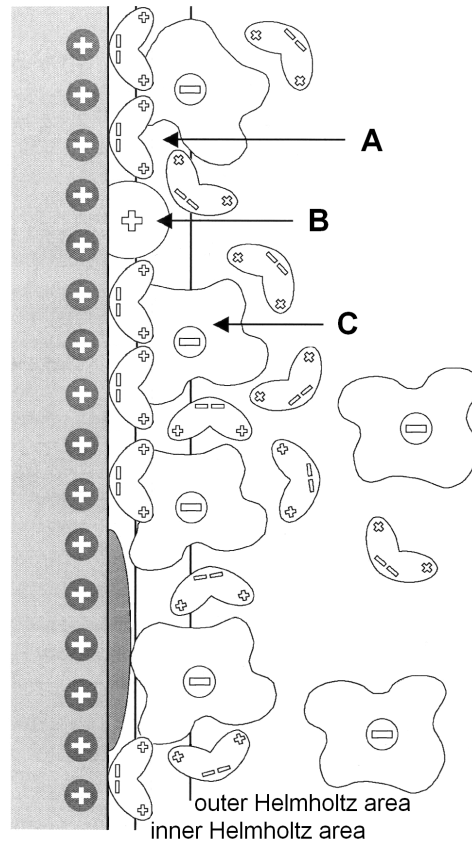
Figure 3.1: *Schematic illustration of the Helmholtz layer, modified from [65, 66]. A indicates adsorbed oriented water dipols, B marks specifically adsorbed cathions, C indicates negative overcharges within the double layer which´s centers built the outer Helmholtz layer.*

Caused by differences in potential an electrochemical double layer is built. It consists of positive charges at the side of the electrode and of negative ions at the side of the electrolyte. The area passing through the centers of the anions, is referred to as the outer Helmholtz Area. According to the Helmholtz theory the ions are directly adjacent to the electrode, so that the outer Helmholtz layer runs parallel to the electrode surface in a distance of half a diameter of the ions (solvate covering included) [67, 68]. More recent models, established by Gouy Chapman and advanced by Stern [69] assume a statistically distributed ion cloud, which contains the opposite charge of the electrode.

The dissolution rate dm/dt (mass per time) for electrochemical etchings can be calculated as follows (modified from [70] and [71]):

$$\frac{dm}{Adt} = \frac{M}{z \cdot F} \cdot j \cdot \gamma \tag{3.1}$$

M - molar mass, F - Faraday constant = 96485 As, z - charge number, j - current density, γ - rate of current yield, A - area subjected to etching

The charge number z depends on the reaction product generated and can, as in the case of iron, be dependent on the current density. The current yield γ in this case indicates the percentage of current, that is used for material dissolution. The fraction 1 - γ is lost through decomposition processes of the etching medium.

3.2 Selective Etching

When employing chemical or electrochemical etchings in order to achieve a differentiation of molecular structures, the processes become much more complex than described above. Materials such as stainless steel consists of grains with different orientation, boundary areas, precipitations, inclusions etc., which all show different electrochemical behavior. Depending on the corrosive medium, the applied potential, the temperature and other parameters certain phases may be corroded to a much higher degree than others. Fig 3.2 illustrates a simplified model of a metal consisting of two phases in a corrosive environment (comp. [72]) at a given potential. Phase A in this case represents the anodic site, Phase B shows cathodic behavior. Phase A may be a site of higher disorder like a grain boundary or a dislocation or an area of different composition like a precipitation. At the anodic site the metal has the tendency to oxidize, whereas at the cathodic site there is a tendency toward a reduction reaction. This reaction can be e.g. the reduction of H^+ to H [72]. It has to be noted that, if a high positive outer potential is applied, as it is the case in all electrochemical etchings described in this thesis, both phases may exhibit anodic behavior. In this case both phases will corrode, however with Phase A being corroded much quicker.

Stansbury describes an approach for a theoretical description of the selective etching of different phases in [71]. It is assumed that *any microregion on the surface has a dissolution rate (current density) that is the same as that observed in a bulk*
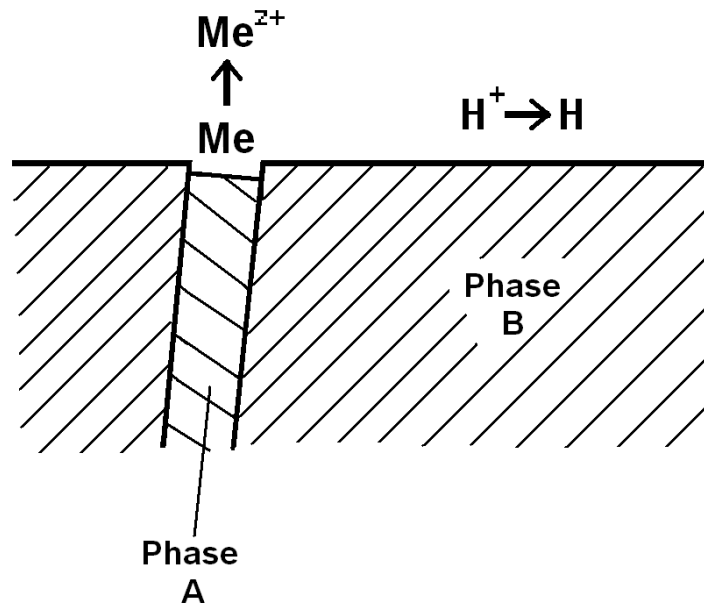
Figure 3.2: *Schematic illustration of the corrosion of a two phase system. Phase B represents the anodic phase which tends to dissolution, phase A represents the cathodic phase which supports the dissolution of Phase B.*

sample identical in composition to the microregion when exposed under the same conditions - e.g. environment and potential. In order to estimate the etching rates of different phases, current density diagrams of the different phases such as fig. 3.3 can be employed, using the ratio of the current densities j_A/j_B of the phases at the respective potential (comp. also [73]). When the current density ratio is known, the ratio of the dissolution rates can be determined using formula 3.1

$$\frac{dm_A \cdot A_B}{dm_B \cdot A_A} = \frac{M_A \cdot z_B}{M_B \cdot z_A} \cdot \frac{j_A}{j_B} \tag{3.2}$$

3.3 The Alloying Elements of 316L

The main alloying elements of 316L are nickel, chromium and molybdenum. The main function of these elements are important for the understanding of the effects of etchings and are explained in the following section.

Nickel

If nickel is alloyed to iron, the area of cubic face-centered austenite, which occurs at unalloyed steels only at a temperature above 723° C (s. Fe-C diagram), is augmented. Above 8 % nickel content a steel is austenitic at room temperature. Austenitic steel is characterized with good formability and increased chemical resistence especially towards non oxidizing acids.

Chromium

Chromium is a ferrite former which, however, increases the austenite area in the presence of nickel. In contents over 10.5 % alloyed to a steel it builds, in atmosphere as well as in most other oxygen containing environments, a protecting surface layer of chromium oxide, that defends the steel from corrosion, especially against oxidizing acids [74, 75]. An increased chromium content in the passivity layer leads to a change in potential towards more noble values and thus to a higher chemical resistance [76]. The passivating layer is explained in detail in the following section.

Molybdenum

Molybdenum supports the passivating effect of chromium. It is alloyed to steel, if an exceptional resistance against pitting corrosion and crevice corrosion is required [77, 78, 79, 80]. The different efficiency of molybdenum, chromium and nitrogen in terms of passivation can be estimated by the following formula, which introduces an efficiency factor W: $W = \%Cr + 3.3 \cdot \%Mo + 30 \cdot \%N$. The corrosion repressing properties of molybdenum are attributed to an increased resistance of the passivity layer against debilitating elements [81, 82] as well as to an improved repassivation characteristic [83]. It was found, that the thickness of the passivity layer increases with increasing molybdenum content [81, 80].

Silicon

Silicon tends to increase resistance by dispersion of chromium and supports the formation of Cr_2O_3. However at high temperatures (800°C and above) silicon activates the formation of the δ phase. The formation of the δ phase leads creates chromium denuded zones and is attributed to a weakening of the corrosion resistance [84].

3.4 Electrochemical Behavior of Cr-Ni-Steels

For austenitic steels the corrosion behavior in various media is determined predominantly through the formation of a passivity layer. The passivity layer consists of a film of metal oxide/ hydroxide complexes having very low conductivity for metal ions [85]. So the metal atoms beneath the layer are prevented from corrosion. The typical behavior of stainless steel in an aqueous corrosive medium is illustrated in fig. 3.3 on the example of 316L in diluted sulfuric acid (comp. [86]).
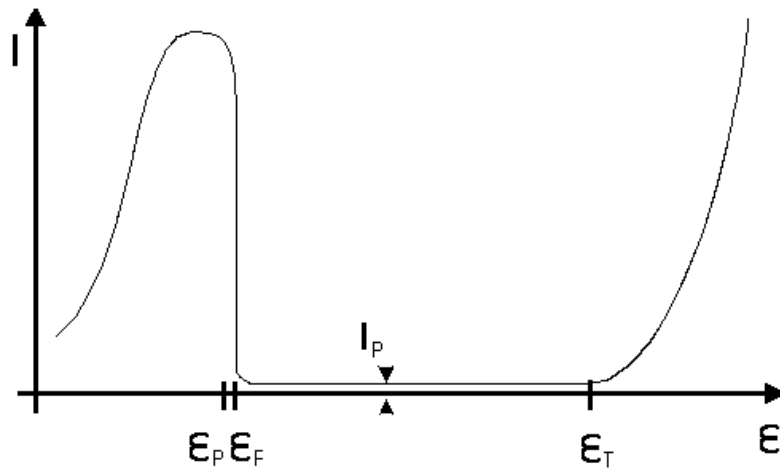

Figure 3.3: *Typical ϵ/I- curve for stainless steel in a corrosive medium. After the passivity potential ϵ_p the current drops to a constant low value, indicating the passivation of the material. After reaching the point of transpassivity (ϵ_t) the current increases again, indicating the breakdown of passivation (comp. [87]). Most etchings described in this work are performed in this area.*

The graph starts at the equilibrium potential of the electrode, the surface being not passivated at that time (left in diagram). At the equilibrium potential no outer current is present. Nevertheless there are anodic and cathodic reactions taking place. These reactions have currents of opposite directions which are in this case commensurate so that the outer current is zero. With increasing potential the current increases, indicating an active dissolution of the material. Toward higher potentials the surface is increasingly covered by hydroxide adsorbates. Above the passivity potential ϵ_p deprotonization of the hydroxides leads to the formation of a passivating film mainly consisting of metal oxides. At this point a continuous protecting passivity layer is formed, so that the current decreases, reaching a plateau eventually.

This area is the potential independent passivity area, in which almost no material dissolution takes place. The (very low) current in this area origins from a very slow decomposition of the passivity layer, which is compensated by a rebuilding of the layer at the side of the metal or from minor dissolution processes at spots where defects in the passivity layer are present, respectively. Accordingly the passive current density gives information about the protecting ability of the passive layer. When the current is further increased, different processes can take place, depending on the material and the corrosive medium. In most cases a point of transpassivity (ϵ_t) is reached where the passivity layer changes in composition and loses its passivation properties (comp. [88]) which results in another considerable increase of current. Another possibility, especially when chloride ions are present, is the formation of pitting corrosion spots, where the material is locally dissolved at a very high rate. Another process at higher potentials which can occur parallel to the aforementioned is a current increase caused by oxygen evolution. If the potential is decreased again from high values, i.e. the diagram is traced backwards, a new increase of current can be noticed after passing the passivity area. This point indicates the begin of depassivation and is referred to as the flade- potential ϵ_f.

The passivity properties are strongly dependent on the composition of the passivity layer [89]. The composition of the passivity layer can be changed by the exposure to corrosive media. Accordingly the corrosion resistance and with it the biocompatibility can be improved considerably by certain pretreatments like e.g. electropolishing or nitric acid treatments. The improvement is mainly caused by an enrichment of chromium within the passivity layer [61]. For alloys like 316L which have improved passivity properties, the area of active dissolution is shifted to the left which is connected with a strong reduction of the active dissolution current, finally leading to a diagram without an active area.

3.4.1 Effect of Hydrochloric Acid on Stainless Steel

Chloride ions own the property of attacking the passivity layer of stainless steel. An analysis of the layer reveals a composition mainly of chromium oxide and -hydroxide as well as a low percentage of iron hydroxide. The thickness is in the range of few nm [90, 91]. Interestingly in most cases neither nickel nor molybdenum can be found in passivity layer [92, 93]. Through the influence of Cl^- on the film on the one hand the integrity of the film is weakened, on the other hand a transport of metal ions to the surface is enabled which perishes the passivity effect of the film [94]. As a

consequence all main alloying elements, Fe, Ni and Cr in pure form at least slowly dissolve in HCl at room temperature without any potential applied. An effective passivation occurs only at high current densities, in case of Cr in the range of 10 mA/mm² [88]. The predominant reactions taking place in HCl containing solutions are the following

$$Me + 2H_2O \longrightarrow Me(OH)_2 + H_2 \tag{3.3}$$
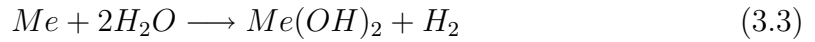
where the hydroxides further react to form oxides or chlorides, e.g.:

$$Me(OH)_2 + 2HCl \longrightarrow MeCl_2 + 2H_2O \tag{3.4}$$
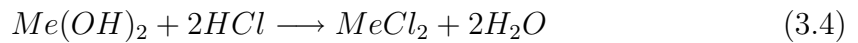
During HCl etchings the amount of metal oxide decreases while the oxy-hydroxid content increases [95]. At lower potentials the attack often manifests itself as pitting corrosion, which is explained in detail in the following chapter.

Pitting Corrosion

Pitting corrosion occurs, if an attack takes place only locally at certain spots, whereas most of the surface remains virtually untouched. This form of corrosion can be observed on metals or alloys which form passivity layers. If the passivity layer is weakened at a single spot, the attack causes the formation of a local anode. Accordingly the surrounding surface acts as a cathode. The result is a quick progress of corrosion at the local anode eventually leading to a local destruction of the material (s. fig. 3.4). For stainless steels pitting corrosion is mainly caused in connection with halogenide ions. These ions are able to weaken the passivity layer locally and thus creating a local anode. Despite intensive research the exact processes of the development of pitting corrosion are not yet fully understood. According to current models, comp. [67], adsorbed halogenide ions cause a local increase of the conductivity of the oxide layer as well as an increased dissolution of the layer. The result is the formation of an active pit beneath the layer where active metal dissolution takes place. Within the pit an increase of halogenide ion concentration as well as a decreasing pH-Value can be observed. These factors itself lead to an additional acceleration of the dissolution process. Critical for the formation of pitting corrosion is the presence of defects and inclusions [96]. It could be shown that pits initiate very often at inclusions of sulfides [97, 98, 99]. Suter and Boehni note a critical size of about 1 μm for manganese sulfites [98]. Other sources relate the creation of pits
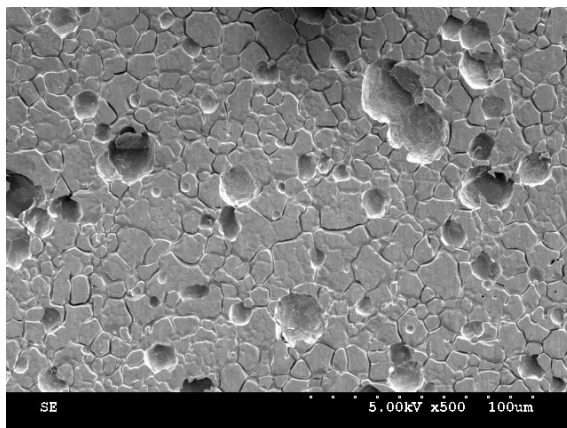
to the formation of the delta-phase [100].

Figure 3.4: *Pitting corrosion of 316L after electrochemical etching in HCl. The local breakdown of the passivity layer leads to the formation of spherical pits.*

Electropolishing

An effect that can occur when etching with chloride ions is the electropolishing effect. In this case the selectivity of the etching process is completely prevented by adjusting the etching parameters in a way that the mass transport (of ions and water molecules) is limited. This way the reaction is not controlled by the reaction rate anymore, but the mass transport becomes the limiting factor and a limiting current density occurs. The result is a leveling and smoothening of the surface. An explanation for the leveling effect is that at uprisings and irregularities the field intensity is increased as a function of $1/r$ (r - curvature radius). As the etching rate is dependent on the field intensity an accelerated removal takes place at this sites [101].

The precondition for an electropolishing effect is a relatively high current density (in the transpassive area). Additionally a high viscosity of the etching solution is advantageous. The higher the viscosity, the better a boundary layer of ions can be maintained at the etching area and the more the mass transport is limited. An increase of viscosity can be achieved for example by adding glycerin to the etching solution.

3.4.2 Effect of Nitric Acid on Stainless Steel

Nitric acid reacts with metals forming nitrates. However 316L as well as pure iron and chromium have a tendency to passivate in nitric acid solutions depending on the concentration of the acid. The higher the acid concentration the higher is the tendency to passivate. Thompson [102] states an almost complete passive behaviour of chromium in 68% nitric acid at room temperature. The reactions are similar to those occuring with HCl, however, the generated hydroxids immediately form nitrates, therefore in the following the intermediate hydroxidation step is waived. Concerning chemical etchings and electrochemical etchings at lower potentials iron, chromium and nickel dissolve in a bivalent state [103, 88, 104].

$$Me + 2HNO_3 \longrightarrow Me(NO_3)_2 + H_2 \tag{3.5}$$
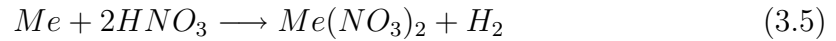
At higher potentials and at higher current densities (acc. to Gmelin [105] for Ni about 0.2 mA/mm$_2$) the metals dissolve in a trivalent state

$$2Me + 6HNO_3 \longrightarrow 2Me(NO_3)_3 + 3H_2 \tag{3.6}$$
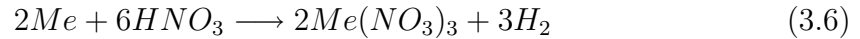
In both cases no gas formation at the anode can be observed. A reason for this is the immediate oxidation of the hydrogen to water (comp. [106]).

$$H_2 + HNO_3 \longrightarrow HNO_2 + H_2O \tag{3.7}$$

Nitric acid preferably attacks the grain boundaries. Therefore nitric acid is used in metallographic etching solutions for visualization of grain boundaries. The etching rate at the grain boundaries is in this case a lot higher then at the grain surfaces. Two reasons can be found for this. Firstly a much higher degree of disorder and an increased number of vacancies and lattice defects is present, so that these sites are preferably attacked. Secondly the composition at the grain boundaries often differs from the composition at the interior of the grains. This difference is mainly caused by segregations of alloying elements. Christien et al. [107] showed that it is possible to quantitatively determine the concentration of certain segregation elements at the grain boundaries with the help of metallographic etching methods. It was found that the depth of the etched grain boundary indents are directly proportional to the content of the segregation element phosphor. A model for the calculation of segregations at the grain boundaries is described by Sahlaoui et al. in [108]. Using microchemical analysis of solution annealed 316L a depletion of the passivating element Mo but no significant depletion of Cr could be determined by Furutani et al. [109]. Another factor favoring the corrosion effect is the presence of chromium rich

carbides of the type $M_{23}C_6$, that can be found at the grain boundaries. In the direct vicinity of these chromium rich precipitations there is a chromium depletion and thus the passivity layer is weakened [110]. Chromium carbides however develop only at high temperatures (above 700°C) or during very long tempering cycles (1000h at 600°C)[111]. All nitrates are soluble in water, so that a deposition of reaction products on the surface can be excluded.
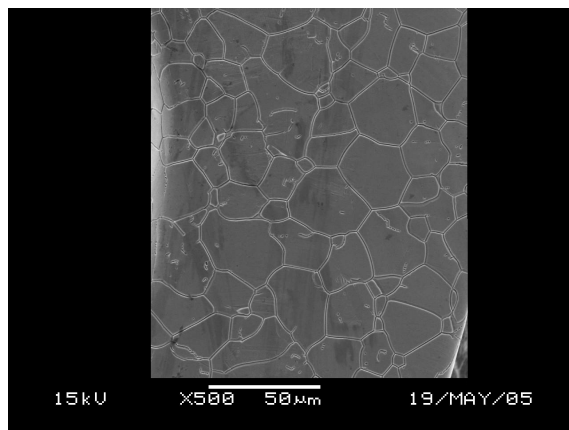

Figure 3.5: 316L slightly etched with nitric acid. The grain boundaries become visible while the rest of the surface remains virtually unaffected.

Nitric acid treatments are sometimes used in order to increase the passivation effect for HNO_3 [62, 112]. This increase is explained by an enrichment of chromium within the passivity layer and by a dissolution of inclusions like MnS (comp. [64]). However some authors also report negative effects of HNO_3 on the passivation [62]. In nitric acid the amount of metal oxide decreases while the metal oxy-hydroxides content increases [95].

3.4.3 Effect of Oxalic Acid on Stainless Steel

Stainless steels as well as pure Fe slowly corrode in oxalic acid containing medium, while pure Cr and Ni act passive in oxalic acid. Chromium and iron mainly react with oxalic acid as follows (comp. [113])

$$Me + 2H_2O \longrightarrow Me(OH)_2 + H_2 \tag{3.8}$$

$$Me(OH)_2 + 3H_2C_2O_4 \longrightarrow Me(C_2O_4)_3 + 2H_2O + 2H_2 \tag{3.9}$$

When ferrous oxide is present it is preferably attacked [114]. Therefore oxalic acid is sometimes used for decontamination and descaling of stainless steels [115]. In

both cases metal oxalates are created. Ferrous oxalate as the main reaction product for stainless steel [116] is yellow in color and has a solubility coefficient of $K_{sp} = 2*10^{-7}$. Therefore it has, like chromium and nickel oxalate ($K_{sp} = 1*10^{-7}$), a poor solubility in water. After chemical etching with oxalic acid deposition of oxalates on the surface was observed, which could hardly be removed by ultrasonic cleaning [117]. In the field of metallography electrolytic oxalic acid etching is used in order to visualize the microstructure of austenitic steels (fig. 3.6)[118]. In some cases it is also used for visualizing dislocations and twin grain boundaries of certain steels [119].
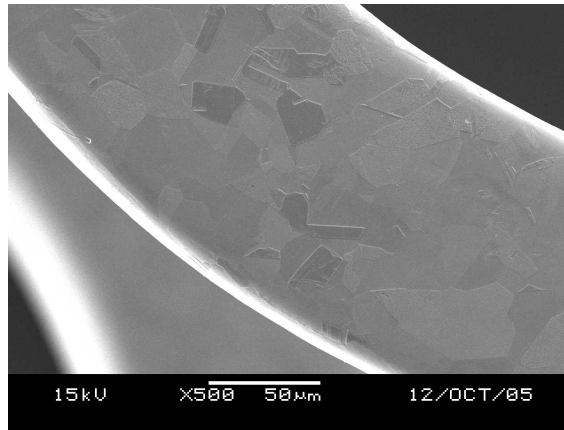

Figure 3.6: *316L etched with oxalic acid. The crystallographic structures are visible.*

3.4.4 Effect of Phosphoric Acid on Stainless Steel

316L as well as all main alloying elements Fe, Ni and Cr passivate in phosphoric acid when no potential is applied. Chromium and iron react with phosphoric acid at lower potentials as follows (comp. [120, 88, 104])

$$Me + 2H_2O \longrightarrow Me(OH)_2 + H_2 \tag{3.10}$$

$$3Me(OH)_2 + 2H_3PO_4 \longrightarrow Me_3(PO_4)_2 + 6H_2O \tag{3.11}$$
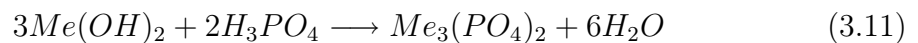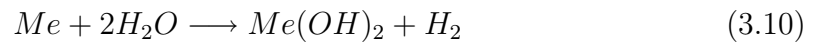
Similar to nitric acid at higher potentials the main dissolution process changes from a bivalent solution of the metal to a trivalent one

$$2Me(OH)_2 + 2H_3PO_4 \longrightarrow 2Me(PO_4) + 4H_2O + H_2 \tag{3.12}$$
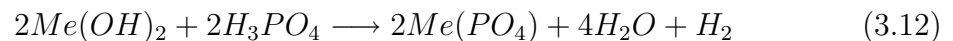
Phosphoric acid features a high viscosity and is used as an electropolishing agent or as an ingredient of electropolishing solutions, respectively [121]. In contrast to

the other acids described, etching with phosphoric acid exhibits, under the applied currents used in this work, exclusively smoothing effects. The processes, that are responsible for this smoothing behavior are described in detail in subsection 3.3.1. In the literature an increase of chromium content within the passivity layer in connection with an increased chemical resistance is reported for surfaces electropolished with phosphoric acid [63]. All phosphates occurring in connection with the phosphoric acid etching of 316L are virtually insoluble in water (K_{sp} for iron phosphate is $1,3*10^{-21}$).
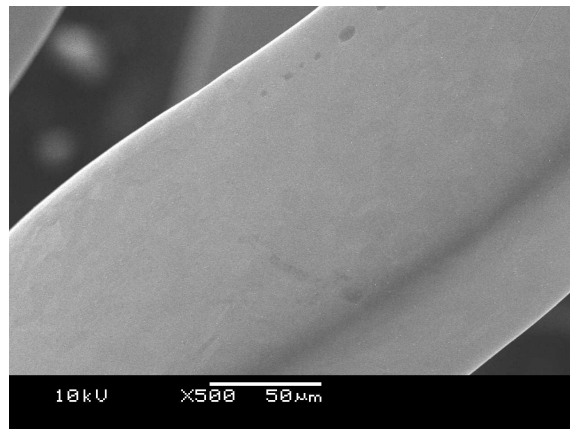

Figure 3.7: *316L etched with phosphoric acid. A uniform smooth surface developed.*

4 Material and Methods

4.1 Material

All experiments were carried out on medical grade 316L steel. 316L is an austenitic chromium-nickel steel with a high chemical resistance. The resistance is achieved by a high chromium content, an addition of molybdenum and a high nitrogen content. 316L is used for a variety of implant materials like bone implants (plates, screws, nails), vessel implants, etc.[122]). The raw material (Minitubes, Grenoble, France) for the stent fabrication are tubes of 1.8 mm outer diameter and 0.14 mm wall thickness. The stents are fabricated by laser cutting and receive a heat treatment after cutting. Both the stents and the raw material (for evaluation experiments and for roughness determinations) were used for the experiments. The material composition is as follows:

C	Si	Mn	S	P	Ni	Cr	Mo	Cu	N	Fe
0,017	0,36	1,8	0,002	0,018	14,72	17,33	2,75	0,08	0,076	bal

Table 4.1: *Composition of 316L in weight-% according to supplier.*

Concerning the mechanical properties the following data is given:

Sample no.	Rm (N/mm^2)	Rp0,2 (N/mm^2)	A (% on 50 mm)
1	943	829	6,5
2	945	811	6,0

Table 4.2: *Mechanical properties of 316L.*

It fulfills the norms ISO 5832.1 and ASTM F 138.92. Roughness of the tubes was determined to Rz = 0,76, Ra = 0,075 (s. p. 34). The average intersectional grain size of the material was determined according to DIN 50601 (lineal intercept method) by measuring etched cross sectional micrographs (fig. 4.1). For a detailed description

s. appendix. The grain size of the tubes was 43.2 μm $\pm$ 8.2 μm in longitudinal direction and 21.1 μm $\pm$ 5.4 μm in transversal direction. The stents have an average grain size of 15.9 μm $\pm$ 3.2 μm, independent of the measured direction.

Unless otherwise noted electropolished stents were used for all etchings. All of the electropolished stents were obtained crimped on a catheter. In order to remove the stents they were dilatated at 6 atms within a polymer tube of 1.7 mm inner diameter. This procedure leads to a slight distortion of the stent. This fact is important to note when etching on a pin (s. following sec.) as it leads to a much worse protection of the inner side of the pin.

Grit blasted stents served as reference for the adhesion tests. Fig. 4.2 shows struts of an electropolished stent and a grit blasted stent.
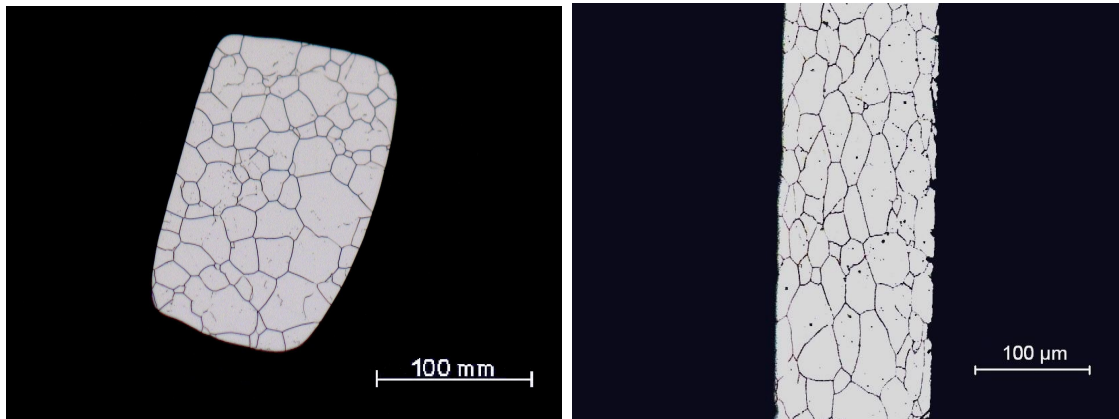
Figure 4.1: *Grain structure of stent material (section), left: stent, right: raw material. A texture in longitudinal direction is visible for the raw material.*

4.2 The Etching Assembly

The following acids were used: nitric acid 65%, hydrochloric acid 35%, oxalic acid (crystalline powder), phosphourus acid 85% (p.A., Merck, Germany). The acids were diluted to the required concentrations with demineralized water. For all etchings the following concentrations were used: nitric acid 40%, hydrochloric acid 24%, oxalic acid 10%. In case of most etchings the stents were immersed into the solution crimped on a stainless steel pin of 1.4 mm diameter, the crimping being performed

Figure 4.2: *SEM images of a grit blasted (left) and an electropolished stent(right).*

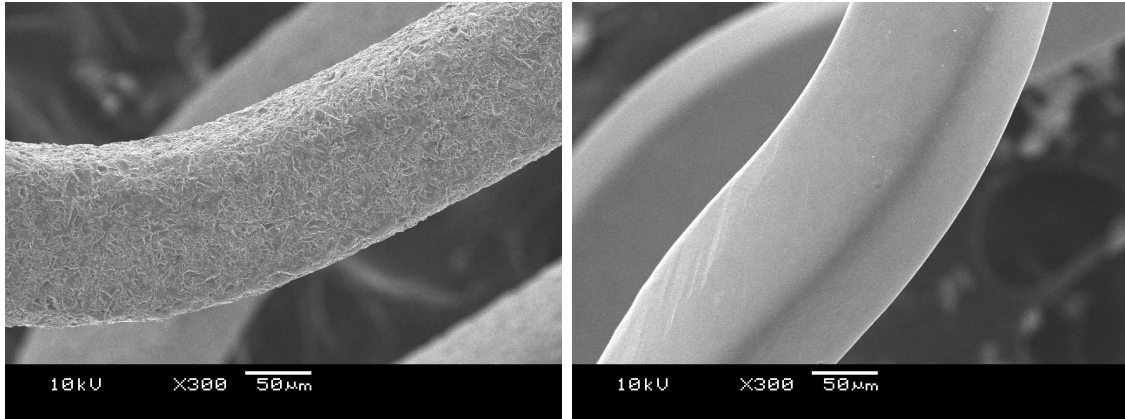manually. In case of most hydrochloric acid the stents were etched without a pin hold by a thin platinum wire. When using 316L tubes the material was hold directly into the etching solution by means of a clamp.

The current was supplied by a DC transformer (PPS 3003, Conrad, Hirschau, Germany) with the stents switched as the anode. The current was measured with an amperemeter. Prior etching the specimens were cleaned in acetone with ultrasonic. After the etching procedure the specimens were hold in 0.5 mol NaOH for 2 min. This step assures that any acid remains are eliminated and, as a side effect, the NaOH promotes a passivation of the surface. After this procedure all specimens were carefully washed with demineralized water and cleaned in an ultrasonic bath for 20 min.

All etchings with the exception of the hydrochloric acid etchings were carried out in a stainless steel block with a 32 mm hole of 16 mm diameter drilled in it (fig. 4.3). The steel block was electrically connected so that it served as a container for the etching solution and at the same time as the cathode for the etching process. The stent on the pin was immersed 20 mm into the etching solution. In most cases hydrochloric acid etchings were carried out without a pin. In this case the stent was immersed into the etching solution on a thin platinum wire.

For the preliminary experiments in order to evaluate the etching parameters of the combination etchings 30 mm stent raw material tubes (1.8 mm diameter) were used. The first etching step was performed as described above. The second step was performed with a special assembly within a small glass cylinder. The cathode
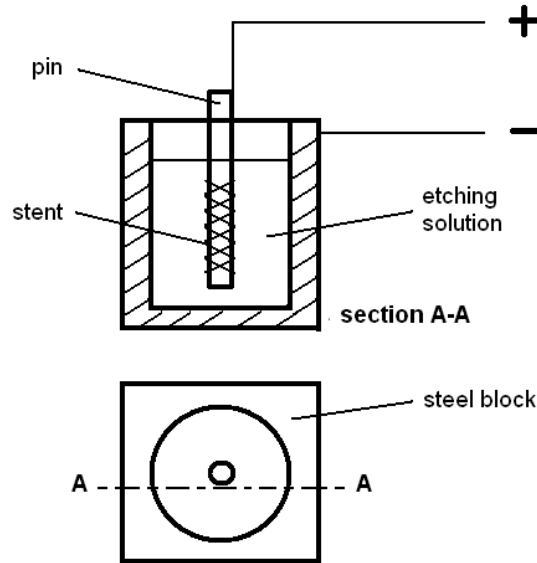
Figure 4.3: *Schematic drawing of the setup of the etching in a steel block. The stent is switched as the anode while the steel block, which is filled with the etching solution, serves as the cathode.*

consists of a cylindrical 316L tube (stent raw material) with 6 mm diameter and 4 mm hight. The tube to be etched was fixed with one end at the middle of the cylindrical cathode by a thin polymer disc with a hole in its center (fig. 4.4). By this a decreasing current density from the top to the end of the tube was achieved. When creating cross sectional micrographs of this tubes different areas of the tube can be investigated representing different etching strengths. A schematic illustration is given in 4.5. Since the electrical resistance of the solution as well as of the tube is nearly constant over the whole length, an almost linear increase from current density j_{min} at the bottom to j_{max} at the top is generated, with an average current density $j_a = 0.5 \cdot (j_{min} + j_{max})$. When the ratio $c = j_{min}/j_{max}$ is known the minimum current density can be estimated by

$$j_{min} = \frac{j_a}{0,5 + \frac{1}{2c}} \tag{4.1}$$

j_a can be calculated by dividing the applied current by the surface area of the tubes which is 30 mm $\cdot$1.8 mm $\cdot\pi$. c can be estimated when comparing the material removal at the top with the material removal at the bottom. The removals were determined to 8 μm and 22 μm, respectively, so that c can be assumed to be approx. 0.37 . A current of 200 mA results in the values $j_{min} = 0.64$ mA/mm^2 and $j_{max} = 2 \cdot j_a - j_{min} = 1.57$ mA/mm^2.
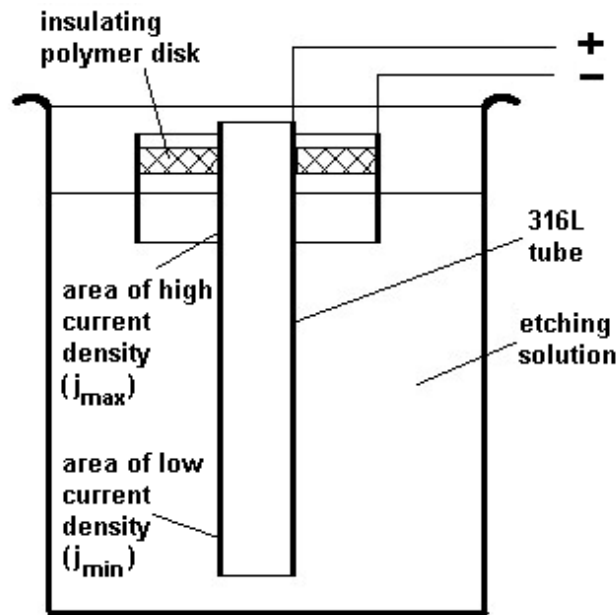
Figure 4.4: *Etching assembly for the preliminary experiments. The setup results in a high current density at the top of the tube which decreases gradually to the bottom.*

For all etchings with hydrochloric acid except the HCl-combination etchings with nitric acid a different assembly with separated electrodes was employed because these experiments were performed using a stirrer. For these etchings an assembly with two separated beakers was used, illustrated schematically in fig. 4.6. The separation of the electrodes holds the advantage that the gas formation at the electrodes is reduced and therefore the dissociation of the solution is inhibited. As a stirrer a polymer coated magnet was used which was adjusted at 270 u/min for all experiments. Each electrode was set in a separate beaker of the same etching solution which were connected with a cellulose membrane soaked with etching solution. As the cathode served a sheet of 316L.

4.2.1 Calculation of Current Densities

For some contemplations the etching currents are converted into current densities in order to provide values that are independent of the experimental design. When etching without a pin the total stent surface area ($4 \cdot 25.9$ mm^2 = 103.6 mm^2 for

1. step, grain boundary etching

2. step, isotropic etching

j_{max}

j_{min}

strong etch effect

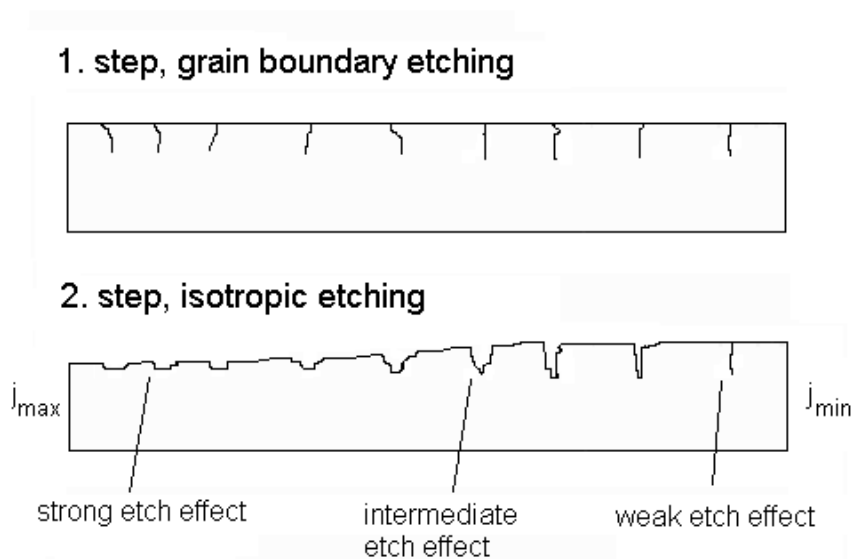intermediate
etch effect

weak etch effect

Figure 4.5: *Schematic illustration of the preliminary experiments. The first step creates small cavities which are hollowed out in a second, isotropic etching step.*

a 16 mm stent) is used for the calculations. The surface area of the pin plus the side surface areas of the (electropolished) stent ($2 \cdot 25.9$ mm^2 for a 16 mm stent) are used when etching on a pin. So the area used for the calculations of the current densities is 1.6 mm $\cdot$ pi $\cdot$ 20 mm $+$ 51.9 mm^2 $=$ 152.5 mm^2. However, the exact area at which etching takes place cannot be determined in this case since part of the stent may not be in contact with the pin and thus contributes to the etched surface area. Also when etching without a pin the actual area varies on the one hand with the material removal and on the other hand with changes in roughness. It is important to note that the current densities and the etching times can be used in order to qualitatively compare the strength of different etchings. However it is not an exactly precise measure of the actual etching strength. Another parameter that can be used as an estimation for the etching strength is the material removal measured as diameter loss.

4.3 Topographic Surface Analysis

The surfaces of all samples were analyzed under SEM at magnifications from 300X to 2000X. For this analysis an S-3500 N, Hitachi Science Systems, Tokyo, Japan was
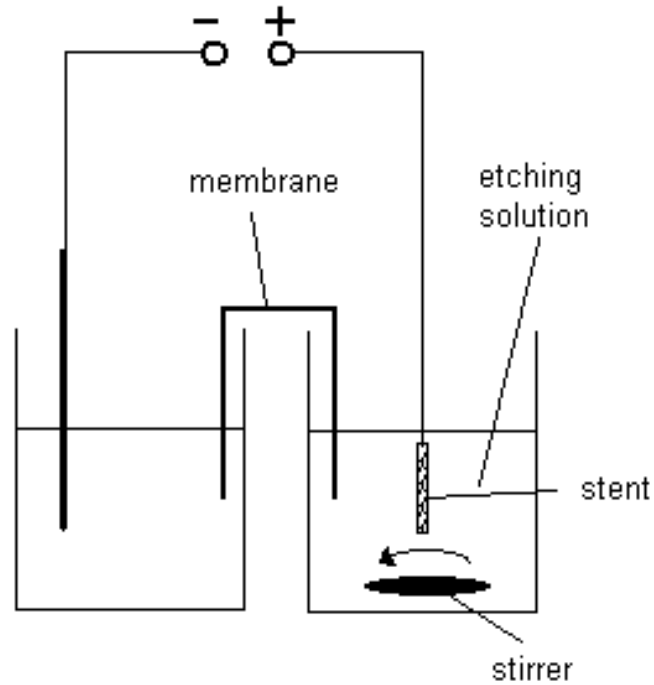
Figure 4.6: *Schematic assembly of the etching with separated beakers. Both beakers are filled with etching solution and are separated with a membrane. This setup enables the use of a stirrer in a way that an influence of the cathodic reaction on the etching process is minimized.*

employed with 5 to 20 kV acceleration voltage.

For both the determination of the grain size in case of the grain boundary etched samples and the characterization of the facets in case of the hydrochloric etched samples the line cut method was used. Ten lines of 100 μm length each were drawn randomly on light microscope images with 200X magnification (Axiovert 25, Carl Zeiss GmbH, Jena, Germany) and the intersections with the grain boundaries or the facets, respectively, were count. It was found that for all etched stents the results of the cut numbers are independent of the line direction, so it can be assumed that the structures are isotropic.

Roughness was determined by mechanical perthometry (M2, Mahr GmbH, Göttingen, Germany) on tube material. The measured parameters were the average roughness depth (R_z) and the arithmetic average roughness (R_a). The most important roughness value for the grain boundary etchings is the R_z value. This value is most sensitive for discrete indentations as it gives an average of the highest peaks and the

lowest valleys. For the hydrochloric acid etchings the R_a values are given, characterizing the average roughness. A limitation of roughness determination (mechanical roughness measurement as well as confocal perthometry) is the correct measurement of slots with very high aspect ratios (like deep narrow crevices). In order to validate the results the values of the measurements were compared to polished sections of the same surfaces. The comparison showed good congruence between the sections and the measured profiles for the hydrochloric acid etched tube samples. For all grain boundary etched surfaces the resulting deep crevices could not be captured by conventional methods because of the high aspect ratios. For these samples as well as for all examination on stents, including the determination of the exact depot volumes of the combination etched samples, an analysis of cross sectional micrographs was performed.

4.4 Cross Sectional Micrographs

For detailed topographic analysis cross sectional micrographs of etched stents were prepared, embedded in two-component epoxy resin (Specifix-40, fa. Struehrs, Willich, Germany). For all stents the sections were created with the stent on a pin in order to fix the stent within the resin. The sections were polished with diamond suspension down to 1 μm particle size and finally sputtered with gold (approx. 10 nm) using a sputter-coater (SCD 005, BAL-TEC AG, Balzers, Lichtenstein) under high vacuum with a current range between 5-15 kV. Besides an exact analysis of the depots it is possible to estimate the material removal of the etchings with polished sections. The removal rate cannot be determined by the width of the stents because for polished sections this parameter varies with the orientation of the struts within the stent netting. Besides the width can vary itself because of inaccuracies of the laser cutting. The thickness, however, does not vary, providing that the stent is mounted exactly vertical.

For the analysis of Rapamycin coated stents, the coated stents were sputtered with gold from all sides prior mounting (process see above). This gold layer prevents the solution of the Rapamycin in the mounting resin. Besides the gold sputtering enables the contours of the Rapamycin layer to be seen well under the light microscope as well as under the SEM, even if the Rapamycin has been washed out by the polishing process.

4.5 Software Analysis of the Depot Structures

The SEM images of the sections were transformed into image-files of a calculation program (MATLAB) for a detailed analysis of the depot properties. For the determination of the depot limits a polygon was generated around the stent as shown in fig. 4.8. The polygon is defined through the attributes of having all edge points on the contour line and having no concave parts. The three- dimensional analog to the polygon model would be a foil in which a stent strut is enfolded. (It is assumed that the height of the microstructures does not vary considerably in direction perpendicular to the cross section. This assumption has to be made in order to exclude minor deviations between the 2D model and the 3D analog.) Determined through this attributes, the polygon covers the strut similar like the artery tissue. Accordingly the areas between polygon and strut can be defined as depots and can be software analyzed. This model is used to describe a state at which the outer drug layer of the stent is already used up. Fig 4.7 shows a cross sectional micrograph of a coated grain boundary etched stent strut after coating with 1% Rapamycin. It can be seen that the drug builds a layer of few μm thickness over the depots. Most of such a layer is normally removed within a few days as already described in the introduction. After this period the depots will predominate the release behavior. At this point the strut is already integrated into the tissue, or covered by a thrombus, respectively, so that the tissue is adjacent to the strut surface as assumed in the model. An example for a stented porcine artery at the third day after implantation is illustrated in fig. 4.7. More details on the release out of the depots are given on p. 104.

4.6 Calculation of Depot Properties

Firstly the contour line of the stent strut was determined through contrast differences between stent and background. This was performed using an object determination function (selectobjectmex) of the MATLAB image processing toolbox. It was found that the contrast was sufficient for all images so that a preprocessing was not necessary. Afterward the polygon was created around the strut (s. fig. 4.8).

A detailed description of the calculation of the polygon points can be found in the appendix. For the analysis of the depots only three of the four sides of the stent
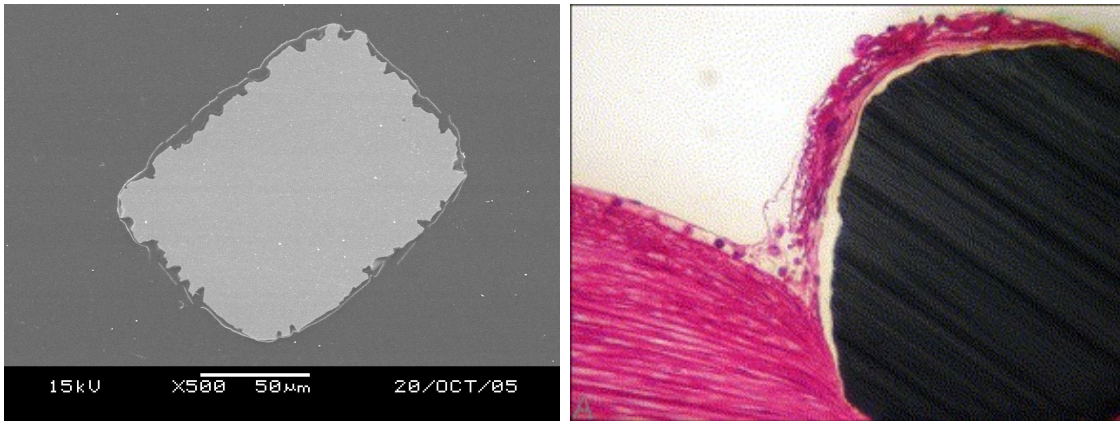
Figure 4.7: *Left: coated grain boundary etched stent strut, section; right: cross sectional view of an (uncoated) stent strut within an artery three days after implantation[123]. A thrombus has already been built around the stent.*
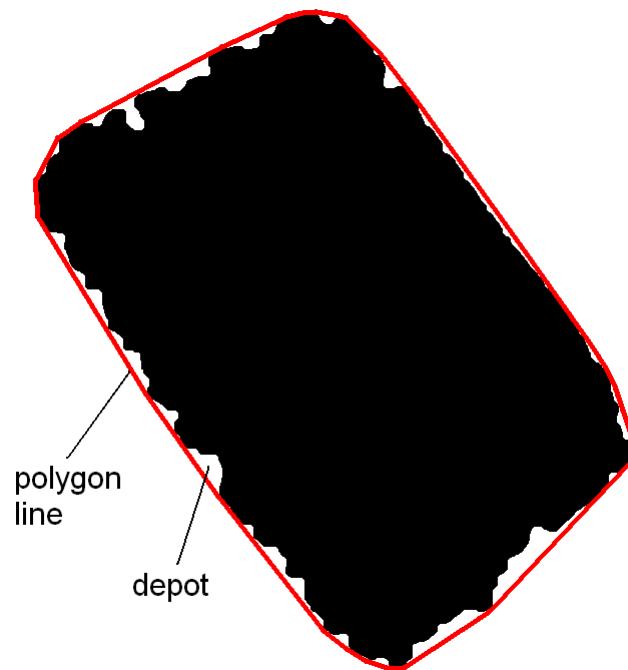
Figure 4.8: *Section of a stent strut with polygon line. The polygon line simulates the artery, circumscribing the microdepots.*

are considered, waiving the inner side of the stent. This side is adjacent to the pin during the etch process and thus protected from the etching attack. Of each single depot the area, the center of the area and its smallest distance from the polygon line is determined. In order to compare different stents the total depot area was divided

by the length of the (three side) polygon line. Since the orientation of the struts within the mounting resin varies, the cross sectional area and with it the lengths of the polygon lines of different struts diverge. Dividing the depot areas by the polygon length yields an average structure depth which is independent of the size and shape of the cross section. This value corresponds to the theoretical storage volume per area of a microstructured surface. E. g. if the average structure depth is 1 μm, the theoretical storage volume would be 0.001 mm^3/mm^2. An even more important parameter than the theoretical storage volume is the effective average depot depth. This value is obtained by multiplying the area of each single depot with the distance of its center point from the polygon line and dividing the sum of this values by the total depot area. The product of this value and the average storage volume can be regarded as a measure for the depot effect. For each etching 6 to 8 strut images were analyzed.

4.7 Coating Process and Analysis of Coatings

The procedure of coating and coating analysis is only summarized in the following chapter, a detailed description can be found in [124]. The stents were coated via a Translumina Magic Box©coating system with 1 or 2% ethanolic Rapamycin solution. Subsequent drying of the stent was not necessary since the system allows the ethanol to evaporate during the coating process. For the quantification of the amount of drug the stent was dilatated with 16 atms and subsequently the Rapamycin was washed off with ethanol and the total amount of Rapamycin was determined by UV-Vis spectroscopy (Specord-210, Jena Analytik AG, Jena, Germany). For the adhesion tests the stent was inserted into an artificial blood circuit and dilatated in an artificial artery. After dilatation the artery with the stent was cut out and the rapamycin was extracted with ethanol. For the determination of release kinetics the coated stents were placed inside a covered plastic tube with Ringer´s solution. In order to achieve a flux of the solution the tubes revolved perpendicular to the tube axis with 20 turns per minute. At constant time intervals a small amount of solution was withdrawn and analyzed in terms of Rapamycin content via UV-Vis spectroscopy. During the release the temperature was hold at a constant 37°C.
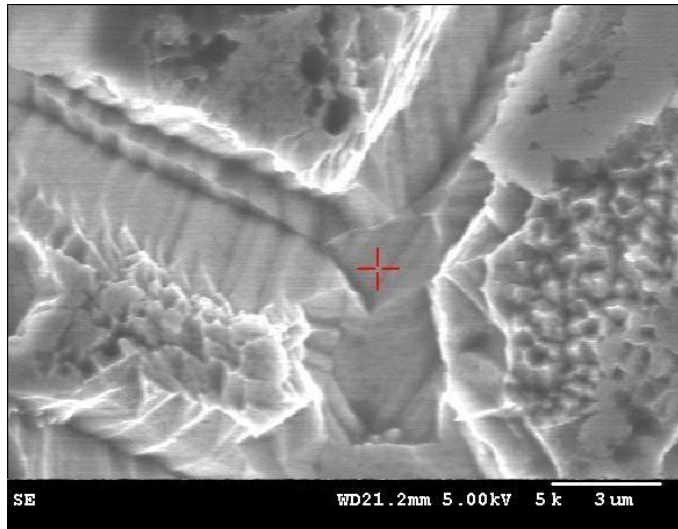
Figure 4.9: *Example for an EDS analysis spot.*

4.8 Chemical Surface Analysis

4.8.1 SEM-EDS

EDS (energy dispersive X-Ray spectroscopy) analysis is used in order to get informations about the composition of a sample through interpretation of X-Ray radiation. The excitation is performed by accelerated electrons. In the case of a SEM-EDS the EDS is combined with an electron microscope which supplies the electron beam. The information depth is dependent on the acceleration voltage of the electron beam. For all analysis in this work the acceleration voltage was 20 kV which yields an information depth of approx. 3 to 4 μm. The lateral resolution is 1 to 2 μm. In order to visualize the grain boundaries the analyzed samples were slightly oxalic acid etched. This combination etching has the advantage that the grain boundaries are made visible without creating crevices which cannot be analyzed by EDS. Fig. 4.9 shows an example of an image of a measured point at the grain boundaries.

4.8.2 Auger Electron Spectroscopy

AES is used in order to analyze the composition of surfaces. In this work it was used in order to obtain informations about the composition of the passivity layers. The information depth is limited to the top 2 to 20 atom layers of the sample surface. Since the passivity layer of stainless steel is in the range of few nm an influence of the bulk material on the results cannot always be excluded. Besides AES is quite

component	conc. in Ringer´s solution (10^{-3} mol/l)	normal conc. in human blood plasma (10^{-3} mol/l)
Na^+	143	137-148
K^+	5,4	4,1 - 5,6
Ca^{2+}	1,8	2,2 - 2,7
Mg^{2+}	0,8	0,7 - 0,9
Cl^-	125	116
SO_4^{2-}	0,8	0
$H_2PO_4^-$	1,0	0,8 - 1,6
HCO_3^-	26	29
Haematin	5,5	3,3 - 5,6
total	310	300

Table 4.3: *Comparison of Ringer´s solution and blood plasma.*

sensitive against surface contaminations so that even minor remains can affect the results. For secondary ion mass spectroscopy or X-ray photoelectron spectroscopy which are the best suited methods for analysis of passivity layers large, plain surface areas are necessary. Therefore these methods could not be used for stents.

4.9 Electrochemical Analysis

All analysis was performed according to DIN 10993-15. For all experiments Ringer´s solution was used as electrolyte (composition s. appendix). Ringer´s solution is used as an artificial substitute for blood plasma or for tissue fluid, which has basically the same composition except a smaller amount of proteins [125]. A comparison of the composition of human blood plasma components and Ringer´s solution is given in table 4.3.

Despite the good replication of the plasma composition in respect to the main constituents, Ringer´s solution can only roughly simulate the complex corrosive properties of body fluids. Besides the listed constituents a plurality of enzymes, proteins, living cells and other complex elements are present within the living body, which cannot be simulated by an artificial solution. Especially enzymes have a great impact on the chemical activity, so that it can be assumed that the corrosiveness in vivo against metals is considerably higher than in Ringer´s solution.

4.9.1 Cyclic Voltammetry

Cyclic voltammetry is used in order to characterize the electrochemical behavior of a material surface in a certain environment. The sample which is immersed in electrolyte solution is initially hold at the equilibrium potential. Then the electrode potential is decreased to a more negative potential (in cathodic direction). This scan is performed in order to guaranty the same initial situation for all samples. From this point the potential is scanned in anodic direction up to a maximum potential. Finally the scan is reversed until the potential reaches the initial starting point. The minimum and maximum potentials are selected in a way that hydrogen or oxygen evolution, respectively, can be observed at the sample. It was not possible to determine the exact surface area of the immersed part of the stent. Therefore a standardization of the currents to current densities was waived.

An example of a measurement is given in fig 4.10. Prior to and after the measurements the specimens were analyzed under SEM and under the light microscope.
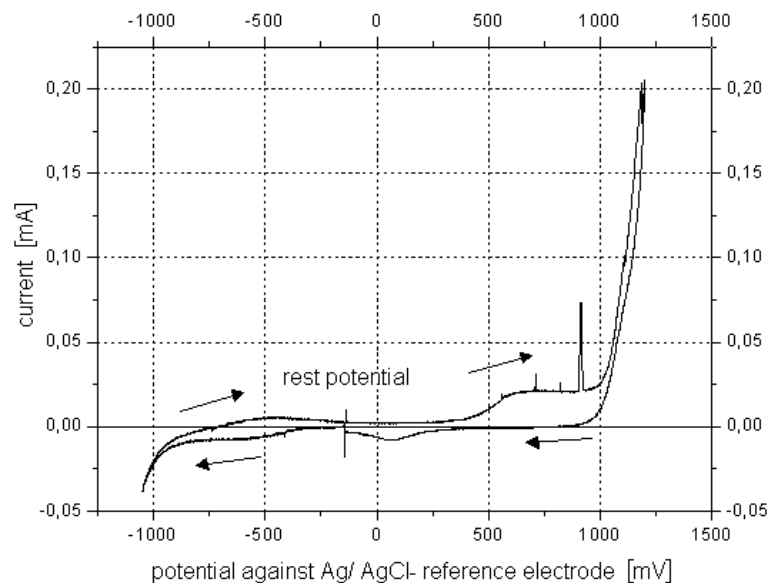

Figure 4.10: *Example for a cyclovoltammogramm.*

The assembly for the cyclic voltammetry is illustrated in fig 4.11 (comp. [126]). For the measurements a three electrodes setup as illustrated in fig 4.12 was used. The potential is measured via a third additional reference electrode. The reason for this setup is the fact that a reference electrode pervaded by electrical current exhibits an overvoltage, making a correct potential measurement impossible.
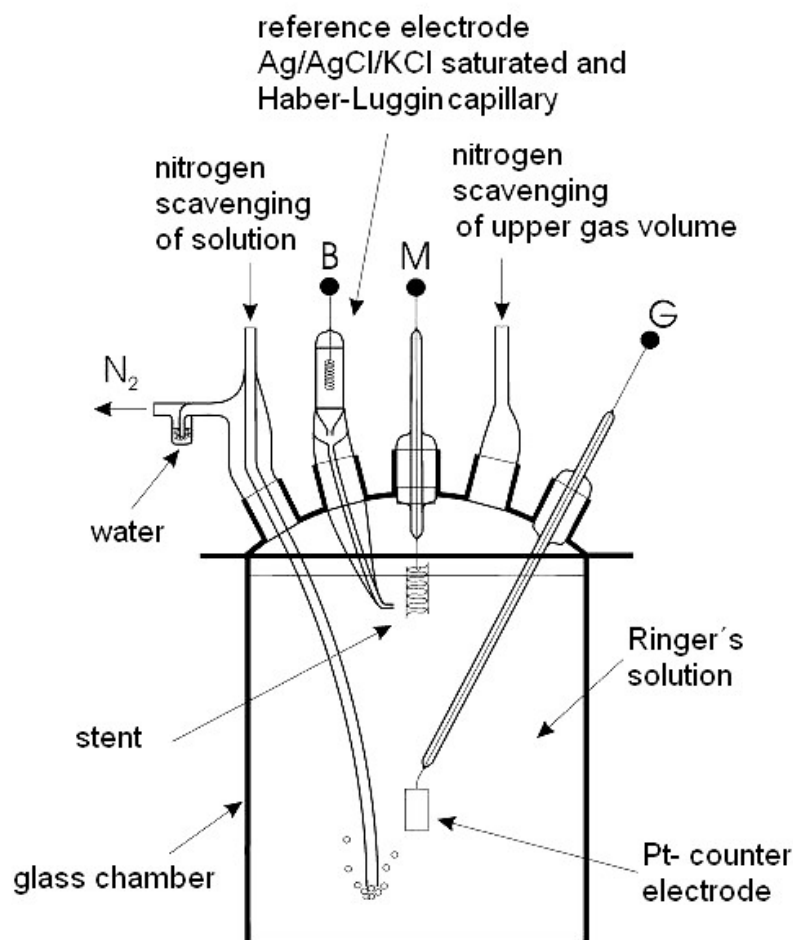

Figure 4.11: *Assembly for cyclic voltammetry (B: reference electrode, M: measuring electrode, G: counter electrode).*

The voltage for the potentiostat (Jaissle, 1030DA) is delivered by a function generator (Prodis 1/16l),the function generator being controlled by a PC. The released analog current measurement signal is sent to the PC via a voltmeter (Keithley 199 System DMM/Scanner) which serves as analog-/digital transformer. The software that was used was purpose-written for the experiments at the Institut for Corrosion

and Surface Technology, Erlangen with the programming software QuickBasic.

The measuring unit for the cyclic voltammetry is illustrated in fig 4.12. The reference electrode is a Ag/AgCl electrode with saturated KCl solution and is combined with a Haber-Luggin-Capillary. The potential of such an electrode is normally $E_{Ag/AgCl/KCl}$ = +198 mV$_{SHE}$ (SHE - standard hydrogen electrode), however for the employed electrode for unknown reasons a stable potential of +220 mV$_{SHE}$ was measured. For the counter electrode and the wire to hold the stent platinum was used. In order to avoid an influence of the platinum on the cyclic voltammogram the stent was not completely immersed into the solution, so that the platinum had no contact with the electrolyte. The complete assembly was surrounded by a metal cage in order to shield electromagnetic disturbance radiation.
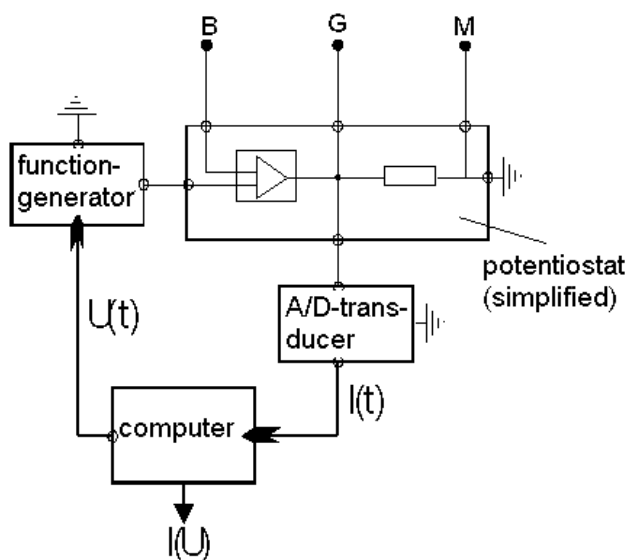

Figure 4.12: *Simplified illustration of the circuit for cyclic voltammetry with three electrodes (B: reference electrode, M: measuring electrode, G: counter electrode).*

Prior each measurement the electrolyte was degased with nitrogen (99,999%) for approx. one hour. Additionally the gas chamber was scavenged with nitrogen during the measurement. Open Circuit potential measurements were performed directly after immersing the stent into the electrolyte solution. For these equilibrium potential measurements a time of approx. 45 min had to be awaited until a stabilization of the value appeared. The measurements were performed in inert gas atmosphere in order to receive a current-potential curve that is not superposed by reduction effects of oxygen. All measurements were carried out at a scan rate of 1 mV/s starting from

the equilibrium potential in cathodic direction till -1050 mV$_{Ag/AgCl}$, subsequently in anodic direction till 1200 mV$_{Ag/AgCl}$ and finally again in cathodic direction till the equilibrium potential.

4.9.2 Potentiostatic Tests for Determination of Ion Release

Due to the high amount of nickel and chromium in 316L a risk of negative side effects caused by released ions is present. Chromium and nickel and also molybdenum are toxic substances that can cause severe allergic reactions. In the case of coronary stents allergic reaction have been attributed to a considerably higher risk of restenosis. [127, 128]. Potentiostatic experiments were performed in order to compare the release behavior of the etched stents with grit blasted stents as reference. It has to be noted that the chosen conditions cannot exactly simulate the in vivo conditions. Nevertheless the experiments give some information about the examined surfaces in comparison to each other.

The test assembly is analog to the cyclic voltammetry assembly, while the ion release experiments were carried out in a glass chamber with a lid (fig. 4.13) (comp. [126]). The filling volume of the glass chamber was 40 ml. The tests were performed at a constant potential of 150 mV above the break through potential for a time period of 72 hours. The current was measured continuously over the whole period. All specimens were subsequently analyzed under SEM and light microscope. The electrolyte solutions with the released ions were analyzed with the graphite tube technique on an Analyst 800 (Perkin Elmer, Wellesley, Massachusetts, USA, detection limit 2 μg/l).
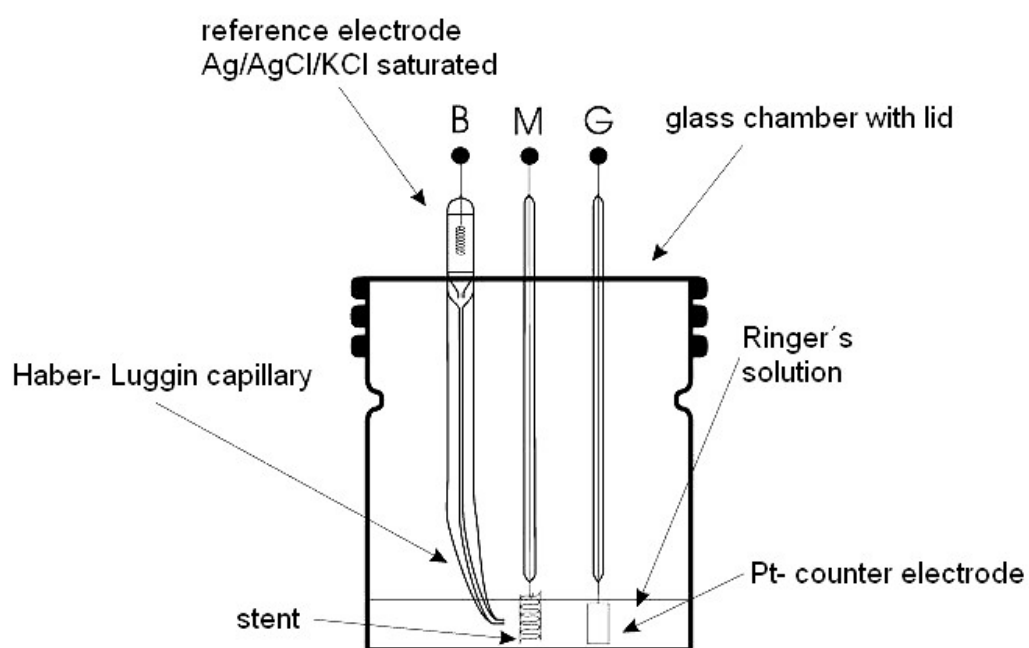
Figure 4.13: *Schematic illustration of the assembly for determination of long term ion release (B: reference electrode, M: measuring electrode, G: counter electrode).*

4.10 Cell Seedings

4.10.1 Seeding Process

Endothelial cells (cell line), stromal cells (primary cells) and fibroblasts (cell line) were used:

- HUVEC: human umbilical vein endothelial cells (Cat# C-015-10C, Cascade Biologics)

- UCSC: umbilical cord stromal cells (inhouse produced, the procedure is described in [129])

- 3T3: embryonic fibroblasts (Cat# CRL-1658, ATCC, Manassas, USA)

All cell seedings were performed on 316L platelet material. Round platelets of 1 mm thickness and 10 mm diameter (corresponding to a surface area of 188,57 mm^2) were machined from stent raw material bars and subsequently ground and polished. The platelets were grit blasted or etched, respectively, according to the stents. It was found that higher currents (600 mA for a platelet roughly corresponds to 200 mA for a stent on a pin) and longer etching times were needed for the platelets in order to generate the same microstructures. The surfaces were examined under SEM before seeding in order to observe the surface topographies. For the seeding process the platelets were inserted into the bottoms of approx. 2 cm high sections of a polyurethane tube, in a way that the platelets seal the tube consistently. In a next step the sections were filled each with 5000 cells in cell medium. The cell number was determined using the Casy 1-Cell Counter Analyzer System, Model TT (Schärfe System GmbH, Reutlingen, Germany). For the analysis a small part of the solution to be tested was diluted one to one hundred using a weak electrolyte (Casy®ton, sterile filtered, Schärfe System GmbH, Reutlingen, Germany) and drawn through a capillary with a constant flow velocity.

The cell cultivation took place under sterile conditions in cell culture incubators (Heraeus Kendro Laboratory Products GmbH, Langenselbold, Germany) at 37°C and 5% CO_2-atmosphere. For subcultivation, culture medium was removed from the Petri dish and washed twice with phosphate buffered saline (PBS-Dulbecco, Biochrom AG, Berlin, Germany). The cell monolayer was removed by trypsinization (Trypsin EDTA Solution, Biochrom AG, Berlin, Germany). A list of all reagents

and culture media used can be found in the appendix. As time points for the analysis day 1, day 4 and day 8 after seeding were chosen. At each time point the cells were fixed and three WST-measurements were performed. Subsequently the cells were prepared for SEM-Imaging. The WST measurements were carried out 30 and 90 minutes after addition of the WST- measuring solution. A detailed description of the procedure is given in the appendix.

4.10.2 Preparation for SEM-Imaging

The cells were washed twice with phosphate buffered solution and fixed for 2 days in glutaraldehyde (VWR, Darmstadt, Germany) at 4°C. The samples were then dehydrated using an increasing alcohol line from 10% to 100%. Subsequently the samples were critical point dried by substituting the alcohol stepwise by CO_2 (CPD-030, Bal-Tec AG, Balzer, Liechtenstein). Afterward the samples were sputtered with an approx. 10 nm gold layer using a sputter-coater (SCD 005, BAL-TEC AG, Balzers, Liechtenstein) under high vacuum. SEM analysis was performed with 10 kV acceleration voltage at magnifications between 30X and 500X.

4.11 Mechanical Tests

During the implantation a coronary stent is subjected to high stresses by the dilatation process. The results are plastic deformations at predefined spots so that the stent remains in the dilatated shape. After the implantation process a static load acts upon the stent, imposed by the dilatated arteria. The magnitude of this load depends on the consistence of the stenosis. Superimposed on the static load is a cyclic load which is caused by the oscillation of the blood pressure. This pressure oscillation has a frequency of approx. 1 Hz, according to the heart beat, and a magnitude of approx. 40 mmHg (s. Fig. 4.14). The pressure change acts as a cyclic load relieving during the heart beat. It is assumed that the worse case in terms of fatigue stress occurs at very soft stenosises. In this case the static load will be smaller, however the pressure oscillation is absorbed least by the artery, increasing the cylclic loads on the stent.
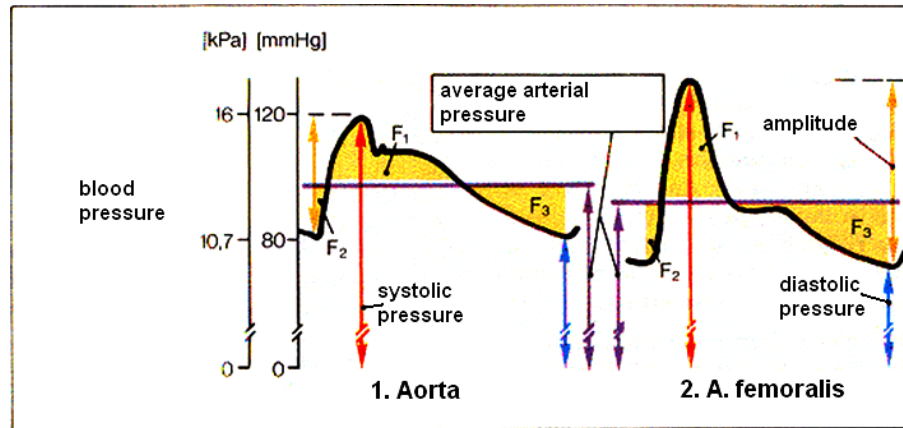
Figure 4.14: *Blood pressure diagramm, modified from [130]. The difference between diastolic and systolic pressure is 40 mmHg.*

The main intention of the fatigue tests was to evaluate the effect of different structures on the fatigue behavior and to give a comparison of the different surface modifications amongst each other at conditions approximating in vivo conditions rather than to make a prediction if the stents would endure a use within the body. The experiments were performed on etched conventional stents that were not especially designed for an etching procedure. For a commercial use a special stent design would be necessary with larger strut thickness in order to compensate the material loss through the etching process.

For the fatigue tests a pressure chamber was developed with which 8 stents can be tested simultaneously. With the assembly described in this chapter it is possible to simulate pressure oscillations at a frequency of up to 70 Hz. The pressure chamber consists of a stainless steel housing filled with Ringer´s solution, which is closed with a membrane on the lower side. On the lower side the membrane is connected with a piezo battery (AgPd stack, 5.2 * 5.2 mm, AN01/8505b, EPCOS AG, Munich, Germany) which height can be adjusted by a differential thread. The tubes with the stents are mounted on top of the chamber in a way that the pressure within the chamber is transmitted to the interiors of the tubes. It is important to assure that no gas bubbles get into the assembly during the filling process. By moving the membrane with the piezo a pressure change can be imposed on the chamber. For the fatigue experiments the piezo is actuated by an amplifier for lower voltage piezo actuators (AVU 200/5P, DASS mbH, Saarbrücken, Germany) with the signal being supplied by a sinus generator (FG 200, H-Tronic GmbH,Hirschau, Germany). The pressure within the chamber is controlled by a pressure transmitter (PR-23 S,

Keller mbH, Jestetten, Germany). That way, with the help of an oscillator, it is possible to directly visualize the pressure oscillation. This method was used for the evaluation of the actuation parameters for the piezo in order to get the required pressure amplitude. The piezo was actuated in a way that an amplitude of 30 mbar was generated at a basis pressure of 40 mbar. For the basis pressure a slightly higher value than the amplitude was chosen in order to prevent negative pressure. For the testing procedure the stents were dilated within a silicone tube sections of 3 cm length, 3 mm inner diameter and 4 mm outer diameter at a pressure of 15 bar. It has to be mentioned that minor pressure loss through the tubes cannot be avoided, so that the basis pressure had to be adjusted on a daily basis during the test using the differential thread. Afterward the pressure chamber and the sections were filled with Ringer´s solution and fixed on the provided spouts. After the testing time of 52 days the sections were removed from the stents and the stents were investigated under SEM. A technical drawing of the assembly can be found in the appendix.
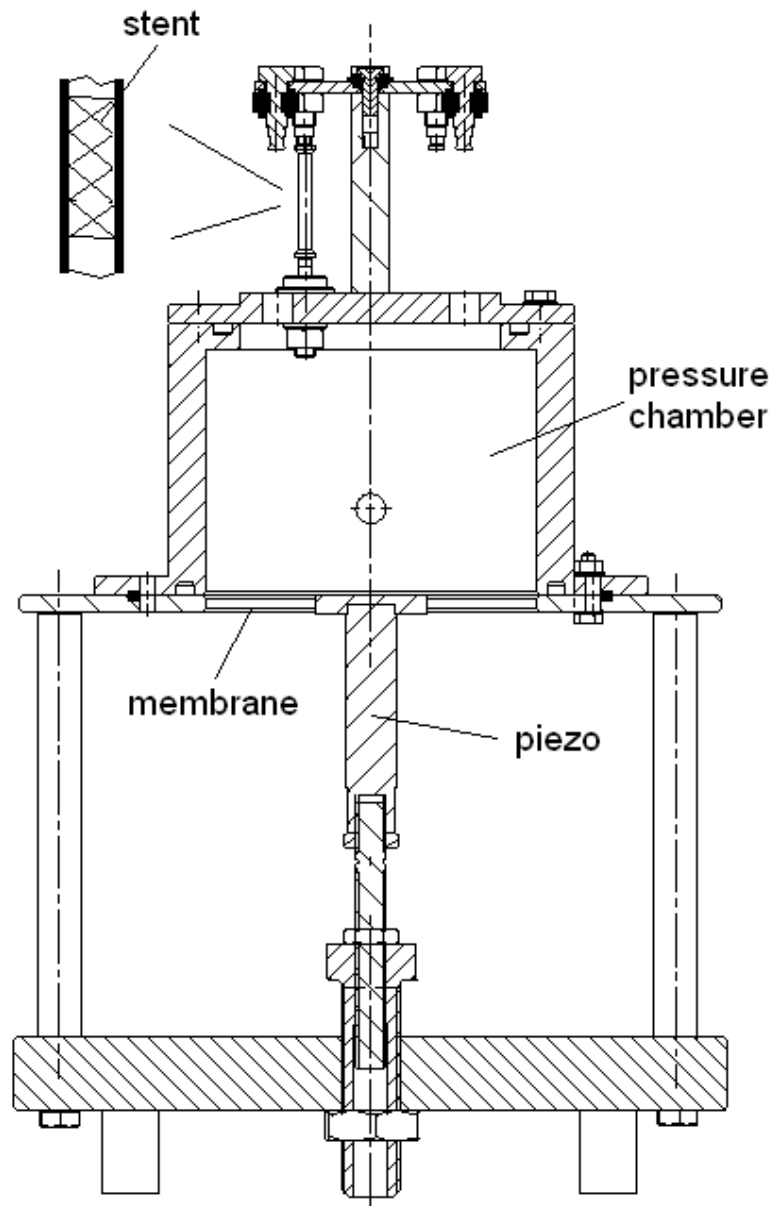
Figure 4.15: *Drawing of stent fatigue tester. The stents are implanted into polymer tubes which are mounted on top of the chamber. Tubes and pressure chamber are interconnected and filled with Ringer´s solution.*

5 Microstructuring with Hydrochloric Acid

5.1 Results

Electrochemical etchings on basis of hydrochloric acid can result in the formation of various surface topographies. Depending on parameters like viscosity of the etching solution, applied current, flow velocity of the etching solution, surface contaminations etc. the result can be anything from an electropolished surface or a local attack like pitting corrosion to an evenly distributed microstructuring. The latter case is subject to the examination of this chapter. This type of etching offers an interesting possibility to generate microstructured surfaces that could have good resistance against wear when coated with soft materials. It could be shown that, under certain circumstances, it is possible to generate an evenly rough faceted surface with HCl. However it was found that these type of etchings are very difficult to reproduce.

Table 5.1 shows the results of etchings on a pin. The samples (four for each current) were etched at currents of 50 mA (0.48 mA/mm^2) to 400 mA (3.86 mA/mm^2) in stirred etching solution. The etching times were 20 min, 10 min, 5 min and 150 sec (for 50 mA, 100 mA, 200 mA and 400 mA). The numbers given in the table indicate the approximated average distance between two facets in μm, calculated by counting the intersections between a straight line of 100 μm length and the facets. A slash indicates that no microstructure was present. When a microstructure was present that, however, did not have countable facets or the value was below 2 μm, it was indicated with n.c.

When etching on a pin, the faceted surfaces were found only in few of the specimens. Most specimens had a smooth surface without any microstructure. An explanation of this phenomena might be found in the generation of a dark black layer consisting possibly of iron oxide between stent and pin, which can sometimes be found after etching. The layers might prevent a sufficient current flow through the stent

Sample no.	50 mA	100 mA	200 mA	400 mA
1	/	14	11	/
2	/	/	8	/
3	n.c.	n.c.	/	/
4	/	/	/	/

Table 5.1: *Average distance in μm between facets for different etching times with pin, measured on 4 stents each.*

in many cases. Nevertheless, interestingly the formation of this layer seems to be connected with the formation process of the faceted structures. In all cases where a microstructure was present the stent surface was covered with the black layer. So a condition for the microstructuring might be the presence of the layer while a sufficient current flow is still sustained. After etching the layer has to be carefully removed when examining the samples. Especially under the SEM it can be easily mistaken with the actual metal surface. Fig. 5.1 shows an SEM image of a stent where the layer was not removed. Fig 5.2 shows one of the two microstructured samples of the 200 mA row (top) and one of the samples where the microstructures could not be counted (bottom).

Table 5.2 shows the results of the etchings without a pin. The samples were etched at currents of 40 mA (0.39 mA/mm^2) to 240 mA (2.31 mA/mm^2) in stirred etching solution. The etching times were 12 min, 6 min, 3 min and 2 min.

Sample no.	40 mA, 12 min	80 mA, 6 min	160 mA, 3 min	240 mA, 2 min
1	3	n.c.	11	/
2	/	3	7	n.c.
3	n.c.	n.c.	4	2
4	/	4	5	/

Table 5.2: *Average distance between facets for different etching times without pin, measured on 4 stents each.*
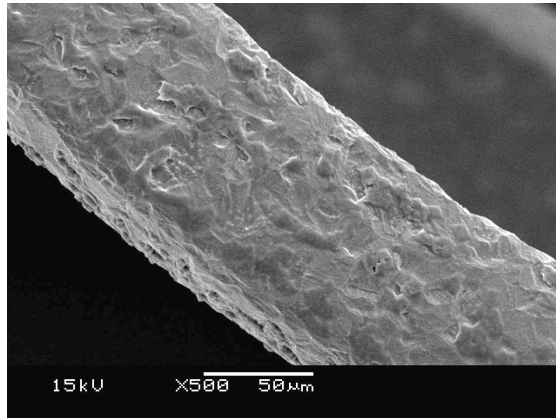
Figure 5.1: *Hydrochloric acid etched stent covered with black oxide layer. The layer can be easily mistaken for microstructures.*
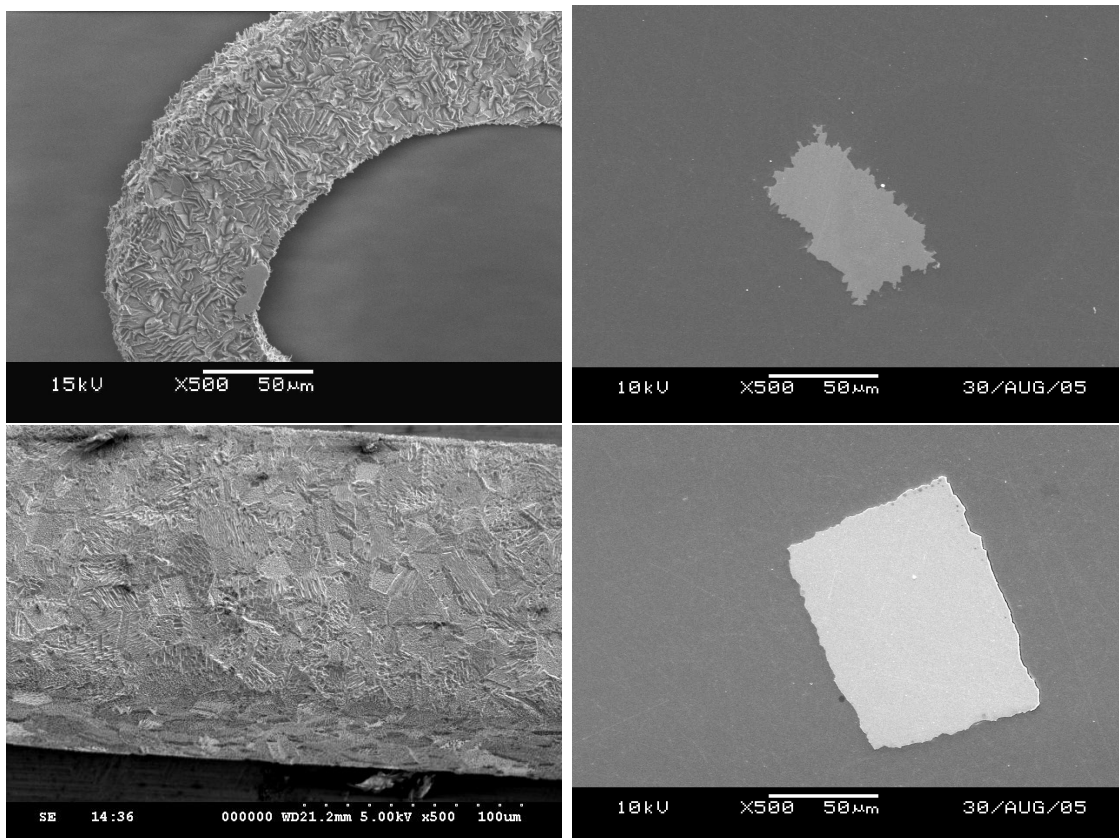

Figure 5.2: *Hydrochloric acid etching with pin, 200 mA, 5 min, two different stents, surfaces and sections. The lower images show a stent where the facetts could not be counted.*

Without the use of a pin, the faceted surfaces were better reproducible. At a current of 160 mA (1.54 mA/mm²) the faceted surface could be generated on all samples. The created microstructures, however, differ to a considerable degree in size and distribution of the faceted structures as shown in fig. 5.4. Roughness values for tubes etched with 1.54 mA/mm² were between Ra = (0.22 μm - 0.71 μm) and (Rz = 0.87 μm - 3.29 μm).
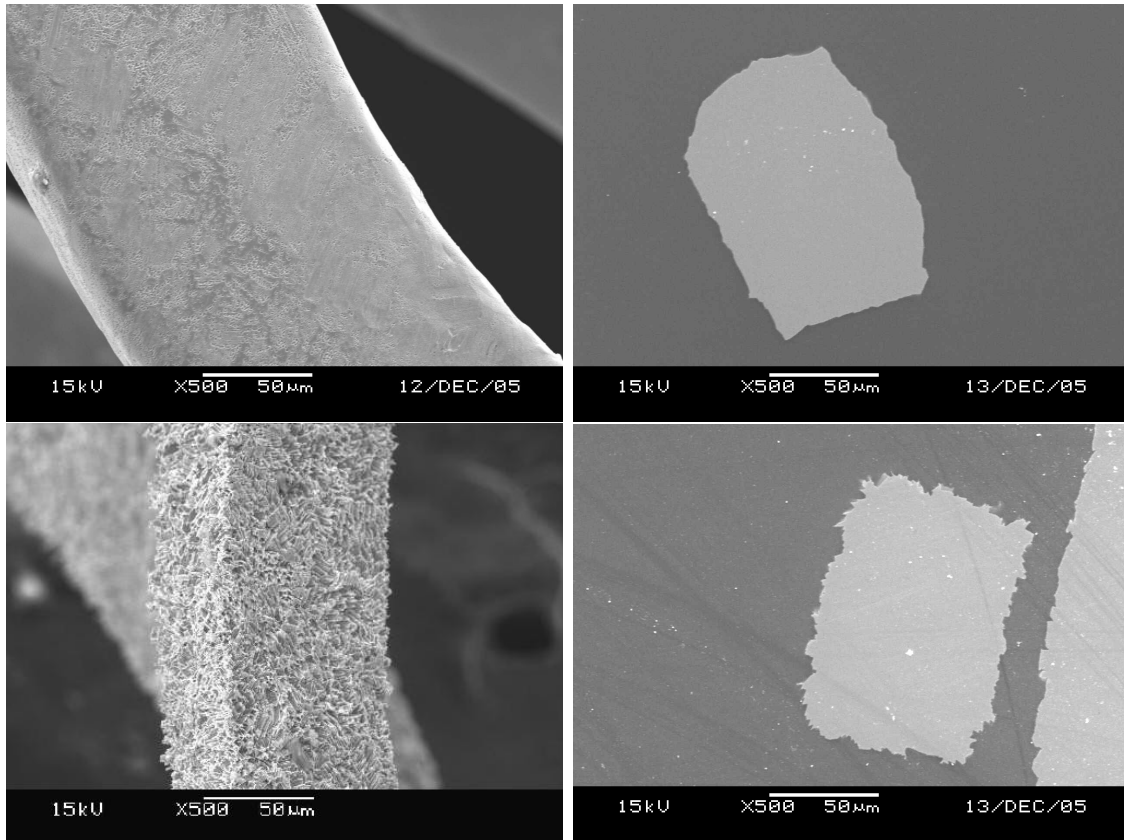

Figure 5.3: *Hydrochloric acid etching 80 mA, 6 min, without pin, two different stents. The lower stent shows generation of microstructures, the upper does not.*
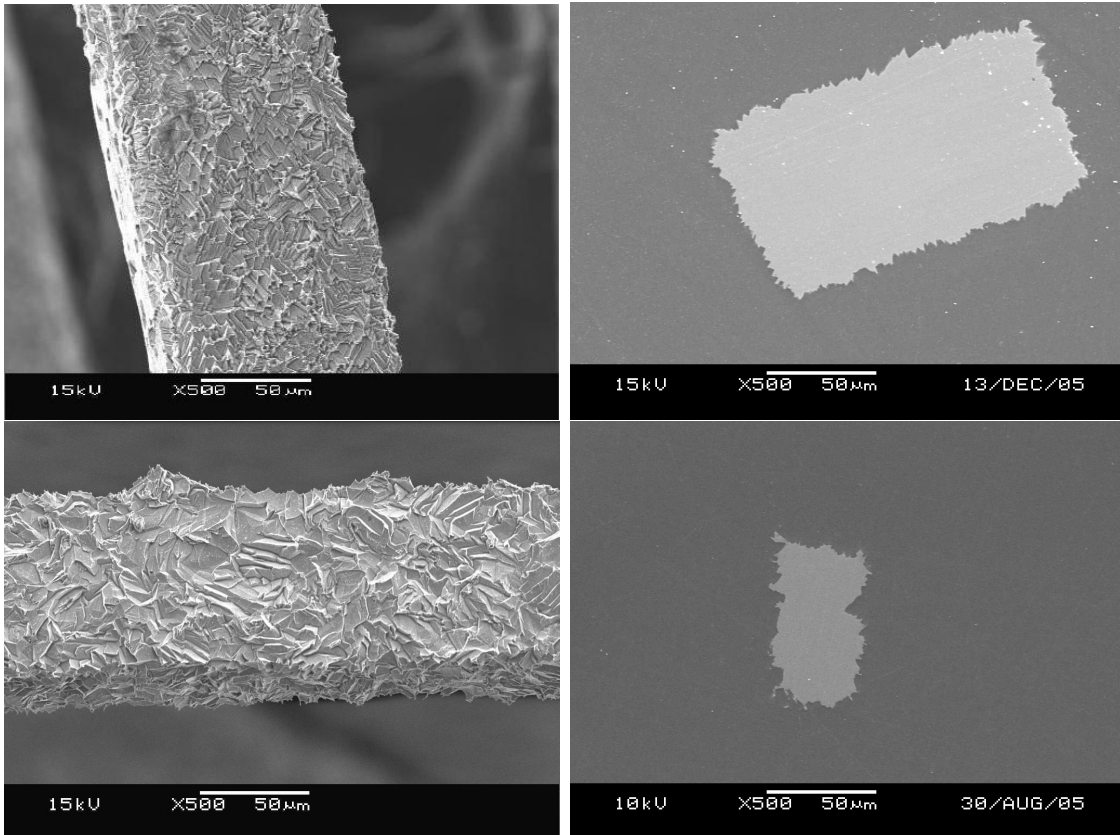
Figure 5.4: *Hydrochloric acid etching, 160 mA without pin, 3 min, two different stents. Note the differences in the generated microstructures.*

5.2 Analysis of the Formation Process

By interrupting the etching process preliminarily a detailed picture can be drawn of the formation of the structures. On picture 5.5 the initial phase of this etching method can be seen. In the highest magnification the creation of evenly distributed small pits of different geometries (small black arrows) can be observed. As described in [131], triangular pits suggest that the attacked surface is orientated in the (111) direction whereas squared pits indicate a (100) orientation and rectangular pits are created at (110) planes. Some of the pits have progressed to cavities of several μm size showing a platelet like surface inside (large white arrows). Several features distinguish this form of corrosion from normal pitting corrosion. Firstly as a result of high mechanical strain during the processing of the tubes a high dislocation density is present, enabling the formation of a high number of evenly distributed small pits. Secondly the effect of the stirrer prevents the formation of a consistent etch film on the surface. By this the etching process becomes activation controlled instead of mass transfer controlled, so that the electro-polishing effect is suppressed. Furthermore presumably no protecting remnant of a passivity layer can be maintained over the growing pits as it is the case in pitting corrosion [132].

Interestingly, as mentioned before, the generation of the microstructures seem to be in connection with an insoluble black layer of iron oxide/ hydroxide. This layer might disturb both the formation of a consistent etch film and the conservation of the passivity layer. Because of these factors no growing hemispheres with smooth inner surfaces can develop. Instead a selective etch attack takes place, which, in the initial phase, creates small triangular or rectangular pits. Where the surface is etched further it shows platelet like appearance according to the orientation of the grains. While the high amount of pits prevents the inhomogeneous growth of single pits an evenly faceted surface is created. Since the formation of pits is largely unpredictable and depends on the presence of slight impurities this model could explain the bad reproductivity of the results [133].

Fig. 5.6 shows a U/I-Diagram of the 316L material in the etching solution. It has to be noted that the U/I curve is dependent on the scan rate which was approx. 0.1 V/ sec. The higher the scan rate, the lower is the resulting current at high voltages, probably due to protection effects by the growing etch layer. This fact also has to be considered when evaluating applicable etching parameters. The formation of the structures seems to be limited to certain current densities within the lower part

of the graph. At higher currents electropolished surfaces occur. At lower current densities than 1.4 mA/mm$_2$ the microstructures occur only occasionally.
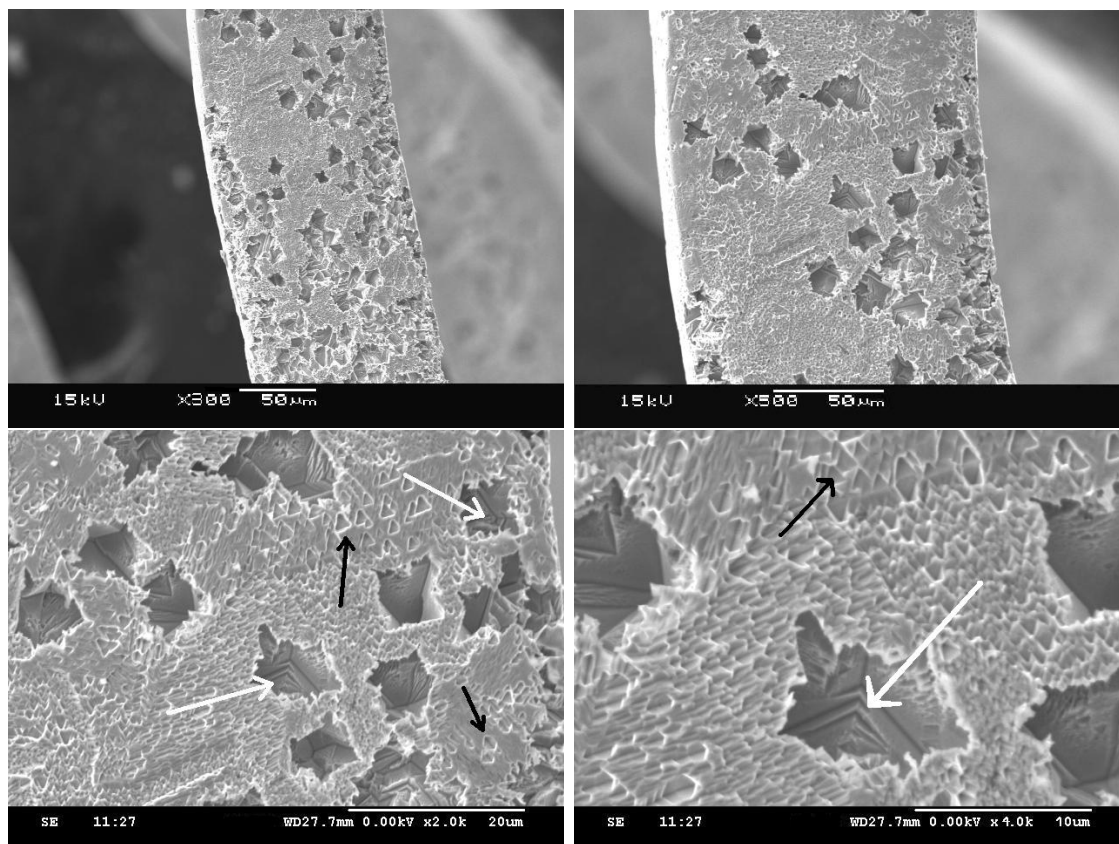

Figure 5.5: *Initial Stage of hydrochloric acid etching. The black arrows mark small pits, indicating the beginning of the formation of the microstructures, the white arrows mark larger cavities, generated through progressed pitting.*
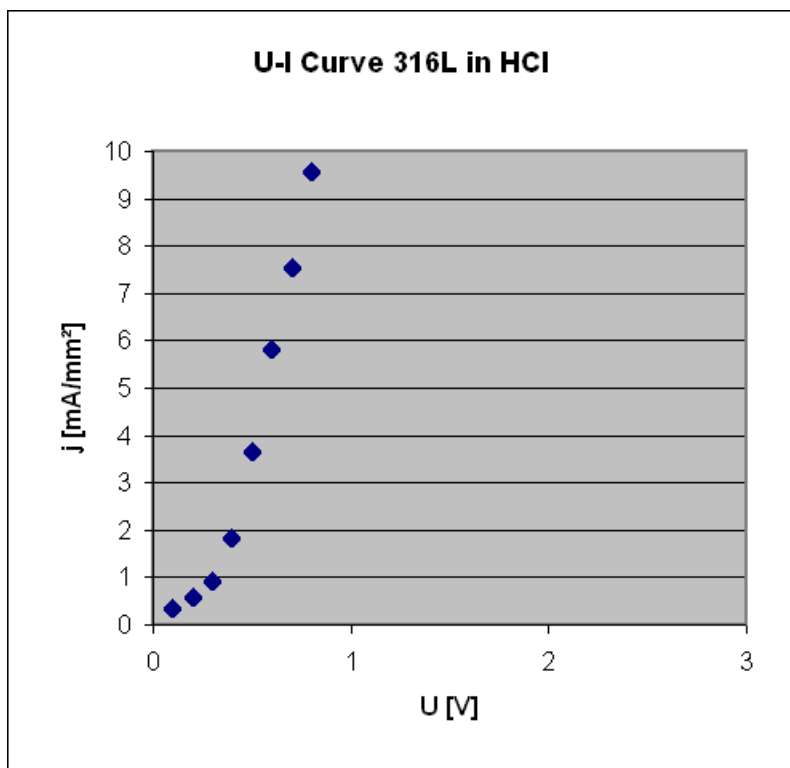
Figure 5.6: *U/I-Diagramm of 316L stent material in hydrochloric acid.*

6 Microstructuring with Nitric Acid

6.1 Results

Electrochemical etching with HNO_3 within the range of the examined etching parameters leads to a highly selective attack on grain boundaries. The generated surface roughnesses (n= 5, measured on etched tubes) were between Rz = 1,96 μm and Rz = 8,87 μm depending on the etch time. However these roughness values can only give some vague indications, about possible adhesion properties for example. They cannot be used for a characterization of the surfaces, since high aspect ratios and crevices are not captured. Therefore cross sectional micrographs were used as the main source for the analysis. It has to be noted that even though the stents are etched on pins cavities are not only limited to the three sides of the stents exposed to the acid, but are also present at the inner side adjacent to the pin. This is due to a slight distortion of the stents by the crimping and dilatation procedure as described in the materials and methods section on p. 30. For the sectional micrographs it is important to consider only the relevant outer sides, therefore on all images the inner side is separated with a black line.

Fig. 6.1 shows the etching structures for different times at a current of 200 mA (1.31 mA/mm^2). The 2 min etching shows a slight grooving of the grain boundaries. Sections show the formation of thin crevices of 2 to 4 μm depth along the grain boundaries. At 4 min etching time the grain boundaries are already considerably broadened. Sections show the formation of cavities with narrow V-shaped appearance. After a 6 min etching a very rough, granulated surface is created through detached grains. An etching process of this strength is to be regarded as unsuitable as a surface modification for implants because of the risk of detached particles.
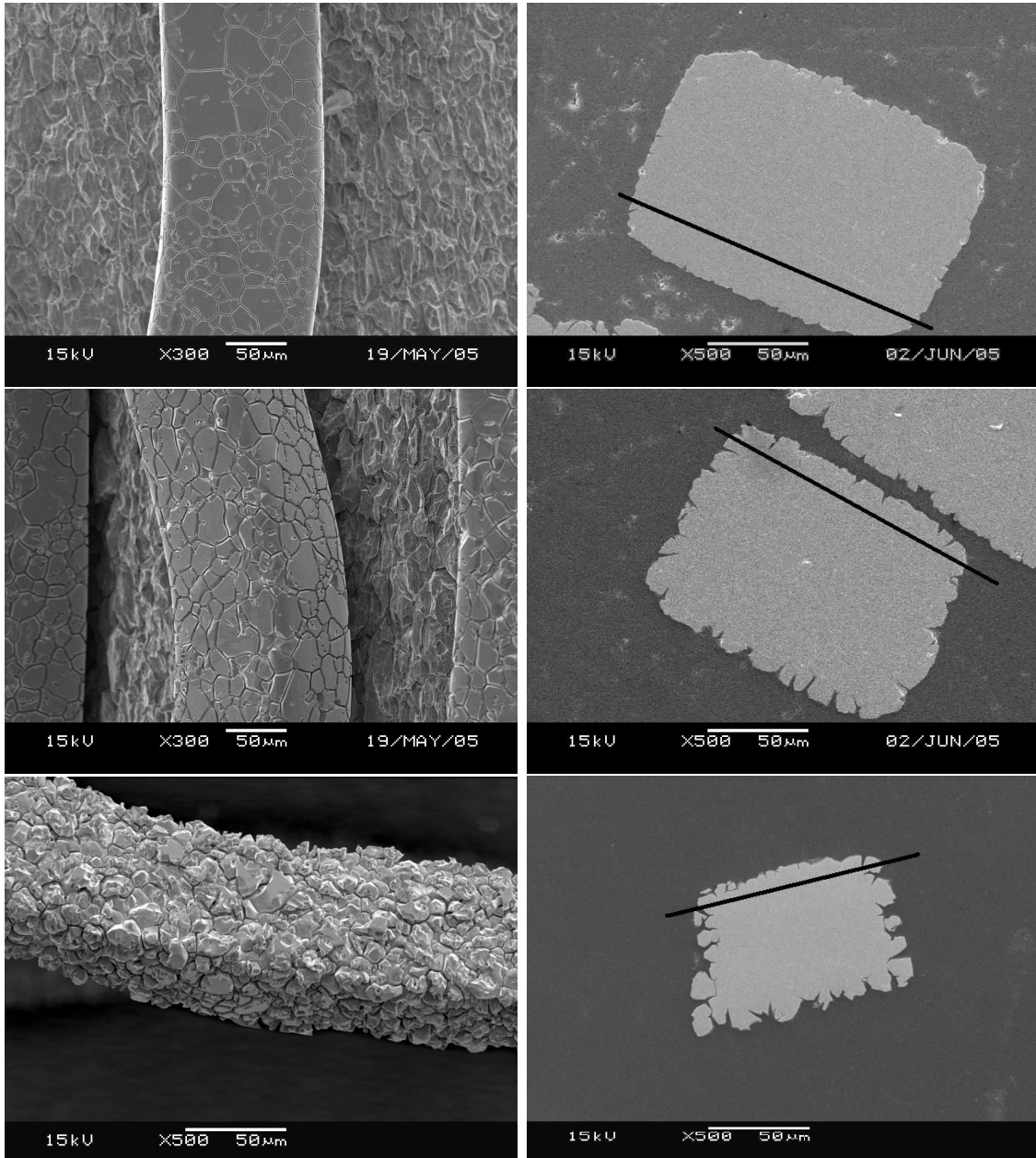
Figure 6.1: *Slight grain boundary etching, 200 mA, 2 min (top), 4 min (middle) and 6 min (bottom). The 6 min etching is to be regarded unsuitable for a use for implants because of the risk of detached particles.*

6.2 Analysis of the Formation Process

Especially for the stronger etchings increasingly spots on the grains are visible, where the surface has been attacked locally without the presence of grain boundaries. In some cases supposedly some surface heterogeneities were present here, leading to a kind of pitting corrosion similar as in the case of chloride etching. On the other hand it also appeared as if in some rare cases single grain boundaries or parts of grain boundaries were not attacked. For more detailed investigation of these phenomenas cross sectional micrographs of different grain boundary etched stent and tube samples were in turn metallographically grain boundary etched (for details s. appendix) to visualize the paths on which the cavities propagate (fig. 6.2). The right image shows an example for a cavity without the presence of a grain boundary. With this image it can not be told if the cavity was caused by a contamination or by intrinsic structures. Therefore a second metallographic etching step was performed with oxalic acid. With this two step method the grain boundaries as well as the interior grain structures are made visible. Fig. 6.3 reveals that the cavity in this case followed a dislocation or a twin boundary. Interestingly, however, most of the twins and dislocations where not affected by the etching. These results indicate that the etch attack reacts quite sensitively toward different partly unknown parameters.
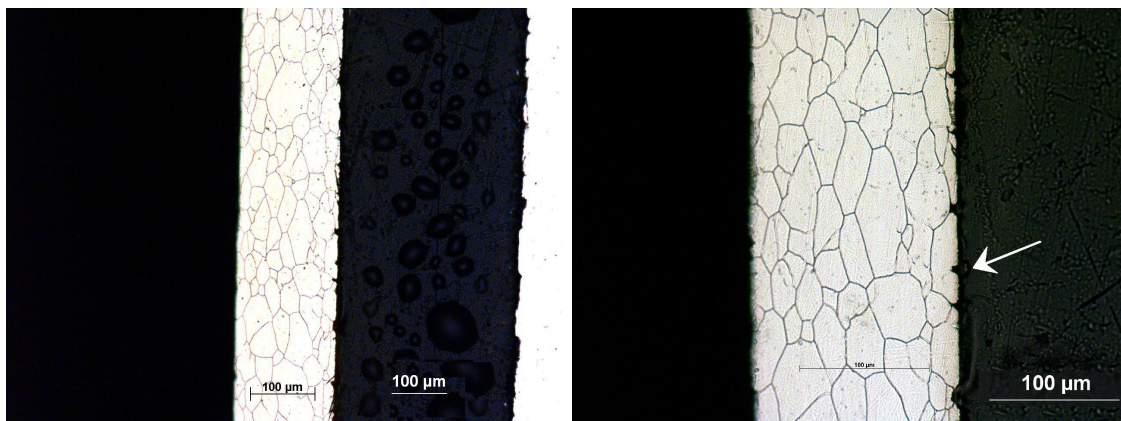

Figure 6.2: *Grain structure of etched tubes, survey (left) and enlarged picture (right). The white arrow on the right image marks an etch attack were no grain boundary is present.*

In order to get detailed information about the selectivity of the etching process in dependence of the applied current, which is important when finding best suited etching parameters, polished sections of stents were created, etched with different current densities j from 0.2 to 6.9 mA/mm^2. The etching times were between 16 min (for 0.2 mA/mm^2) and 40 sec (for 6.9 mA/mm^2). That way it is provided that the
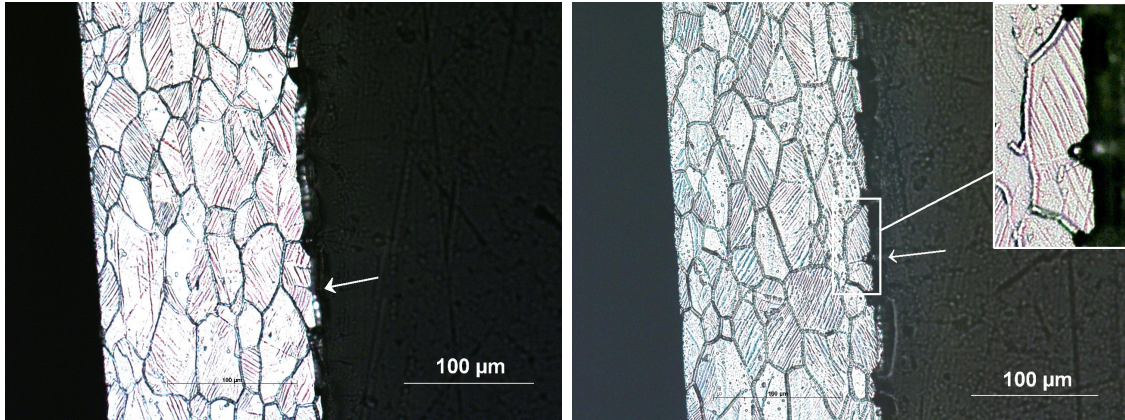
Figure 6.3: *Crystallographic structure of etched tubes. At the sites where etch attack occurred without the presence of grain boundaries, dislocations or twin boundaries, respectively, become visible (white arrows). On the left image a twin boundary can be recognized, the cutout on the right image reveals a dislocation (visible as a faint light line running from the cavity to the grain boundary).*
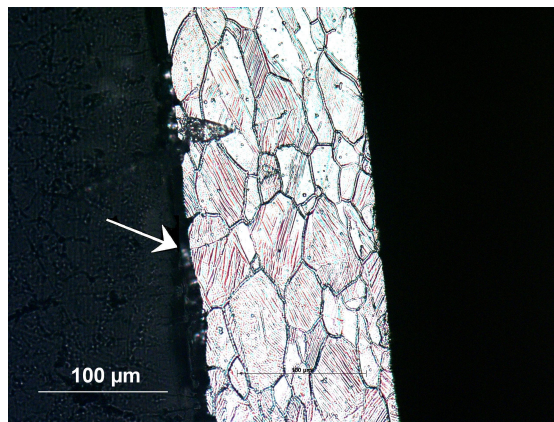

Figure 6.4: *Crystallographic structure of an etched tube. The white arrows mark a twin boundary (left image) which was not affected by the etching.*

etching strengths are in approximately the same range for all current densities. From each stent the lengths of at least 15 crevices as well as the widths of the crevices at the surface were measured on different struts. The ratio of half the width to the length of the crevices is used as a value to compare the selectivity of grain boundary etching processes. This selectivity factor is illustrated in detail on p. 69. When a high selectivity is present deep, narrow crevices develop. When a low selectivity is present the bulk material removal is much higher, resulting in short, wide crevices 6.5. Using this index for the selectivity it is important to exclude outliers, which may result from twin grain boundaries or the like.

It could be shown that the selectivity declines gradually from low currents to high currents without having a distinct peak at any of the analyzed current densities (fig. 6.6). This observation is in contrast to conventional grain boundary etching models as described by Bell in 1976 where the U/I curve of grain boundaries and matrix is assumed as illustrated in fig. 6.7 [134]. In this diagram the grain boundary curve is assumed to have an offset toward both higher currents and lower potentials. The offset toward lower potentials would result in a large difference between local currents and thus a high selectivity at the area where a high slope is present. This area is marked as the grain boundary etching range in the diagram. An offset only toward higher currents, however, would result in gradual differences in selectivity without a distinct peak (fig. 6.8). An explanation for this offset is not given in [134], however it can be assumed that a current shift is rather due to the higher degree of disorder at the grain boundaries while a potential shift should originate from deviation in the material composition at the grain boundaries. According to this the selectivity varies with the slope of the curve only if the etching process is dominated by a composition deviation. In this case the highest selectivity would be achieved in the range of voltage with the highest slope. A constant current shift as it would be caused by a higher degree of disorder at the grain boundaries, would result in a gradually declining selectivity over the whole range. So the measured results indicate that chemical differences between grain boundaries and matrix may play a less important role in the etching process than hitherto assumed. In order to obtain additional informations about this phenomenon chemical analysis was performed on grain boundary etched specimens.
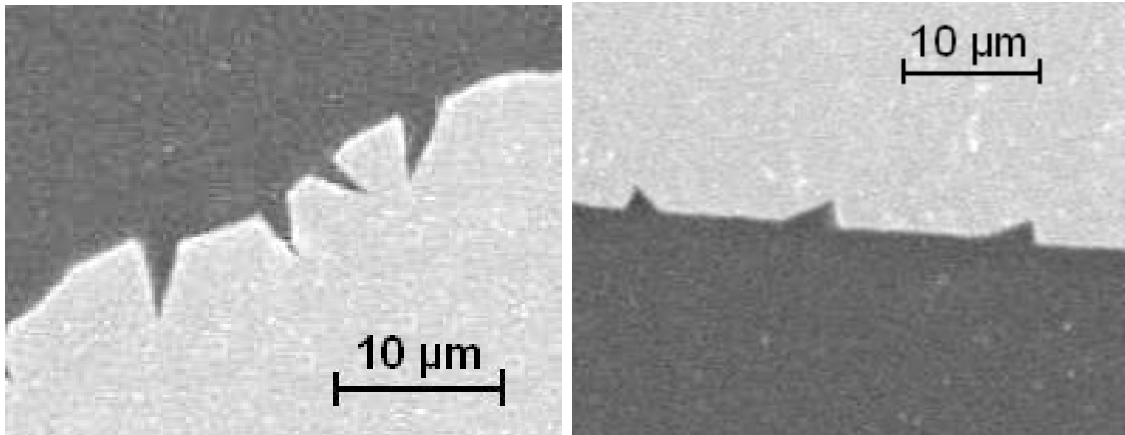
Figure 6.5: *Different crevice structures, on the left image a high selectivity (narrow crevices) can be seen, the right image is an example for a low selectivity (broad crevices).*

Figure 6.6: *Selectivity of the etchings for different current densities.*

Figure 6.7: *U/I-Diagramm of 316L in nitric acid modified from a diagramm in [134].*

Figure 6.8: *U/I-Diagramm of 316L in nitric acid based on a diagramm in [134](left) and as measured for the analyzed stents.*
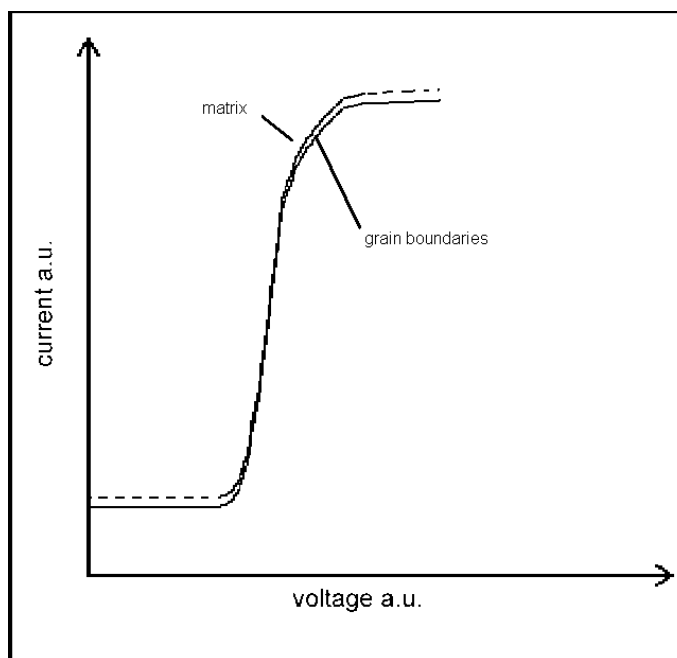
Figure 6.9: *U/I-Diagramm with offset only towards higher currents.*
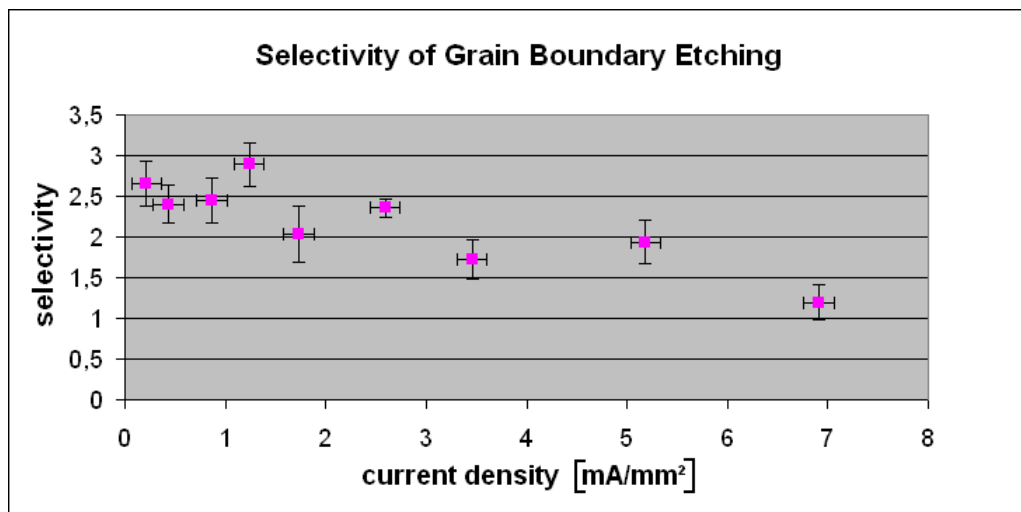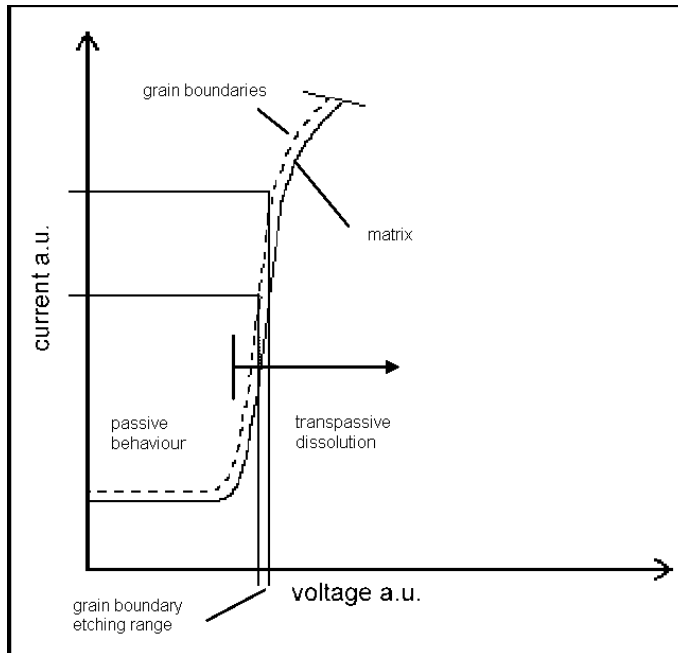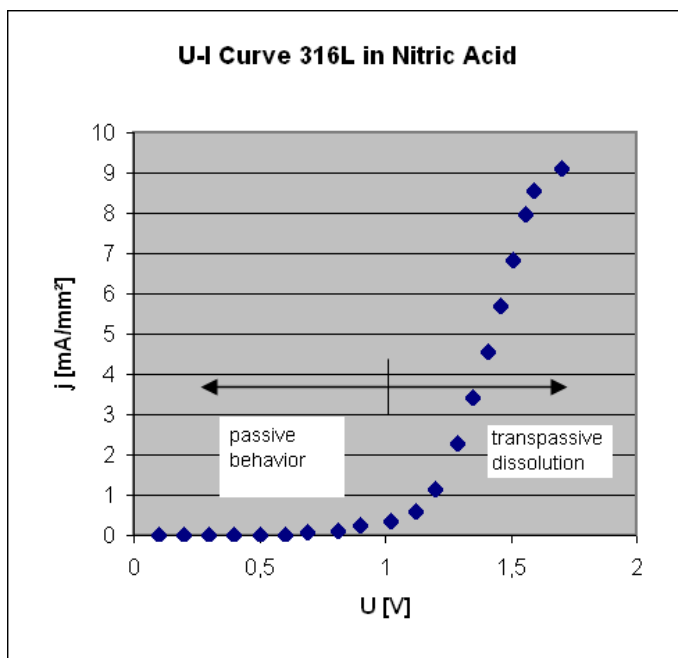
6.3 Chemical Analysis

EDS analysis was carried out in order to investigate the composition at the grain boundary area and the grain area of the stents. The analysis gave no indication for any depletion of passivating elements in the area of the grain boundaries. Even a slight enrichment of chromium could be found at the grain boundaries. The enrichment, however, could be caused by chromium rich precipitates at the grain boundaries, which do not lead to a higher resistance.

It has to be noticed that the main composition variations at the grain boundaries are found within a range of less than 100 nm while the spot size of the EDS is 1 to 2 μm in diameter. Therefore it would be only possible to detect major deviations in composition within such a limited zone. For a detailed analysis of the grain boundaries a transmission electron microscope EDS would be necessary which was not included in this work.

6.4 Mathematical Description of the Etching Process

In the following section a model of the etching process is established with the aim of calculating the crevice depth, the crevice width as well as the material removal from the etching parameters. Fig. 6.10 shows a schematic image of an etched surface with one grain boundary which is the basis for the following contemplations.
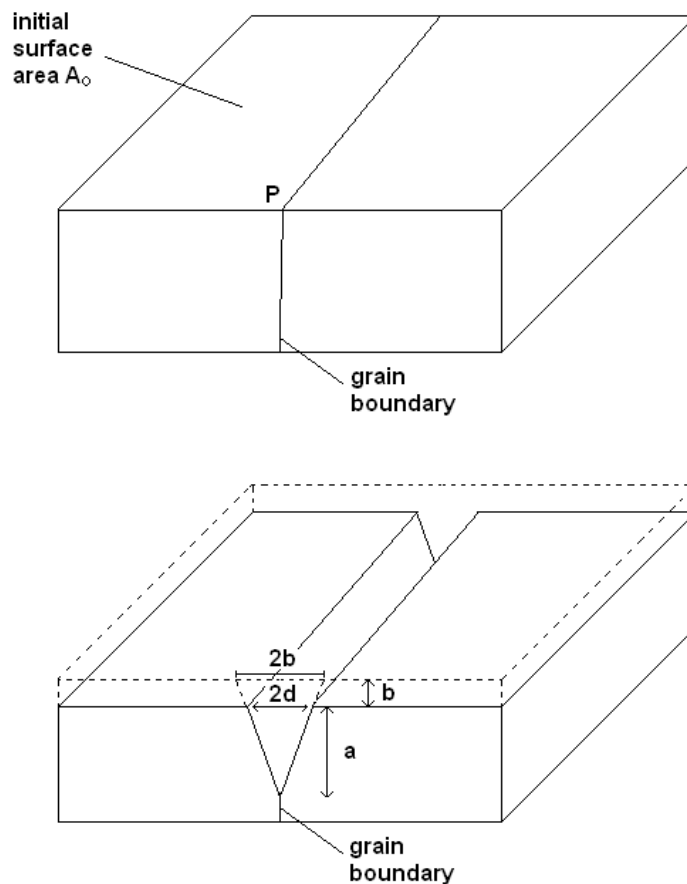

Figure 6.10: *Schematic illustration of grain boundary etching process, top image t = 0, bottom image t > 0.*

The mass loss rate dm/dt occuring at an area A can be calculated from the current density j (comp. p. 18)

$$\frac{dm}{dt} = M \cdot \frac{\gamma}{z \cdot F} \cdot j \cdot A \qquad (6.1)$$

It is assumed that the efficiency factor is constant over time. The surface area is not constant, it increases during the etching process. However the product j · A can be regarded as constant when contemplating a fixed base area A_0 of the original surface as illustrated on the drawing, since the total current is hold constant during the etching process. Therefore the current j · A can be substituted by the constant j_0 · A_0. Now the mass loss rate can be integrated into an amount of dissolved material Δm per etching interval Δt.

Since geometrical aspects are contemplated, the mass has to be transformed into a volume:

$$\Delta V = \frac{\Delta m}{\rho_{316L}} = \frac{M \cdot \gamma \cdot j_0 \cdot \Delta t \cdot A_0}{z \cdot F \cdot \rho_{316L}} \tag{6.2}$$

With the volume of the dissolved material known, the spacial distribution of the dissolved material has to be modeled. It is assumed that the grain boundary is very thin so that a point P can be defined which marks an intersection of the grain boundary and the surface (Fig. 6.10, top). During the etching this point travels downwards, at a constant factor faster than the remaining surface. This factor, which is the ration between the etching rate at the grain boundaries and the bulk material, indicates the selectivity of the etching process. Beside a material removal in vertical direction, a material removal from point P toward both horizontal directions occurs. The latter determines the width of the crevices. When it is assumed that the bulk material removal rate is independent of the direction, the ratio between the material thickness loss b at the surface and the crevice width 2 · d can be calculated (Fig. 6.10, bottom) applying the intercept theorems

$$\frac{2d}{a} = \frac{2b}{a+b} \quad => \quad d = \frac{a \cdot b}{a+b} \tag{6.3}$$

a being the depth of the crevice after the etching. a can be expressed in terms of d by applying a selectivity factor s_j, which describes the ratio of d/a at a current density j:

$$d = \frac{s_j \cdot d \cdot b}{s_j \cdot d + b} \tag{6.4}$$

Solving the equation for b yields

$$b = d \cdot \frac{s_j}{s_j - 1} \tag{6.5}$$

s_j must be > 1, since a value below 1 would mean that the grain boundaries are etched slower than the bulk material. Now a second equation can be set up which describes the volume ΔV in dependence of the crevice width d:

$$\Delta V = A_0 \cdot \frac{s_j}{(s_j - 1)} \cdot 0.5 \cdot d + \frac{l_k}{A_k} \cdot A_0 \cdot d^2 \cdot s_j \tag{6.6}$$

The first part of the equation is the volume loss at the surface, namely the contemplated area A_0 times b. The second part is an approximation of the volume fraction of the crevice. This part comprises the cross sectional area of the crevice $d^2 \cdot s_j$ (= d · a) as well as a factor l_k/A_k which indicates the total length of the exposed grain boundaries per surface area. An influence of the knot points where two grain boundaries touch is neglected. The factor l_k/A_k can be measured from microscope images of slightly etched stents. For the stent material it was determined to 77 mm/mm².

Equating both terms for ΔV and solving for d finally yields

$$d = -\frac{A_k}{l_k \cdot (s_j - 1)} \pm \sqrt{(\frac{A_k}{l_k \cdot (s_j - 1)})^2 + \frac{A_k \cdot M_{316L} \cdot \gamma \cdot j_0 \cdot \Delta t}{l_k \cdot s_j \cdot \rho_{316L} \cdot z \cdot F}} \tag{6.7}$$

The selectivity factor s_j can be taken from diagram 6.6. The charge number z can be assumed as 3 for j > 0.2 mA/mm² (comp. p. 25). The Faraday constant F is 9.6485 · 10⁷ mAs. The rate of current yield γ is 1 for the contemplated etching process, the current yield γ is assumed as 0.95 (comp. [135]). The average molar mass of 316L has to be calculated from the corresponding molar masses of the alloying elements (comp. [106])(M_{Fe} = 55.85 g/mol, M_{Cr}= 51.99 g/mol, M_{Ni} 58.7 g/mol, M_{Mo} = 95.94 g/mol):

$$M_{316L} = 0.632 M_{Fe} + 0.173 M_{Cr} + 0.147 M_{Ni} + 0.0275 M_{Mo} = 55.46 g/mol \tag{6.8}$$

The density of the material was determined to 7.73 g/cm³ = 7.73 · 10⁻³ g/mm³.

Calculating the crevice width for a current density of 1.3 mA/mm₂ with a selectivity of 2.9 and an etching time Δt = 180 sec yields a value of 3.3 μm for the crevice width and 4.7 μm for the crevice depth, respectively. These values are in accordance with measured values (6 μm ± 2 μm crevice depth).

When plotting the crevice width against time it becomes visible that the crevices growth approximates a root function, which is most pronounced for low selectivities.

For higher selectivities and smaller times the growth of the crevices is almost linear. This effect origins from the decreasing effective current density due to the increasing surface area. For large times t the decreasing effective current density can cause a change in selectivity, so that the formula cannot be applied for large etching times where the surface area $A_t >> A_0$.

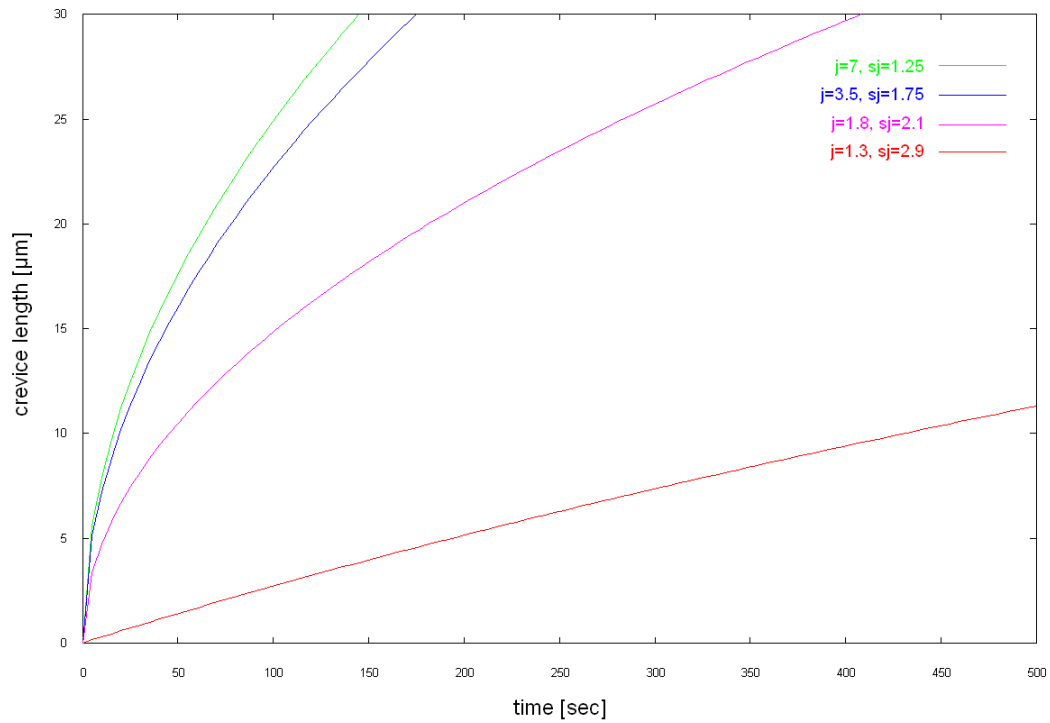**Figure 6.11:** *Crevice length plottet against time, according to formula 6.7 for different current densities (j=1.3 mA/mm^2 to j=7 mA/mm^2)) with the corresponding selectivities sj. For small times and for low selectivities the graph resembles a square root function, for larger times and for higher selectivities the graph approximates a linear function.*

7 Combination Etchings on Nitric Acid Basis

The basic idea of the combination etchings is to use microcrevices generated by nitric acid etchings in order to create a grid of evenly distributed depots. This is realized by a combination of the nitric acid etching with a second, isotropic etching step. The aim of the second step is to broaden the grain boundary furrows generated by the grain boundary etching so that larger, wider depots without sharp crevices are created. There are two types of etching solutions suitable for this purpose. One type are electropolishing solutions, analyzed on the example of phosphoric acid. With this method, smooth surfaces are created so that the risk of progressing crevices is minimized. The disadvantage of this method is the fact that the depot volume is to some extent decreased because the material removal on the surface is relatively high. So the volume that is gained by broadening of the depots is at least partly lost by a decreasing depth of the depots. The second possibility is to use an isotropic microstructuring like the HCl-etchings analyzed in chapter 5 as second step. With this method a fine microstructure is superimposed on the grain boundary etched structures in a way that the furrow volume is increased while crevices are hollowed out. This method is analyzed on etchings with HCl. Since the reproductivity of this etching method is limited as it was already found in chapter 5 an alternative acid was analyzed in terms of suitability. For that purpose oxalic acid was chosen. A schematic illustration of the three combination etchings is given in fig. 7.1. Electrochemical etching with oxalic acid creates similar, but finer microstructures than HCl with good reproductivity.

For each etching solution a suited first grain boundary etching step was evaluated as a basis for further examinations. These evaluations were carried out on stent raw material tubes as described on p. 31. Using this first step basic etching, different etching strengths for the second step were investigated. For a first evaluation SEM images of surfaces of the etched stents and cross sectional micrographs of embedded stents were contemplated. The cross sectional micrographs were then used for a
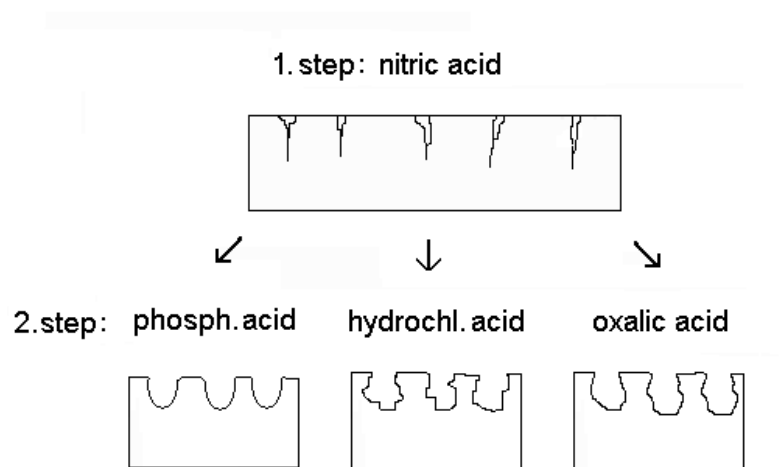
Figure 7.1: *Schematic illustration of different combination etchings. Phosphoric acid yields smooth rounded cavities, HCl yields faceted, rather nonuniform cavities, the effect of oxalic acid is in between.*

software analysis of the depot properties. The software creates a polygon around the stent section, determining the limits of the depots, so that features like the depot depth and the storage capacity can be determined.

Notes on the sectional images

When contemplating the cross sectional micrographs it is important to exclude the inner side of the stent from the analysis. This side will be within the blood stream after implantation, so a rough surface should be avoided. When etching virgin stents the inner side is almost completely protected from the etching process. However, as described on page 30, previously crimped stents were used for all experiments, unless otherwise noted. So in most cases an etching of the inner side could not be avoided, which can lead to confusion. Therefore on all images the inner (luminal) side is separated with a black line. The sections were performed on undilatated stents. It was shown by cross sectional micrographs in directions parallel to the stent axis (comp. p.102), that the size of the depots within the areas affected by the strain does not significantly increase during dilatation. A short approximation of the theoretical strain validates this observation (s. appendix).

7.1 Phosphoric Acid

Phosphoric Acid was used at currents between 200 mA (1.31 mA/mm^2) and 400 mA (2.62 mA/mm^2) in undiluted form. Phosphoric acid causes a leveling and smoothening of the surface. It has to be assured, that a sufficient cleaning of the stents is guarantied after etching, since etching with phosphoric acid produces insoluble reaction products.

7.1.1 Parameter Analysis on Stents

As a basis for the phosphoric acid combination etchings a first etching step with HNO$_3$ with 4 min at 200 mA (1.31 mA/mm^2) was used. This etching yields an average grain boundary furrow depth of about 7 to 8 μm (s. fig 7.2). Slighter grain boundary etchings were regarded as less suitable in preliminary experiments because the depots lost a large amount of their volume as a consequence of the leveling effect of the phosphoric acid. The phosphoric etching step was carried out on a pin at etching strengths between 200 mA * 120 sec and 400 mA * 180 sec.
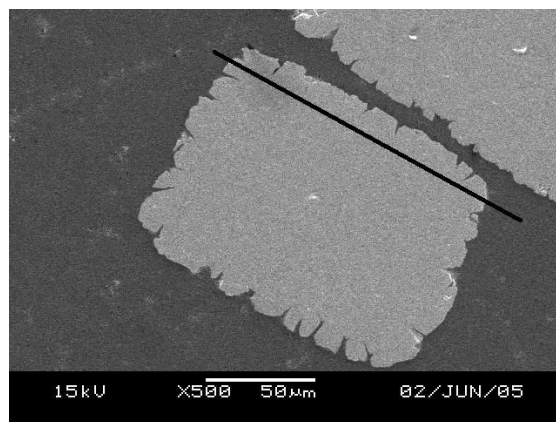
Figure 7.2: *Grain boundary etching, 200 mA, 4 min, section. This etching was used as the basis for all phosphoric acid combination etchings.*

A phosphoric acid etching at 200 mA for 90 sec yields a slight smoothening of the crevice tips as visible on the polished sections. The shape of most of the depots is not noticeably changed (fig. 7.3, top). Increasing the etching time to 180 sec produces widened and rounded, but still V-shaped depots. Etching at 400 mA for 120 sec produces more evenly hollowed out depots (fig. 7.4, top). The depth of the depots, however, is diminished. At this stage no crevices are present anymore at the

74

relevant sides of the stent. A 180 sec etching at 400 mA finally levels all depots, so
that the storage effect seems to be considerably diminished.
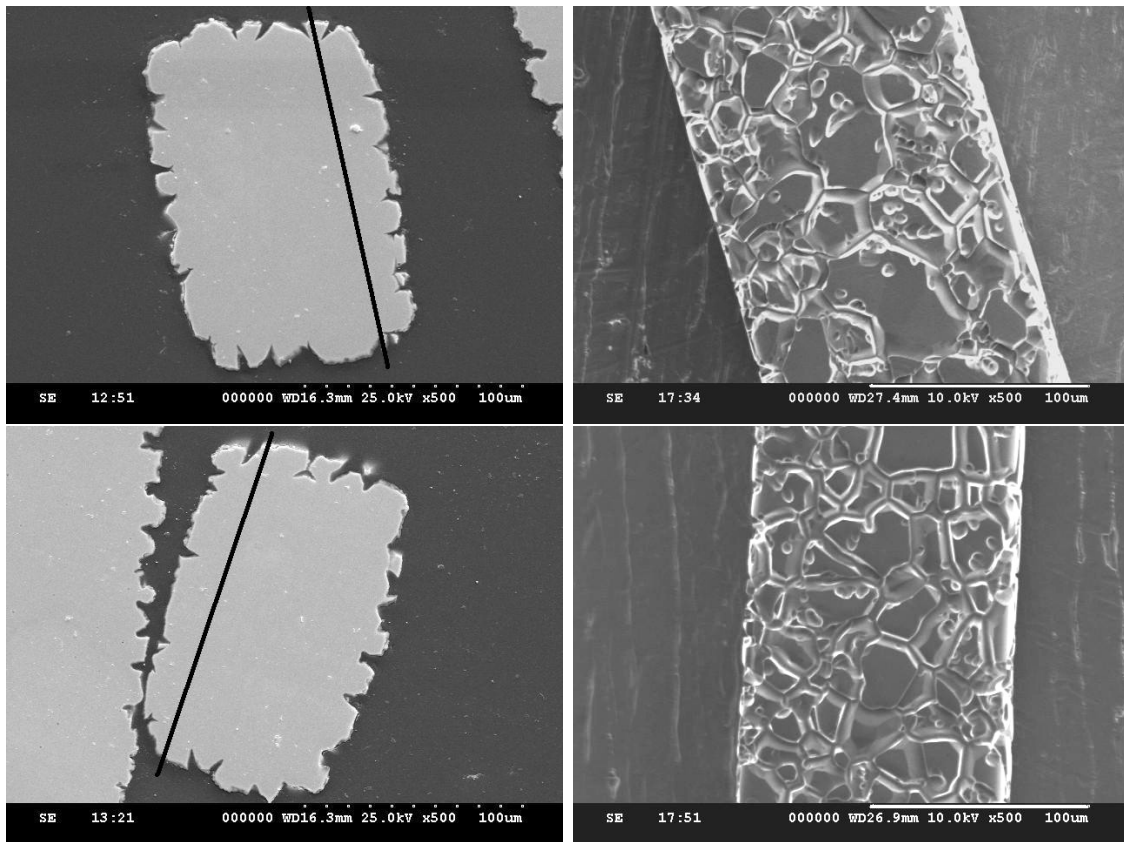
Figure 7.3: *Phosphoric acid combination etching, 200 mA, 90 sec (top), 200mA, 180 sec
(bottom).*

At most of the illustrated pictures the inner side of the stent is also affected by
the etching. This effect is due to bad protection by the pin during the first etching
step which is a consequence of using electropolished stents (88). This is a rather
undesired side effect which can cause damages on the balloon catheter. The crevices,
however, can be leveled if the second etching step is carried out without a pin. A
picture of an intermediate phosphoric acid combination etching without a pin is
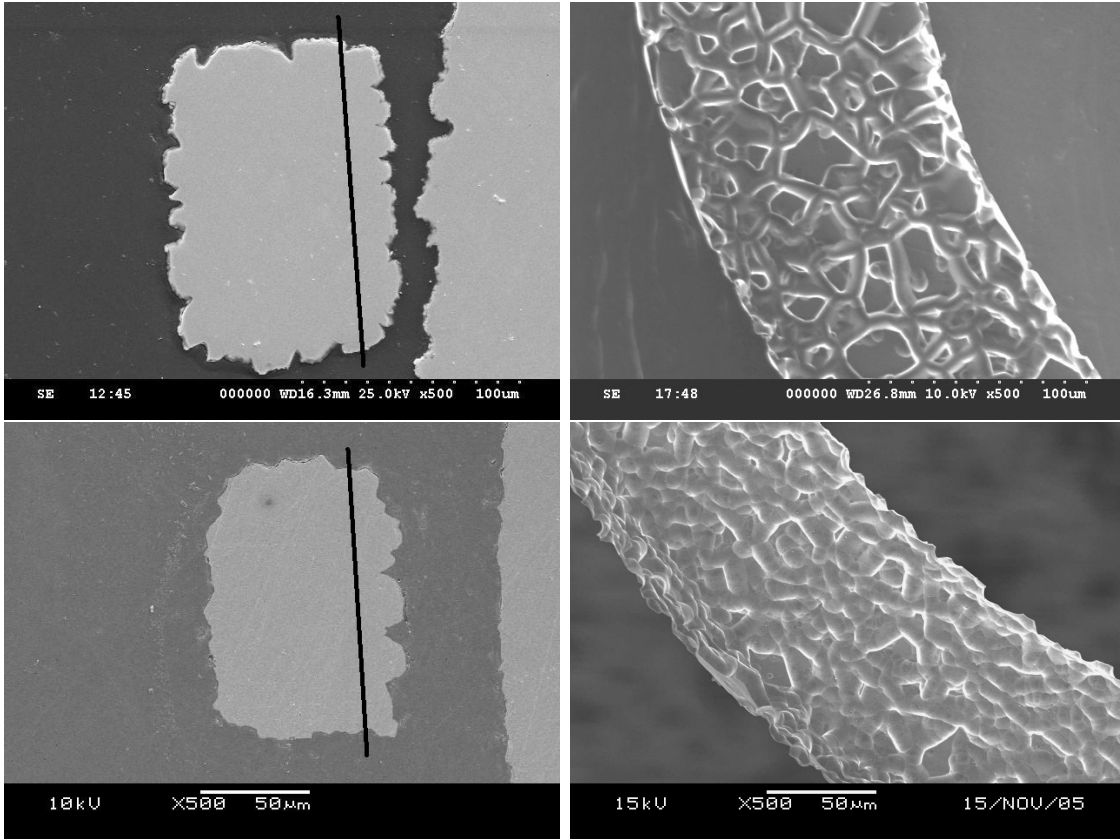shown in fig 7.5.

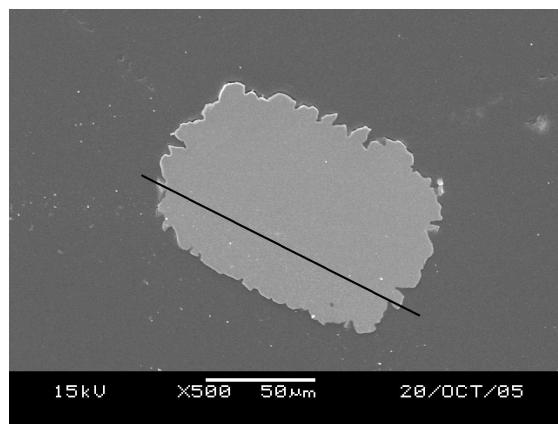**Figure 7.4:** *Phosphoric acid combination etching, 400 mA, 120 sec (top), 400 mA, 180 sec (bottom).*

Figure 7.5: *phosphoric acid etching, 200 mA, 180 sec, second step etched without pin.*

7.1.2 Software Analysis

Fig 7.6 shows an example for a slight phosphoric acid etched stent after software analysis. The begin and the end of each depot are marked with green crosses, the center points are marked with light blue crosses. Red crosses mark the polygon edge points. In fig. 7.7 the average depot area divided by the length of the three side polygon line (storage capacity) as well as the average effective depot depth are illustrated for all etchings. A maximum of the average storage capacity and the depot effect can be found within the range between 200 mA * 120 s and 200 mA * 180 s. Contrary to the observation on the cross sections both values do not seem to greatly decrease at high etching strength. The reason for this are few very large spaces that contribute a large fraction of the calculated storage capacity. These spaces are caused by large areas spanned by the polygon due to coalescence of cavities at stronger etchings (comp. fig. 7.8). Such large space may also occur at slighter etchings, when a cavity is incidentally cut exactly in its longitudinal direction. However this occurs rarely, so a cumulative occurrence is a strong indication for coalescence of cavities.
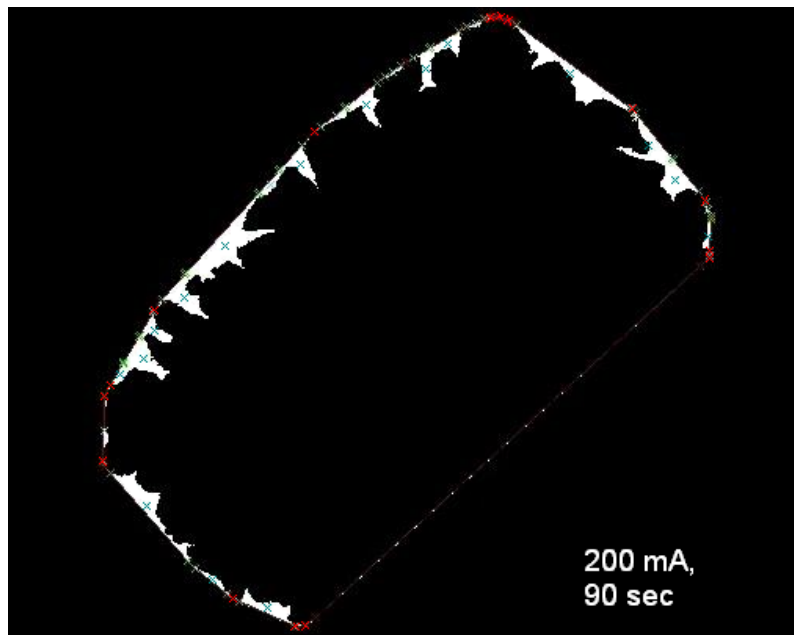
Figure 7.6: *Example for a software analysis of an etched stent, phosphoric acid combination etching, 200mA, 90s.*

Figure 7.7: *Depot effect of phosphoric acid etched stents.*

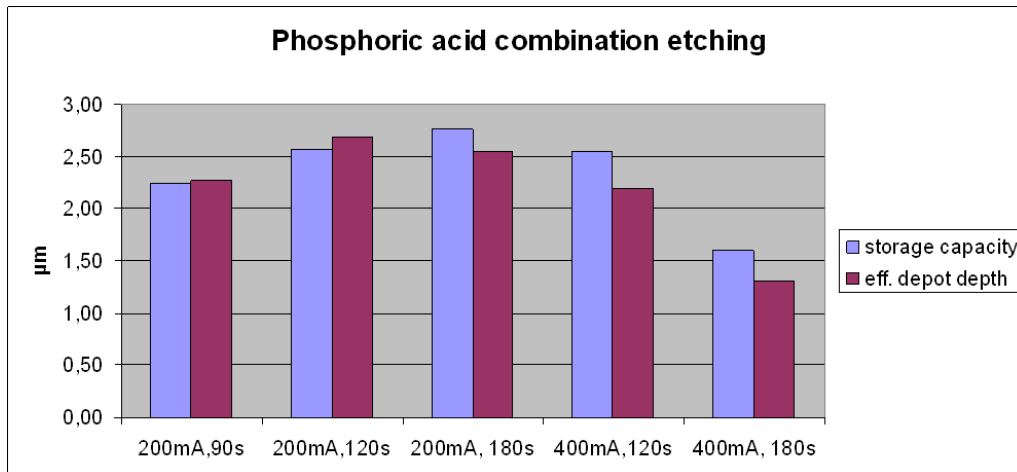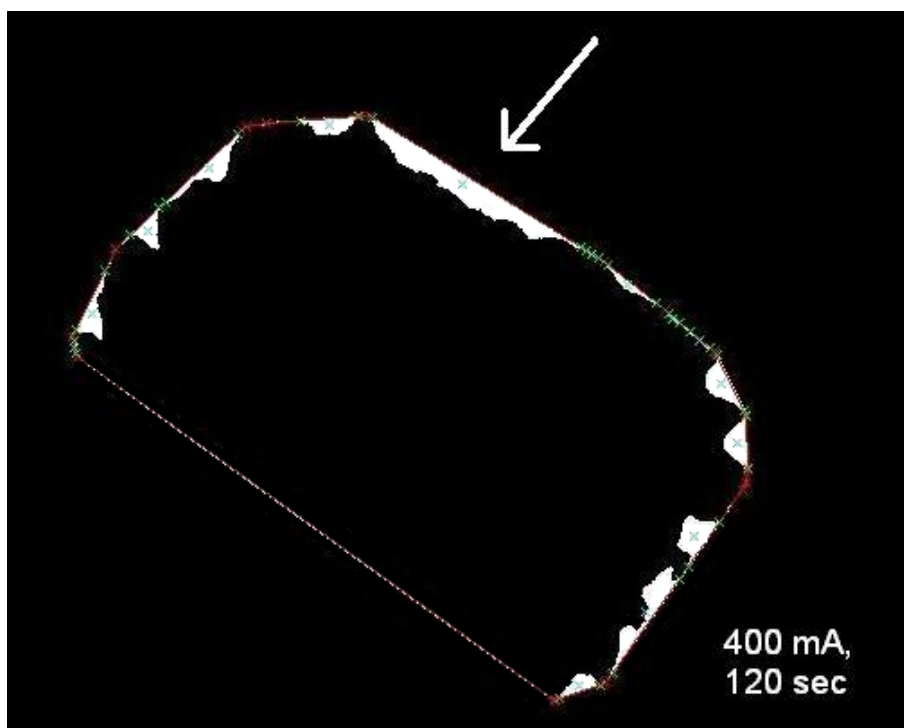**Figure 7.8:** *Software analysis of an etched stent, phosphoric acid combination etching, 400mA, 120s, the white arrow marks a large depot generated through merging depots.*
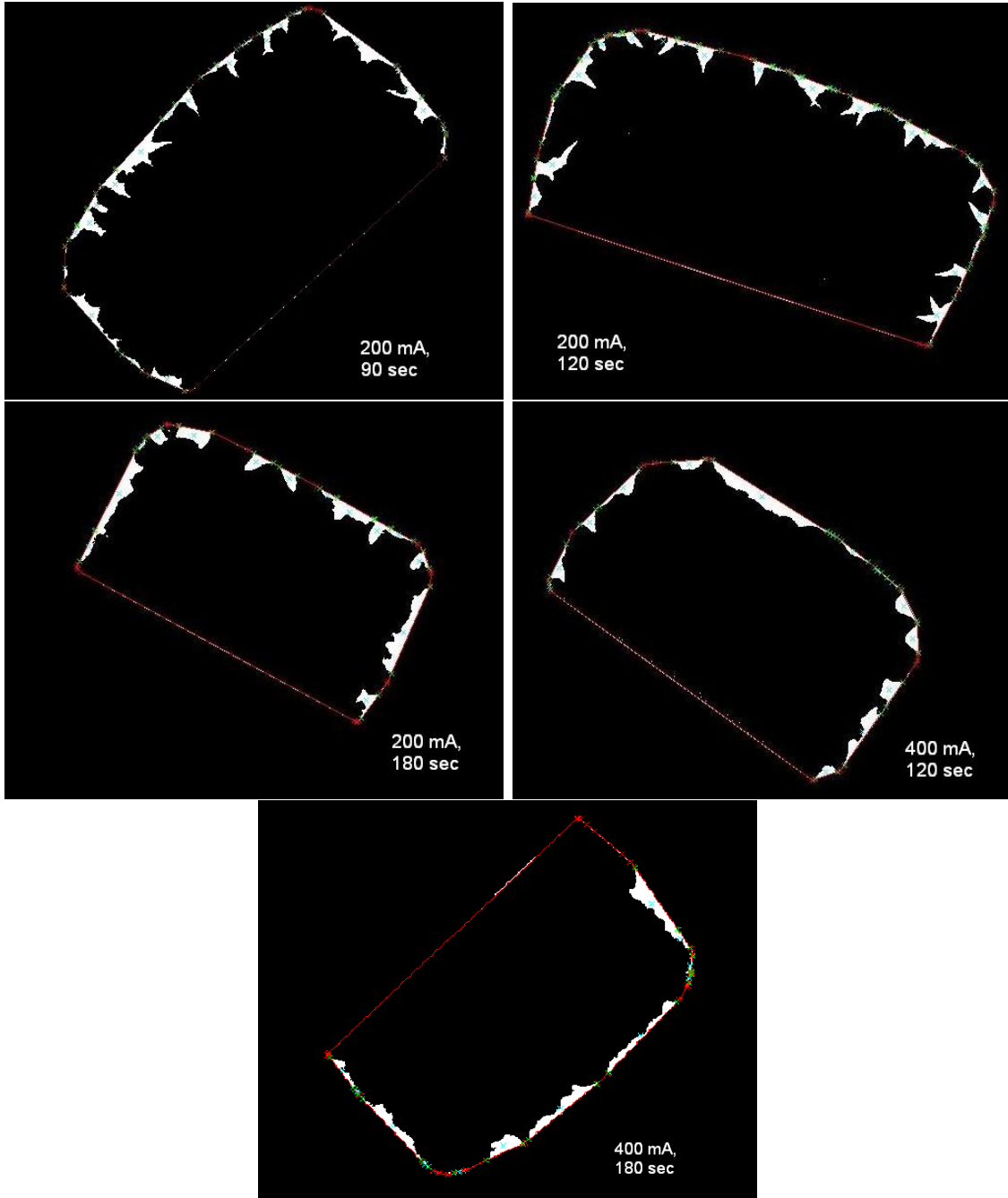
Figure 7.9: *Software analysis of etched stents, phosphoric acid combination etching, survey.*

7.2 Hydrochloric Acid

The acid was used in form of 20% HCl at a current of 200 mA (1.31 mA/mm^2). The results range from a smoothing effect similar to the phosphoric combination etchings to a microstructuring effect as described in chapter 4. Reasonably reproducible results could only be achieved by etching without a pin. Still with this method etching several samples with the same parameters did not yield exactly identical results.

7.2.1 Parameter Analysis on Stents

It was found in preliminary experiments that a 3 min HNO$_3$ etching at 200 mA (1.31 mA/mm^2) yield the largest depots. This etching yields an average grain boundary furrow depth of about 6 μm (fig. 7.10).
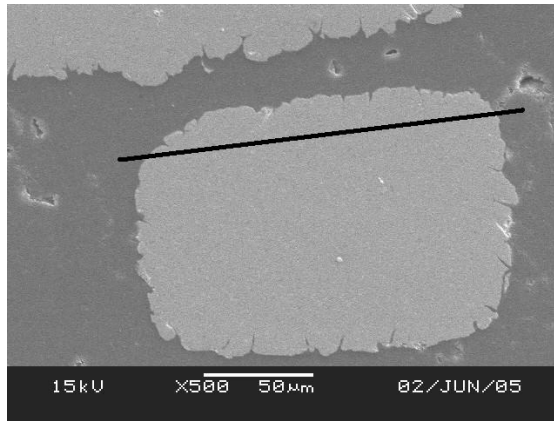
Figure 7.10: *Grain boundary etching, 200 mA, 3 min, section. This etching was used as the basis for all combination etchings except the phosphoric acid etchings.*

For the second step HCl etchings without a pin between 100 mA (0.96 mA/mm^2) * 30 sec and 200 mA (1.91 mA/mm^2) * 60 sec were examined. The combination etching obviously led to a superposition of the rough, faceted surface of the HCl etching over the grain boundary furrow structure. 100 mA applied for 30 sec produces small, even depots with the depot tips already being rounded (fig. 7.11). Increasing the current to 200 mA leads to much larger depots. However, it was found that the depot sizes and shapes varied between different stents. At 50 sec etching time most of the depots have been discreated. Strikingly the top view image seems to reveal less microroughness compared to the 30 sec sample.
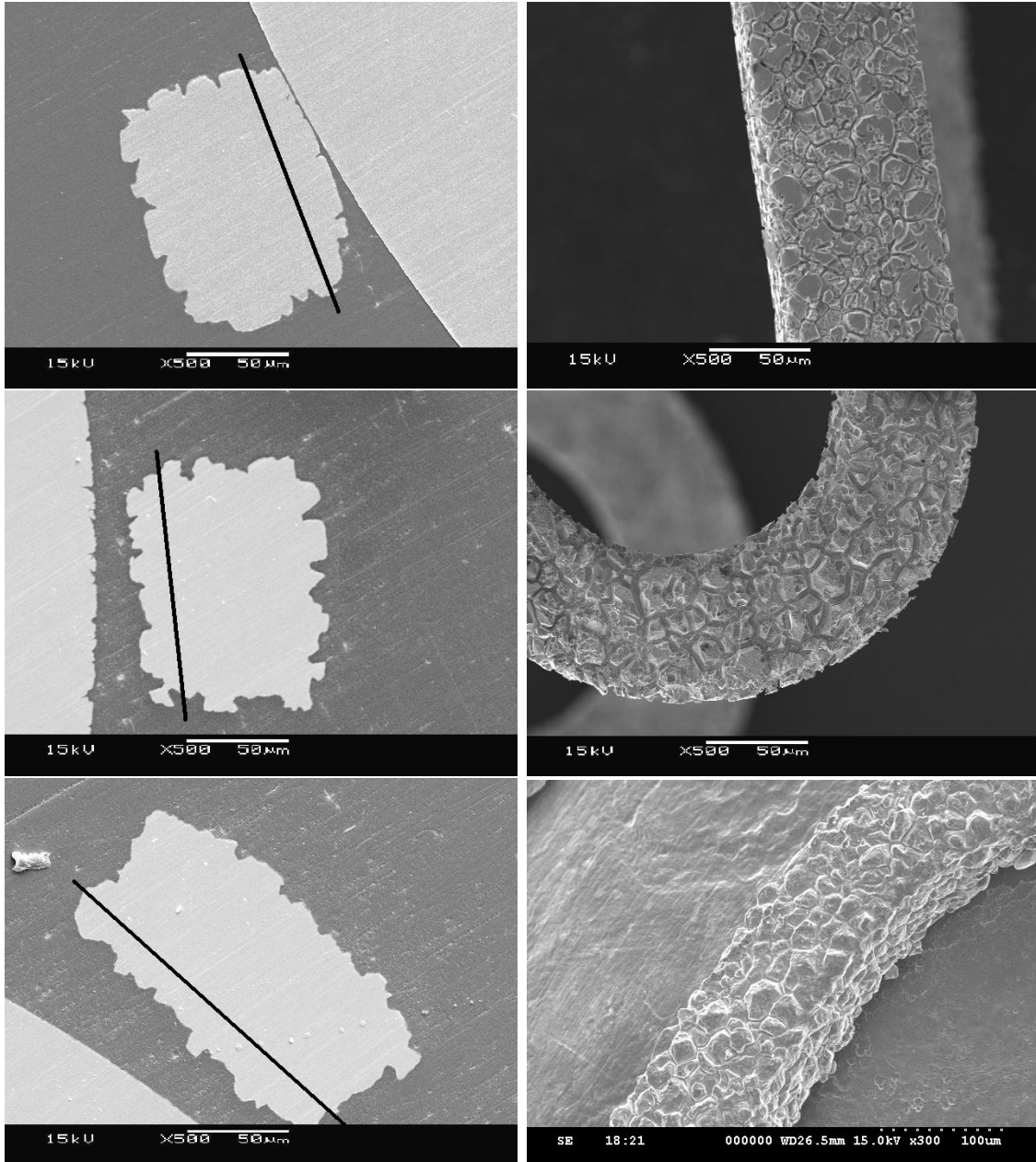
Figure 7.11: *Combination etching HCl, 100 mA, 30 sec (top), 200 mA, 30 sec (middle), 200 mA, 50 sec (bottom).*

7.2.2 Software Analysis

In Fig. 7.12 the results of the software analysis of the depot structures are shown. A maximum of the average storage capacity (3,06 $\mu m^3/\mu m^2$) at a large effective average depot depth (2,54 μm) can be found at an etching strength of 200 mA * 30 s. In contrast to the phosphoric combination etchings a considerable drop of both storage capacity and effective depot depth is present when increasing the etching strength.

Figure 7.12: *Depot effect of hydrochloric acid etched stents.*
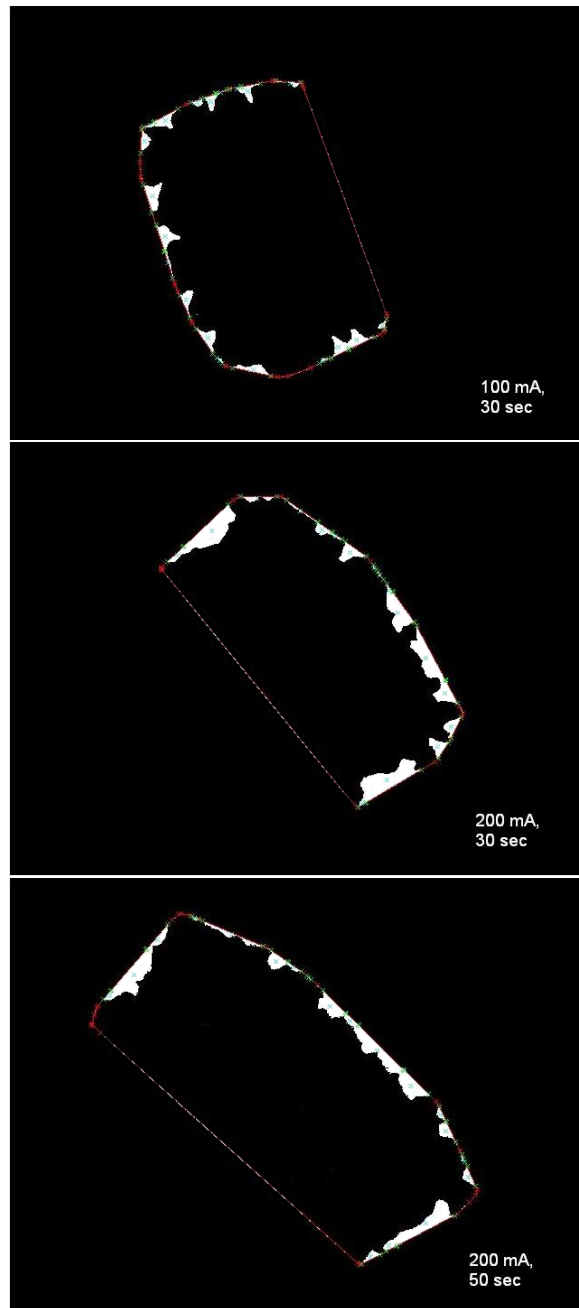
Figure 7.13: *Software analysis of etched stents, hydrochloric acid combination etching, survey.*

7.3 Oxalic Acid

The effect of electrochemical etching with oxalic acid, when used as a combination etching, is in between the effect of phosphoric acid and hydrochloric acid. Besides a leveling effect, a fine superimposed surface microroughness similar, but finer than for HCl is generated. Twin boundaries, dislocations and grain boundaries are etched slightly favored when etching with oxalic acid. This grain boundary etching effect is not nearly as pronounced as it is when using HNO_3. However if oxalic acid is used as a combination etchant with HNO_3, the effect of the first grain boundary etching step is slightly supported. It has to be assured, that a sufficient cleaning of the stents is provided, since oxalic acid etching produces hardly soluble compounds. The etchings were carried out on a pin with 10% oxalic acid at currents from 200 mA (1.31 mA/mm^2) to 400 mA (2.62 mA/mm^2).

7.3.1 Parameter Analysis on Stents

In preliminary experiments etching with HNO_3 at 200 mA (1.31 mA/mm^2) for 3 min yielded even and reproducible depots for oxalic acid combination etching. When using stronger HNO_3 etchings the structures were less uniform and the depot volume did not increase noticeably. Thus a 3 min first etching step was chosen as first etching step.

Both etching steps were performed on a pin. The oxalic acid etching step was carried out at etching strengths between 200 mA * 150 sec and 400 mA * 120 min. The etchings yielded depots similar to these of the hydrochloric acid etchings but with a finer and less pronounced faceted submicrostructure superimposed on the grain boundary structures.

A 150 sec etching at 200 mA produces rather small, but quite uniform depots (fig. 7.14). Increasing the current to 300 mA at 120 sec does not yield noticeable differences to the previous etching. At a time of 180 sec first grains start to detach, creating large shallow depots. The depot depth seems to be decreased in comparison with the previous etching (fig. 7.15). At 180 sec at 400 mA most of the single depots have merged, creating an inhomogeneous surface without distinct depots.
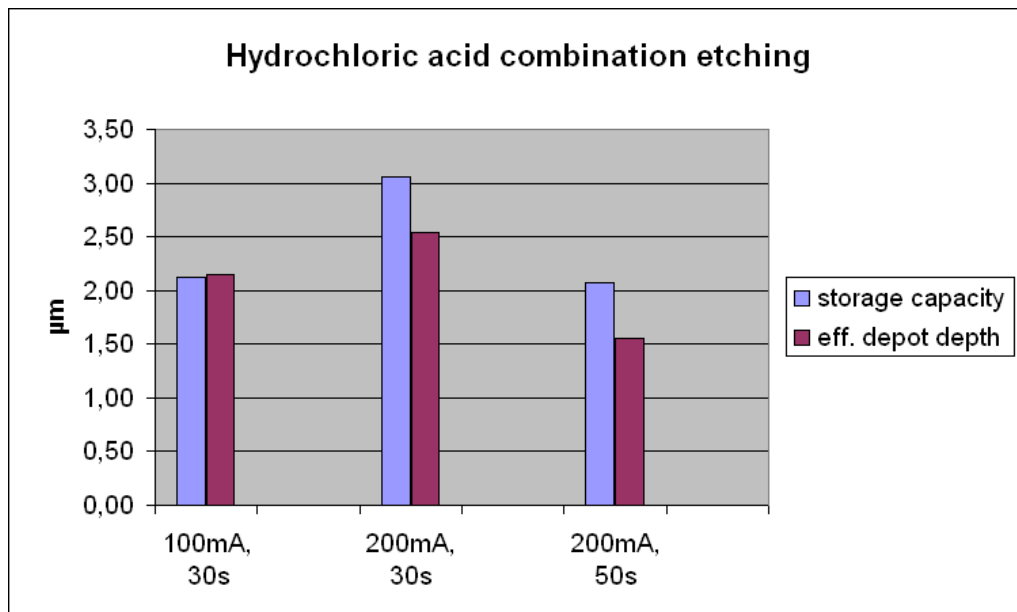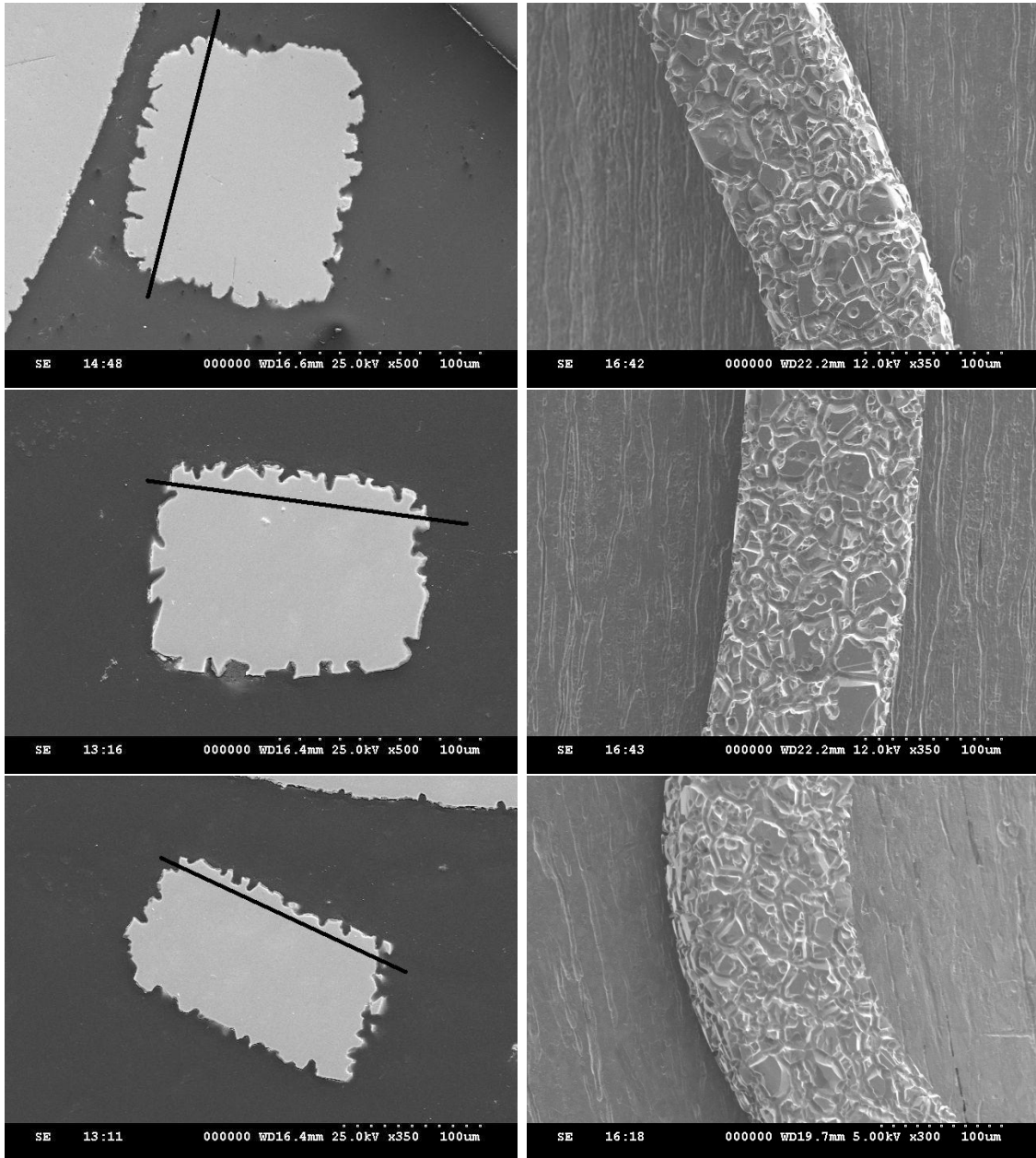
Figure 7.14: *Combination oxalic acid etching, 200 mA, 150 sec (top), 300 mA, 120 sec (middle), 300 mA, 180 sec (bottom).*
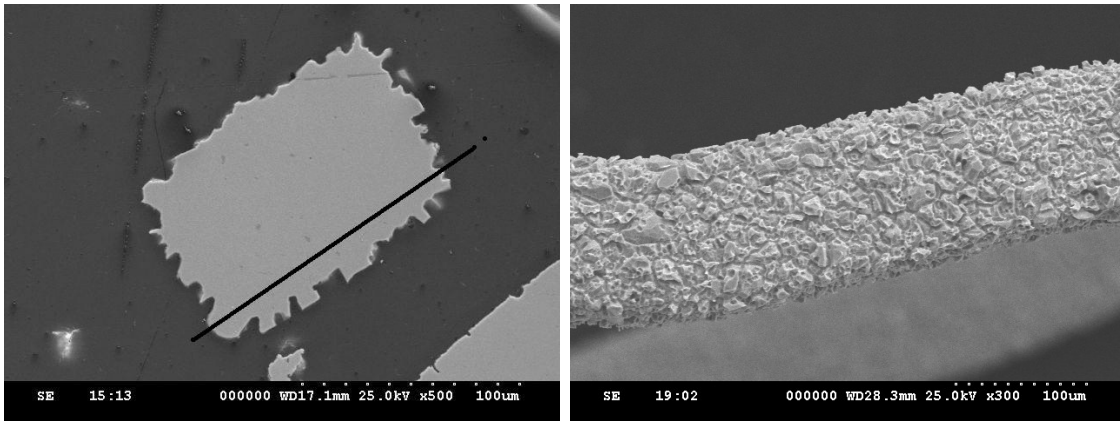
Figure 7.15: *Combination oxalic acid etching, 400 mA, 180 sec.*

7.3.2 Software Analysis

Fig. 7.16 shows the results of a software analysis of the depot structures. A maximum of the storage capacity as well as the effective depot depth can be found in the range of an an etching strength of 300 mA * 120 s. The result is in good accordance with the observations on the images. At lower etching strength the depots are only slightly broadened, at higher etching strength much of the depot effect is lost through material removal and merging of depots.
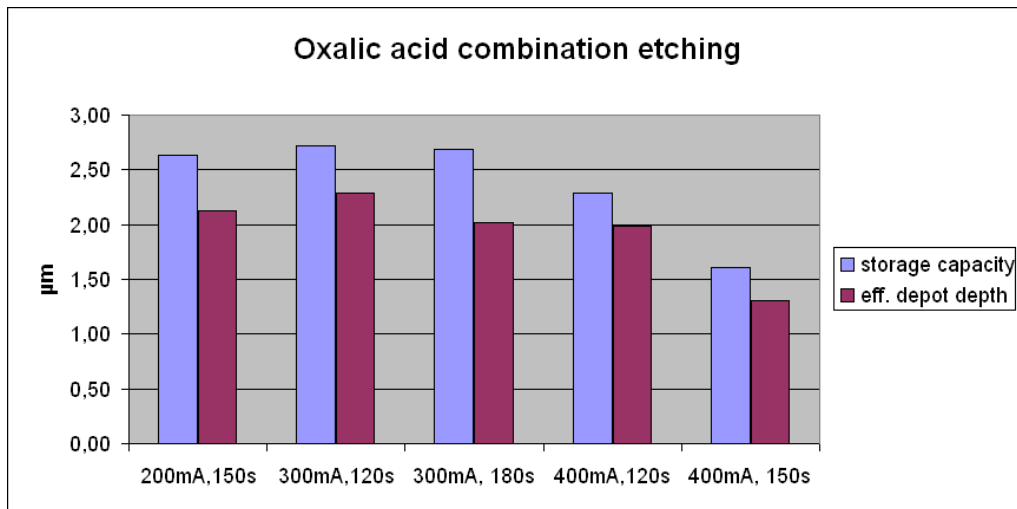
Figure 7.16: *Depot effect of combination oxalic acid etched stents.*

200 mA, 150 sec

300 mA, 120 sec

300 mA, 180 sec

400 mA, 120 sec

400 mA, 180 sec
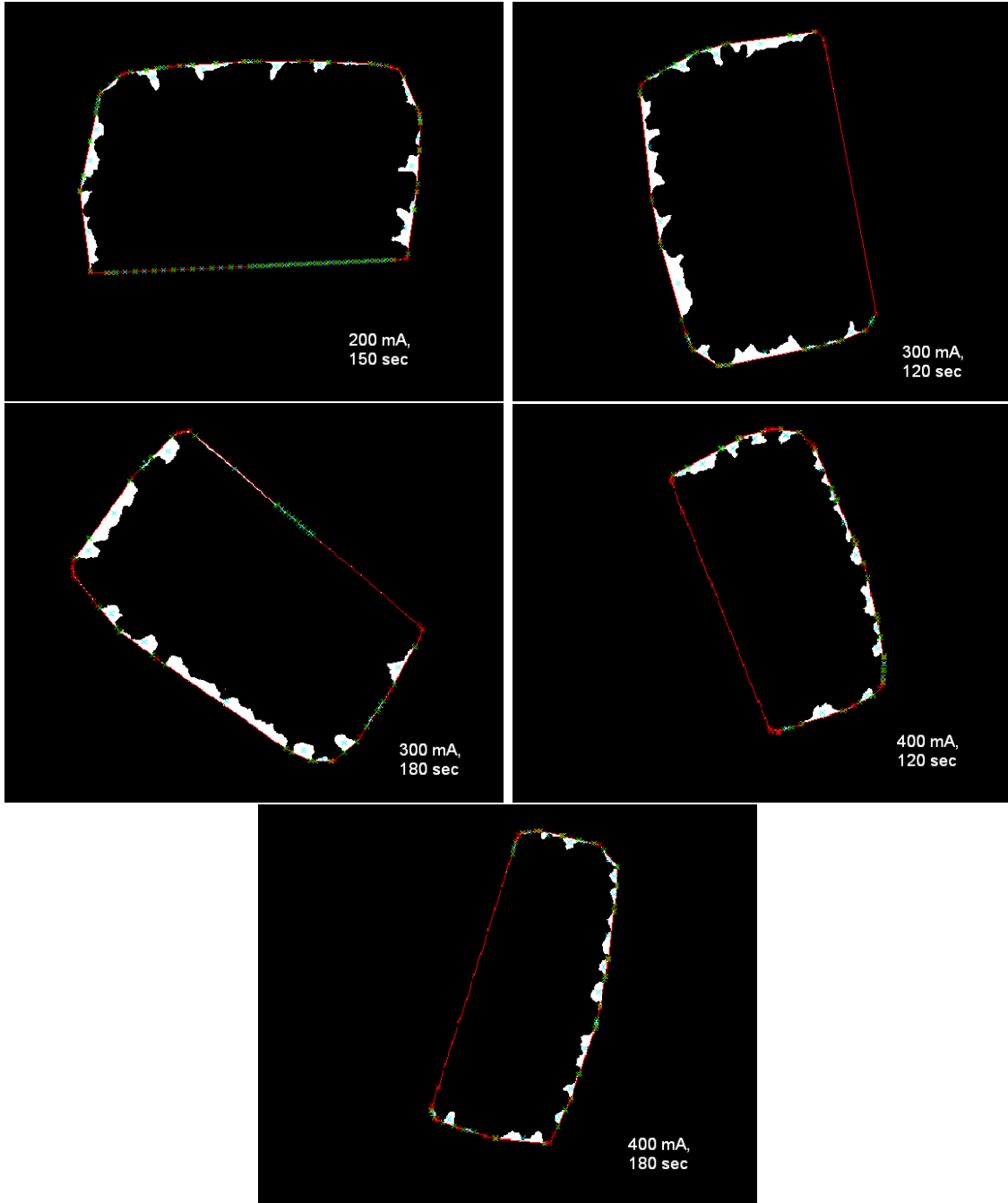
Figure 7.17: *Software analysis of etched stents, oxalic acid combination etching, survey.*

7.4 Etchings without previous Electropolishing

All of the above etchings were carried out on electropolished stents. On the example of the oxalic acid combination etching method it was evaluated if it is possible to waive the electropolishing process by using raw stents. These stents are only subjected to a pickling treatment directly after the laser cutting process in order to remove slag and excrescent oxide layers. The stents were etched in the as produced state. That means in contrast to all other stents used in this work the stents were not mechanically stressed before etching (compare sec. Materials).

The upper pictures on fig. 7.18 shows a stent etched with 1. HNO_3, 200 mA, 4 min and 2. oxalic acid 300 mA, 2 min, both steps etched on a pin. The square shaped geometry of the stent was almost completely maintained with more or less sharp angles. A rounding of the edges can hardly be observed. Strikingly the inner side of the stent is almost completely spared by the etch effect having only small microstructures. These small microstructures could promote the proliferation of endothelial cells without the risk of damaging the balloon catheter. Primarily the good protection will be due to the much better contact to the pin of the as produced stents. However another important factor are the unrounded edges which prevent acid of getting between stent and pin. The picture below shows a stent where the second step was carried out without using a pin at 150 mA for 2 min. The inner side (the bottom side for the left picture and the right side for the right picture) shows much more etch attack than the first stents. However the protection of the inner side is still better than for the electropolished stents. Concerning the sharp angles the second etching step without a pin resulted in rounding of the edges. Interestingly not only the inner angles but also the outer angles are much more rounded. Two reasons can be found for this. Firstly without the pin a better acid flow develops around the stent struts. Secondly the depth of all depots indicate that the current density of the second etching step was probably higher than for the first stent. Although it was attempted to use the same parameters for both stents the current densities of etchings with and without pin cannot be directly compared (comp. 33).
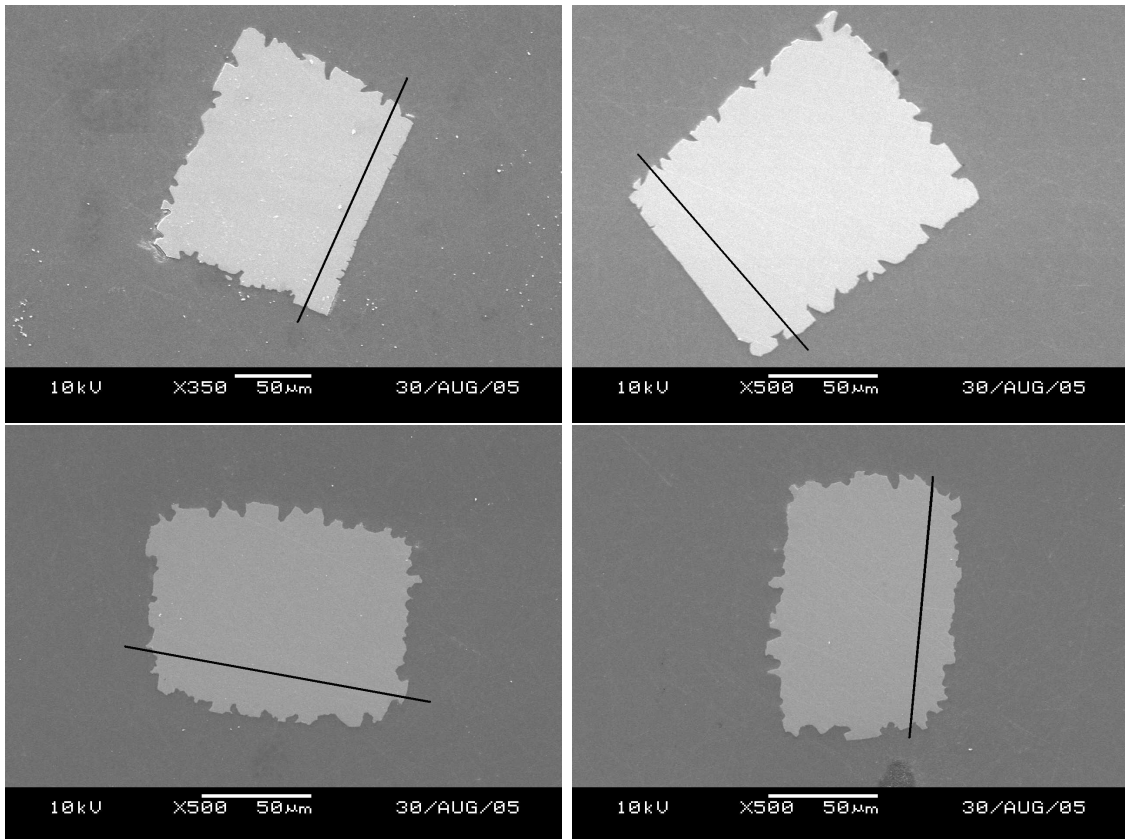
Figure 7.18: *Virgin stent (without pretreatment), combination etchings without pin, top: 1. step: 200 mA 180 sec, 2. step on a pin: 300 mA, 100 sec; bottom 1. step: 200 mA 210 sec, 2. step without a pin: 300 mA, 120 sec (bottom). The slighter etchings above still show the sharp edges generated by the laser cutting. At the stronger etchings below the edges are rounded by the second, isotropic etching step.*

8 Performance of the modified Stents

In the previous chapters five electrochemical surface modification methods have been developed, hydrochloric acid etching, grain boundary etching and three combined methods with grain boundary etching as basis (phosphoric, hydrochloric and oxalic acid etching). One of the methods, the mere grain boundary etching, apparently is not suited for the use on stents. Two methods, the hydrochloric acid etching and the hydrochloric combination etching, turned out to be not sufficiently reproducible. However, there might be other possible applications for these etching methods. Imaginable is a use in the area of other implants like e.g. bone implants. A possible application could be surface modification of any complex, sensitive part where a high surface roughness is required and grit blasting is not possible. Therefore all five methods have been investigated in terms of their chemical and biological performance. The phosphoric and oxalic combination etchings, with which reproducible surface depots can be generated, were also examined in terms of coating behavior, release performance and mechanical properties. For these investigations the following parameter sets were chosen. The HCl etchings were carried out without pin, all other etchings were performed on a pin.

step	single HCl	grain boundary	H_3PO_4 comb.	oxalic comb.	HCl comb.
1. step, HNO_3	/	200 mA	200 mA	200 mA	200 mA
	/	5 min	4 min	3 min	3 min
2. step	80 mA	/	200 mA	300 mA	200 mA
	5 min	/	3 min	2 min	30 sec

Table 8.1: *Etching parameters all analyzed stents.*

8.1 Chemical Performance

8.1.1 Cyclic Voltammetry

Cylclic voltammogramms were recorded for all etchings. Fig 8.1 gives a survey of the different etched surfaces in comparison with grit blasted and electropolished stents. The figure shows only the most significant part of the cyclic voltammogramms which is the passivity area occurring at the scan in anodic direction. The fact that the current at the passivity area differs considerably (about two orders of magnitude) can probably be attributed to a different surface (micro-) roughness and thus a different effective surface area of the stents. Accordingly the smooth electropolished and phosphoric combination etched stents show a much lower passivity current than the grit blasted and the oxalic acid etched stents which have a very high microroughness.

The rest potentials of different etched stents are shown in fig. 8.2. The rest potential is the potential which is measured when no outer potential is applied. It gives an indication for the chemical activity of the surface. A rest potential close to zero indicates chemical inactivity. The potentials were recorded after a constant value was reached, which last about one hour for most of the specimens. In most cases the potential varied to some extend before reaching a constant value, so it can be assumed that initially some chemical surface reactions took place. The etched stents show a rest potential similar to the grit blasted stent. Only the (absolute) value of the electropolished stent is slightly lower than that of the other stents.

Fig. 8.3 shows a comparison of the passivity areas of the different samples. The passivity area indicates the range between the the flade potential and the break through potential. The flade potential indicates the point at which passivation begins and is defined by the inflection point after the first (prepassive) maximum. The break through potential in this case is defined by the potential at which the current increased to twice the value of the (lowest) passivity current. The passivity areas of all stents are similar, except the oxalic acid etched sample, which has a markedly extended area.

Besides the characteristic curves all samples show some current transients when approaching the breakthrough potential (s. fig. 8.1). Most pronounced is this phenomenon for the hydrochloric acid etched and the phosphoric acid etched surfaces. A reason for this could be pitting corrosion. SEM images of the specimens did not show
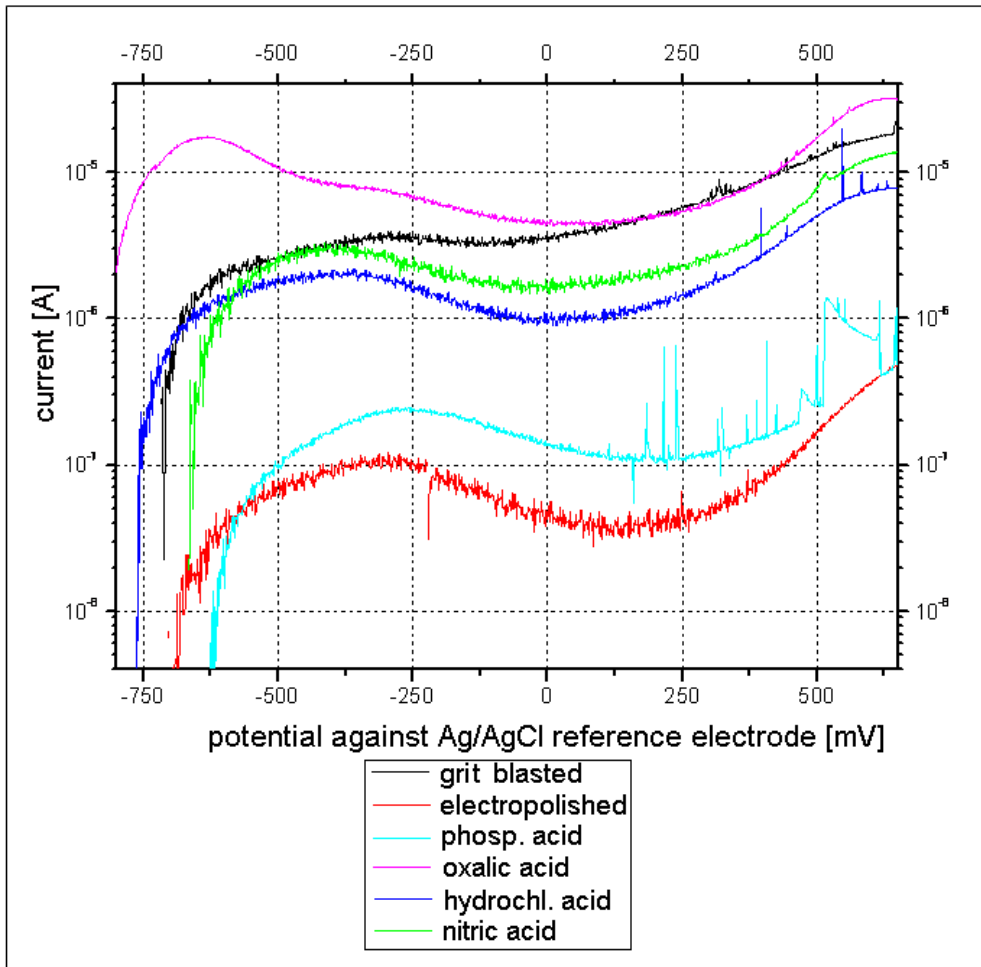
Figure 8.1: *Curves of passivity area of different modified surfaces.*
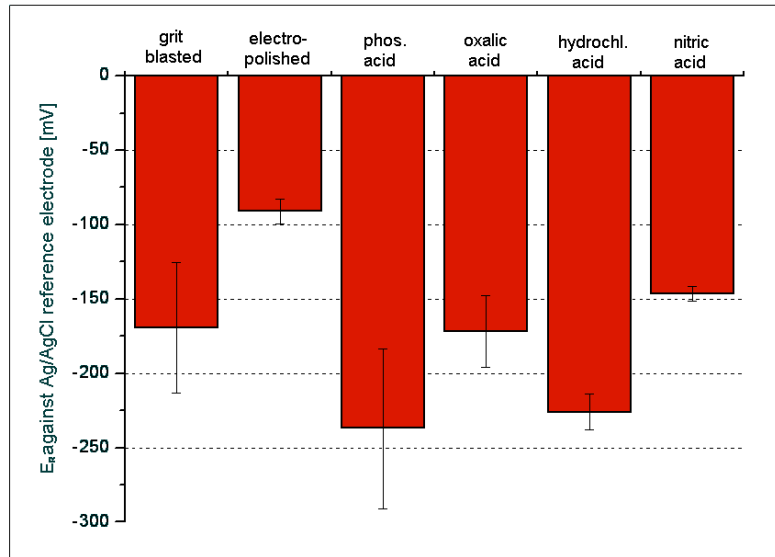
Figure 8.2: *Rest potentials of different modified surfaces. The surfaces are comparable with the electropolished having a slightly lower potential.*
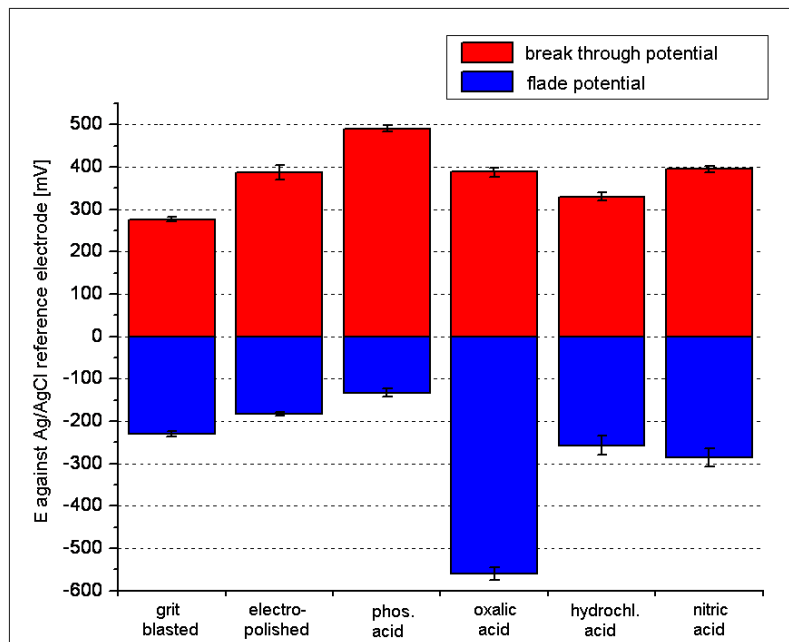
Figure 8.3: *Passivity areas of different modified surfaces. The passivity area of oxalic acid is markedly increased.*

any evident pitting corrosion on the surface. However within the microstructures pitting corrosion could still have occurred without being visible [126].

8.1.2 Release Tests of Nickel

All analyzed surfaces have been subject to an analysis of the ion release properties. The interest was focused on the release of nickel and chromium since these are the most critical ions in terms of toxicity. The breakthrough potential was used as a reference for this tests. The amount of released ions was determined after 60 min in Ringer´s solution at 37°C at a potential of 50 mV above the breakthrough potential. The chromium release was below the detection limit of 2 μg/l for all specimens except one sample, namely the grain boundary etched one (6 μg/l). The release of nickel is illustrated in 8.4. The value for the grain boundary etching has to be contemplated with caution, since with this sample problems occurred with the potential control, so that the test had to be canceled after 40h. When the test was repeated the nickel release could still not be determined due to technical problems during the analysis. However the chromium release, which could be determined, was in good congruence with the previous value (5 μg/l), affirming the high release of the grain boundary etched samples.
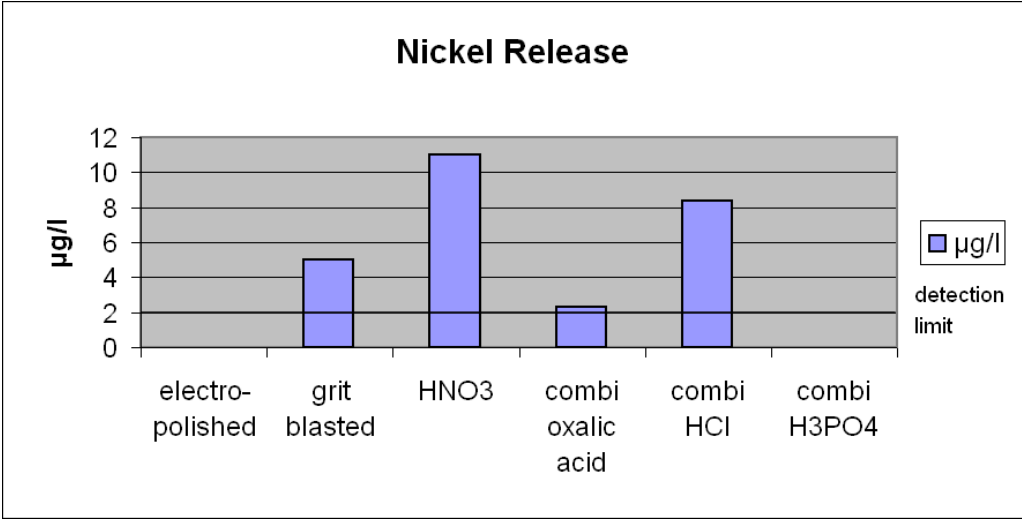
Figure 8.4: *Nickel release of different modified surfaces.*

According to the measured data the nitric acid etching seems to produce the most critical surface. HCl etchings produce slightly better results. The oxalic acid etching

with 2,3 μg/l and the phosphoric acid etching (below detection limit of 2 μg/l) had the lowest release of nickel ions. The release of the electropolished stents was below the detection limit. An obvious conclusion of these observations would be that nitric acid or hydrochloric acid change the properties of the passivation layer in a way that the passivation and release properties are effected in a negative way. However this would be in contrast to most examinations that can be found in literature. Nitric acid as well as electropolishing solutions are mostly reported to support the passivation properties [89] of stainless steel by increasing the chromium content within the passivity layer [62, 112]. Oxalic acid on the other hand is rather attributed to a denudation of chromium [136]. (An analysis of the passivity layers can be found in the next section.) An explanation for this contradiction can be found in the topographies of the different surfaces. A striking accordance can be seen on the occurrence of narrow crevices or high microroughness with a high release of nickel. One explanation that suggests itself is the increased surface area. Another aspect is the presence of acid remains within crevices that are not removed by the cleaning process. These acid remains might cause an accelerated ion release. Especially nitric acid etching creates very narrow crevices in which acid could remain. The electropolished surfaces as well as the phosphoric acid etched ones create very smooth surfaces which could explain the low release [126].

8.1.3 Analysis of the Passivity Layer

An analysis of the passivity layer composition with AES for an oxalic acid etched stents and for an electropolished stent is shown in 8.5. All samples show a relatively high content of iron compared to literature and the presence of nickel [121, 89]. However, the nickel peak may result from an influence of the bulk material. Interestingly no change in composition of the passivity layer could be found, neither between the two stents nor between the surface at the grain boundaries and the matrix [126].

8.2 Biological Performance

8.2.1 Cell Seeding

In the previous sections the effect of the etching treatments on the chemical performance of the surfaces have been investigated. Although no significant differences
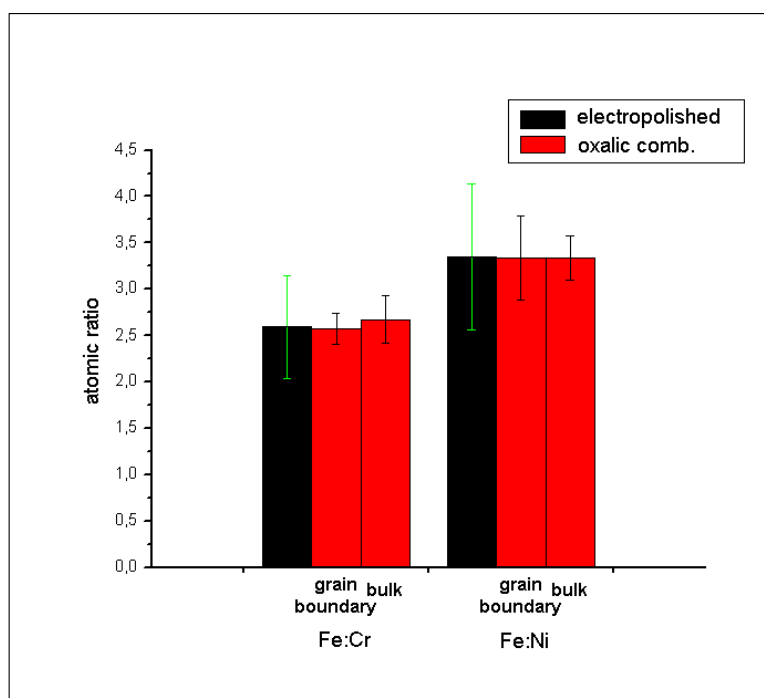
Figure 8.5: *Auger Analysis of stent surfaces. No differences can be detected between grain boundaries and bulk.*

in the composition of the passivity layer could be measured, the electrochemical behavior of the modified surfaces differed. In order to get informations about the effect of the electrochemical differences as well as the effect of the surface topographies on cells, seeding experiments were carried out. All etching treatments were analyzed, except the mere hydrochloric acid etching. A survey of all surfaces is given in 8.6. As reference served grit blasted surfaces. Three types of cells were chosen: endothelial cells (primary cells), myo-fibroblasts (USCS, primary cells) and fibroblasts (cell line). For details s. appendix. As described on p. 6 endothelial cells constitute the inner layer of an artery. The recreation of this layer after the stenting process decides about the occurrence of restenosis. Myo-fibroblasts were chosen as precursors of smooth muscle cells. As Restenosis is a result of an excessive proliferation of smooth muscle cells the proliferation behavior of myo-fibroblasts may give some indications for possible toxic reactions. The endothelial cells and the myo-fibroblasts showed no noticeable proliferation for all examined specimens. Also for the grit blasted reference specimens the cells did not proliferate. Nevertheless for all seeded specimens some cell activity maintained until the end of the time period. This indicates that all of the surfaces are at least not cytotoxic. However no information in terms of a comparison between the specimens could be obtained from

these cells. Primary myo-fibroblasts and endothelial cells are very sensitive, so that a direct seeding on a metal surface may be problematic in general. In literature [32] comparable experiments were performed with endothelial cells where migration on 316L surfaces could be observed. However in this case the metal specimens were implanted into a confluent endothelial cell seeded surface and migration was supported by simulated blood flow. It has to be noticed that in in vivo performance, endothelial cells or smooth muscle cells will not be in direct contact with the stent material. Normally between stent and cells a thin layer of fibrin and other organic material will be present[137]. Instead of further experiments with sensitive arterial cells more robust fibroblast were used for the following tests in order to give comparable information about the general biological performance of the surfaces.

The following etch parameters were used, analog to the previous sections (comp. p. 90).

step	grain boundary	H_3PO_4 comb.	oxalic comb.	HCl comb.
1. step, HNO_3	600 mA 7 min	600 mA 5 min	600 mA 5 min	600 mA 5 min
2. step	/ /	600 mA 7 min	600 mA 7 min	600 mA 5 min

Table 8.2: *Etching parameters for the seeded specimens.*

Fibroblasts proliferated on all surfaces, to varying extent (fig. 8.9). While the sandblasted as well as the mere grain boundary etched surfaces showed only moderate proliferation (fig 8.7), on the oxalic and hydrochloric combination etched surfaces considerably increased proliferation could be observed (fig 8.8). SEM analysis of the fibroblasts showed a coverage of 100 % in case of the HCl combination compared to 65 % in case of the grit blasted samples. A comparison between the different combination etchings showed a markedly decreased proliferation for the smooth phosphoric acid etchings and an intermediate result for the oxalic acid etching. (s. 8.9)
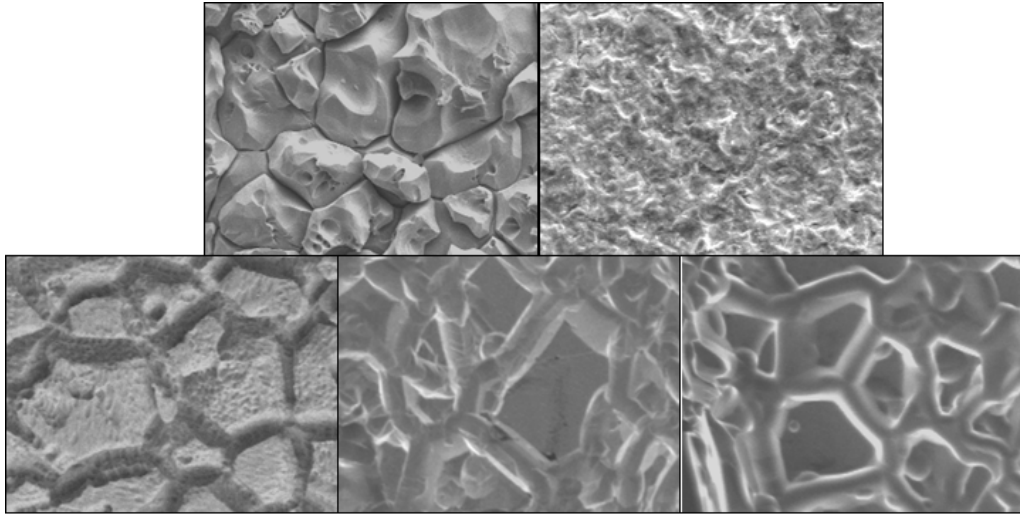
Figure 8.6: Surfaces used for seeding tests (from left to right), top: grain boundary etched and grit blasted, bottom: hydrochloric, oxalic and phosphoric acid combination etched surface.
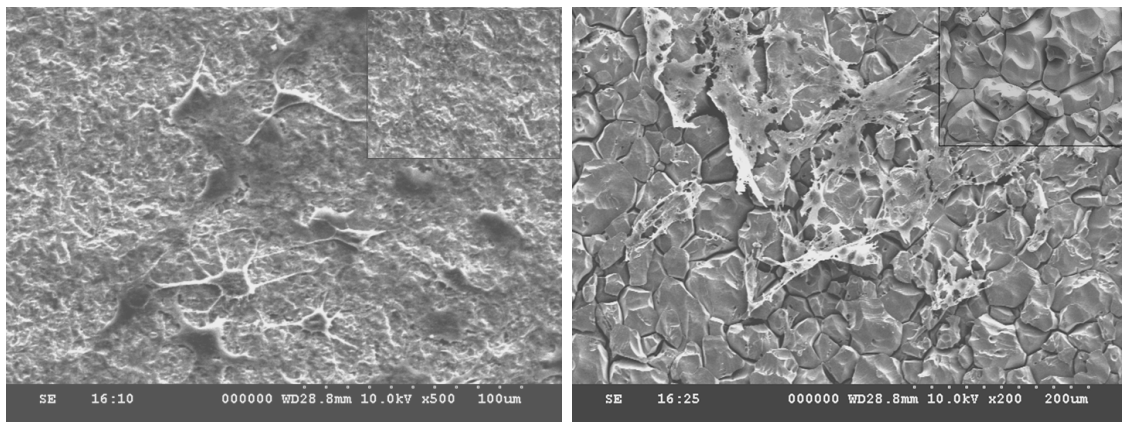
Figure 8.7: Fibroblast seeding on grit blasted and grain boundary etched surfaces (small picture unseeded surface). The surface is seeded incomplete.
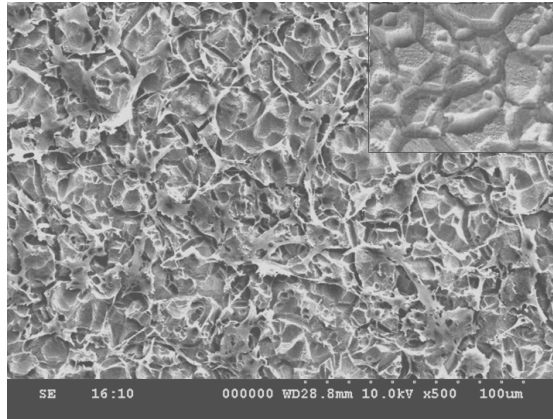
Figure 8.8: *Fibroblast ceeding on HCl combination etched surfaces (small picture unseeded surface). The surface is completely covered.*
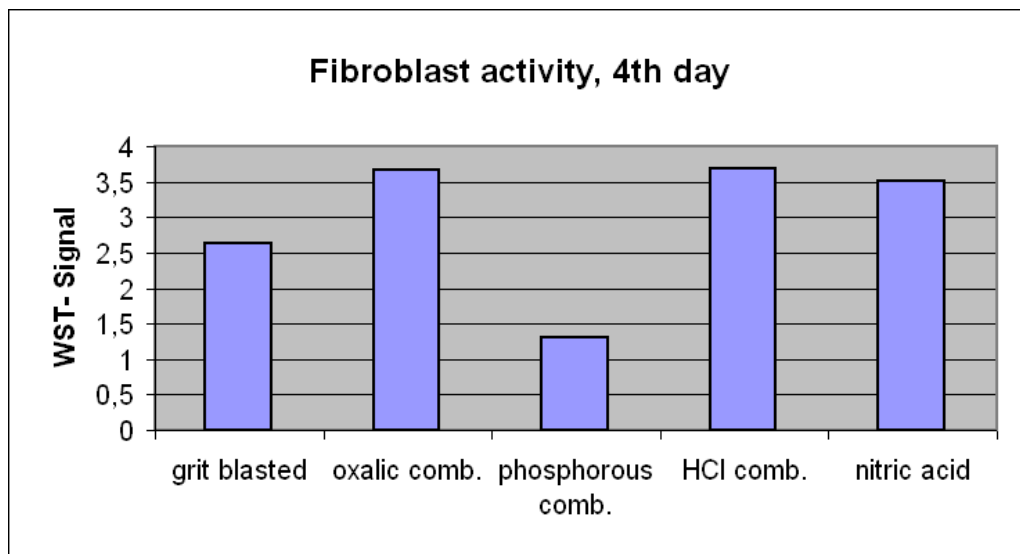
Figure 8.9: *Comparison of cell activity signals of different surface treatments. The WST-signals indicate the metabolic activity of cells providing an index for the proliferation and the viability of cells. Note the weak signal of the phosphoric acid etched surface.*

8.3 Mechanical Performance

For stents, according to DIN-EN 12006 for not active surgical implants, static and dynamic stability has to be proved. According to DIN-prEN 14299 dynamic stability has to be proved for 380 mio. cycles under simulation of in vivo conditions. Especially surface etchings can lead to a change in mechanical properties through various effects. On the one hand etching of surfaces means a material removal so that the load bearing cross sectional area is diminished. This effect can be compensated by a proper adaption of the stent design, namely the allowing for the expected material removal. A more critical problem is the modified surface in respect to the high cycle fatigue behavior. The furrows generated through the etching process work as notches and may represent initial points for crack propagation during the cyclic strain of the heart beat. Fig 8.10 shows a comparison of different modified surfaces in respect to their notch effects. Shown is the average number of notches on a stent strut, split into three categories according to their notch effects. A number larger than 10 indicates critical notches while a number lower than 1 indicates shallow depots with low depot effect. A notch number of ten was chosen as a critical limit as intern studies showed no notch numbers higher than ten for conventional (grit blasted) FDA approved stents. The notch effects were obtained by dividing the length of the depots by the curvature radius of the notch tip. The mere grain boundary etched samples exhibit almost only critical depots with a notch number of 10 and above. With the phosphorous and the oxalic acid combination etchings all of these depots can be converted into less critical notches. Interestingly also for the grit blasted stents few notches with high notch effect could be found.

8.3.1 Radial Strength Tests

Radial strength test were performed with two oxalic acid combination etched stents and two phosphoric combination etched stents. Details on this procedure can be found in [138]. The tests showed that the radial strength is considerably weakened for both etchings. The collapse pressure of the phosphoric acid etchings was 0.19 and 0.20 bar, the pressures measured for the oxalic acid etchings was 0.35 and 0.32 bar. The reference stent, in comparison, had a collapse pressure of 0.66 bar. This results were not unexpected since all etching procedures lead to a material removal as well as to a diminished load bearing area through the microstructures. As a consequence, for commercial use of the surface etched stents, a new stent design would

100
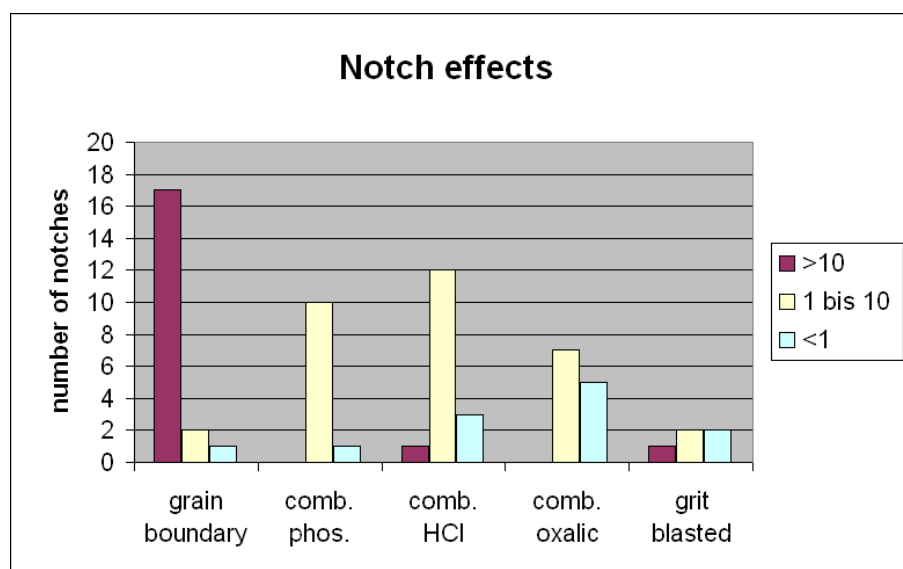
Figure 8.10: *Average number of notches on modified surfaces (referring to one stent), split into three categories, high, intermediate and low notch effect. The combination etching considerably decreased the notch effects without leveling the depots.*

have to be designed with which the material removal as well as the diminished load bearing area is compensated.

8.3.2 Fatigue Tests

To evaluate the fatigue behavior of the etched stents, a test chamber was constructed which simulates the in vivo conditions with an accelerated frequency of 70 Hz. Three stents each, oxalic acid and phosphoric acid combination etched were tested, with an electropolished stent as reference. Besides a grain boundary etched stent was tested simultaneously as negative control. The etchings with hydrochloric acid were not tested due to their insufficient reproductivity.

Polished sections were prepared of all tested stents creating horizontal cuts. Special interest was paid to the depot tips at the inner and outer surfaces of the bends. Up to a magnification of 2000 no fatigue crevices could be observed at any stent. Surprisingly even for the grain boundary etched stents used as negative controll no fatigue crevices could be observed (fig. 8.11). The strains imposed during the tests

seem to be beyond relevant strains for the material.
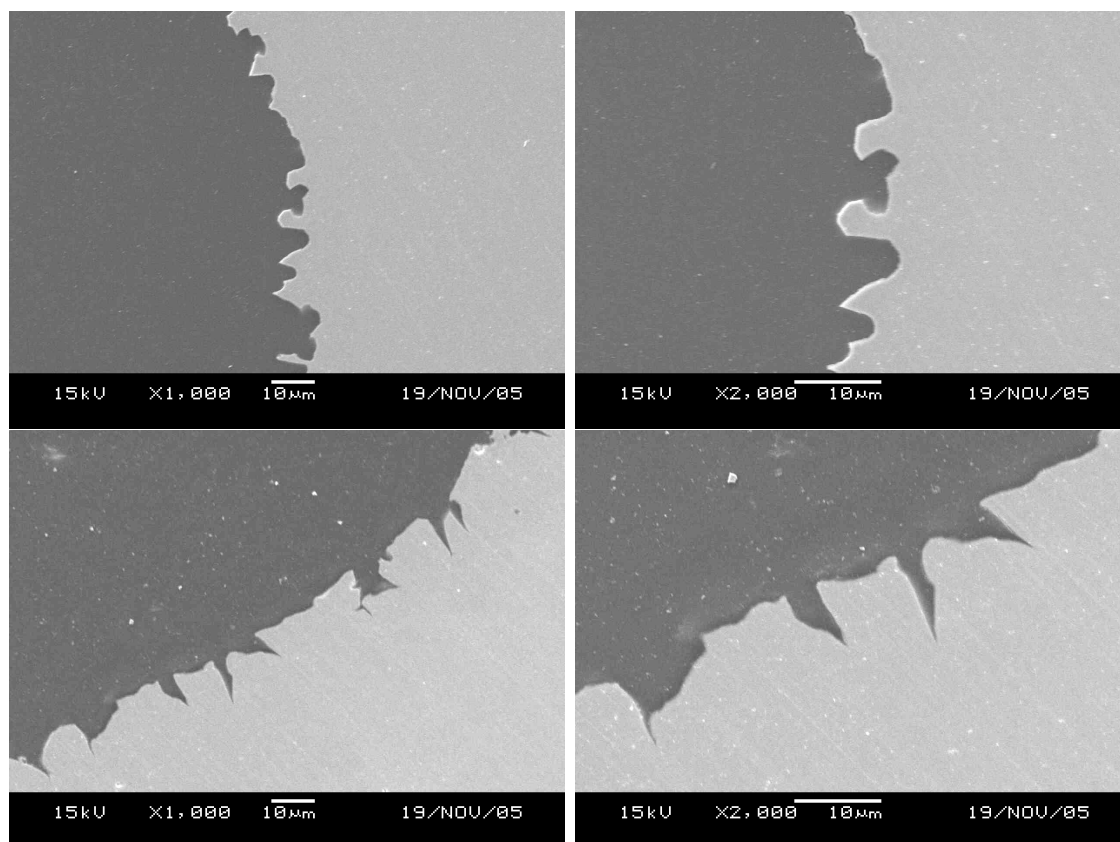
Figure 8.11: *Section through curvatures of a tested stent, top: oxalic combination etching, bottom: grain boundary etched stent. At none of the observed sections any indications could be found for cracks propagating from the etched structures.*

8.4 Coating Behavior

In the following section the performance of drug coatings on the surface modified stents is examined using the original coating method which is employed in the catheter laboratories.

All combination etched stents were coated with Rapamycin using 1% and 2% solution in ethanol. The coatings are uniform, with the Rapamycin apparently being absorbed by the microstructures (s. fig. 8.12). Sections of the coated stents (s. p.
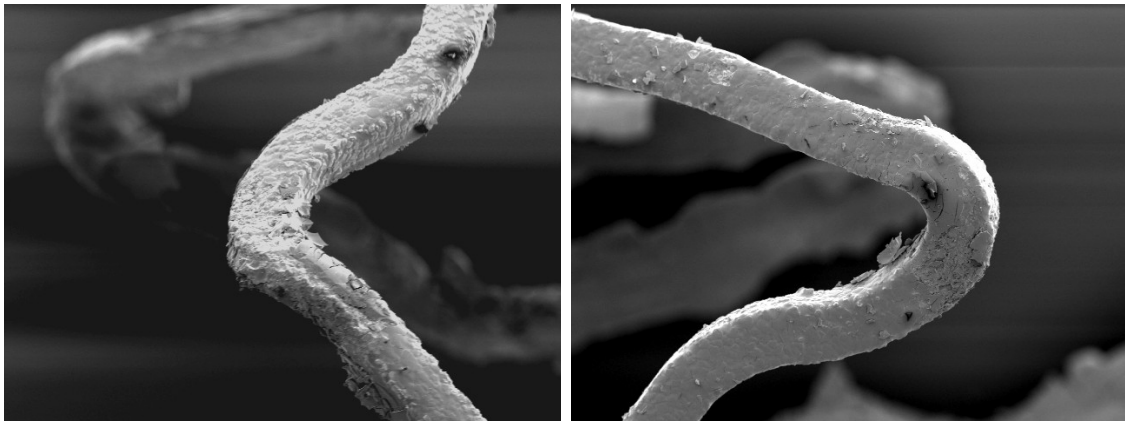
Figure 8.12: *Oxalic acid combination etched stents coated with 1% (left) and 2% rapamycin, after dilatation. The coatings appear uniform and intact.*

38) revealed an approximate thickness of about 10 to 15 μm. With this method, however, it could not be shown to what extent the depots were filled with Rapamycin, since most of the drug was washed out during the polishing process.

More detailed information could be obtained by in vitro performance tests. Adhesion tests as well as release kinetic simulations were performed with all three combination etchings as well as with the faceted hydrochloric acid etched stents (fig. 8.13). The stents were coated with 1% Rapamycin. For detailed information see [124]. Very poor adhesion properties were found for the faceted surfaces (>50% loss during the simulated implantation process). Interestingly the properties were much worse than those of the electropolished stents (approx. 25% loss), although the roughness of the etched stents is considerably higher. An explanation could be the edges of the microstructures acting as break points for the crystalline drug layer. Obviously the layer is weakened by the structures while the microadhesion is not improved. The adhesion properties of the phosphoric and the hydrochloric acid combination etched stents also seem to be considerably deteriorated compared to grit blasted stents. The surface of the phosphoric acid etched stents is probably too smooth to provide a sufficient adhesion, while for the HCl etched stents the same problem as described above may occure. The oxalic acid combination etched stents show the best adhesion properties being similar to that of grit blasted stents.
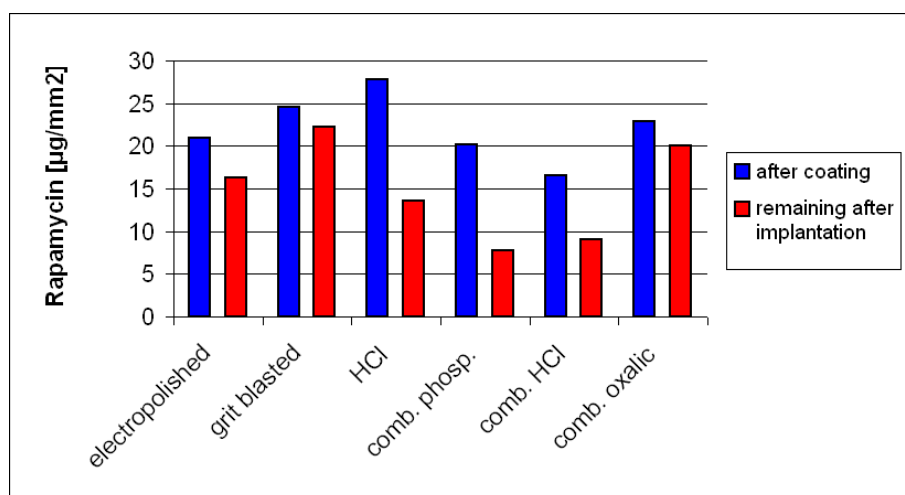
Figure 8.13: *Adhesion of rapamycin on different stent surfaces.*

8.5 Release Kinetics

As described in the Materials and Methods chapter (p. 37) the strut is quickly covered by tissue so that the main release takes place through tissue. It is assumed that, when covered with tissue, the removed Rapamycin within the depots is substituted by tissue fluid, which further assists in solving Rapamycin. Tissue fluid is similar in composition to blood plasma (from which it origins), but unlike blood it contains from 2.5 to 6% lipids [125]. As a consequence the lipophile Rapamycin should dissolve to some extent. The surrounding tissue/ cells in this case act as a semipermeable membrane so that the release from the depots is governed by diffusion/ permeation processes. The concentration of rapamycin within the cells as well as the Rapamycin evacuation processes are not known so the exact release kinetics can only be evaluated by in vivo vascular tissue examinations. However a statement about the general depot effect as well as an evaluation of the rapamycin loss during the first state when the stent is in direct contact with the blood flow can be obtained by in vitro experiments as described below.

For all three combination etching methods drug release experiments were carried out in order to evaluate the storage effect of the surfaces. For this purpose three stents of each type were coated with 1% ethanolic Rapamycin solution and placed in plastic tubes containing Ringer´s solution (comp. p. 39).

It was found that all three combination etchings yielded different release kinetics (fig. 8.14). The release kinetics were decelerated for all stents, compared to grit

blasted stents which released 90% within the first week. The total amounts of released Rapamycin were between 290 and 370 μg/ stent corresponding to 1.9 to 2.4 μg/mm^2. Interestingly the phosphoric acid etching was found to be the most efficient in terms of deceleration. 15% of the drug was stored for as long as three weeks. Fig. 8.15 shows that on all three phosphoric acid etched stents more than 30% (on average 40%) of the drug still remained after the first week. The hydrochloric acid etched stents showed sligthly faster release with approx. 25% released within the first week (fig. 8.16). Surprisingly the oxalic acid stents revealed a relatively quick release. The oxalic acid etchings were expected to be as efficient as or more efficient than the phosphoric acid etched stents due to the higher surface roughness in the submicrometer range. However, the release was found to be considerably faster than the release of the other stents with only 15% of the drug remaining after the first week. Because of the unexpected result the experiment with the oxalic acid etched stents was repeated, yielding a similar result, which makes an experimental deficiency unlikely. A reason for the relatively quick release of the oxalic acid stents could not be found.
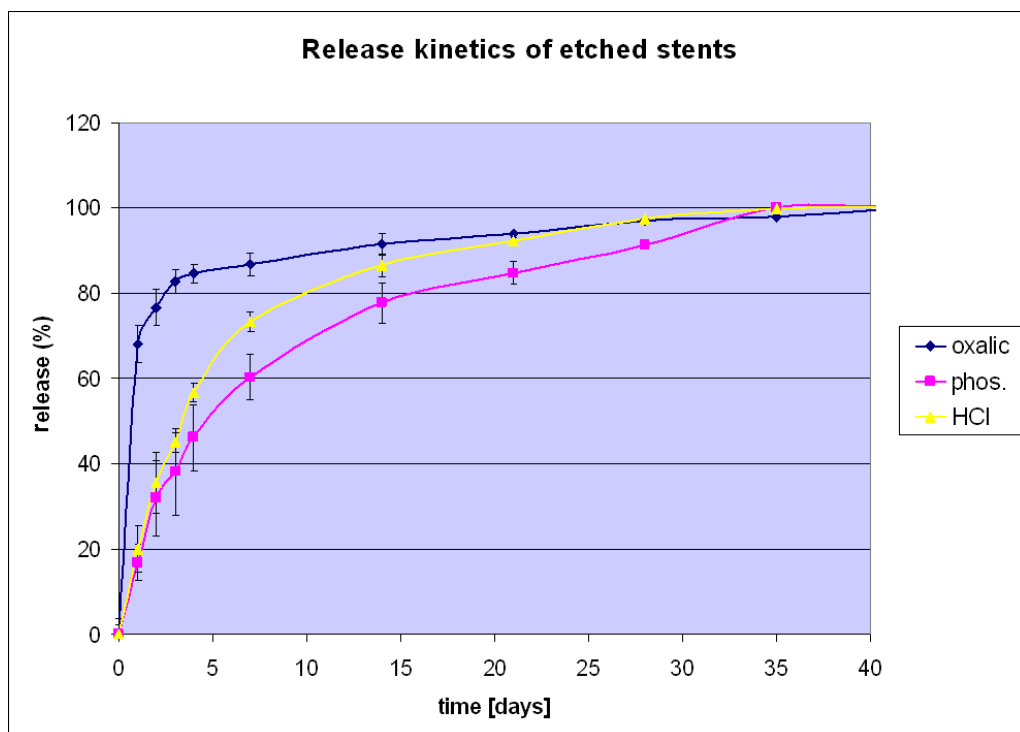
Figure 8.14: *Drug release of different surface treated stents, average values of three stents each.*
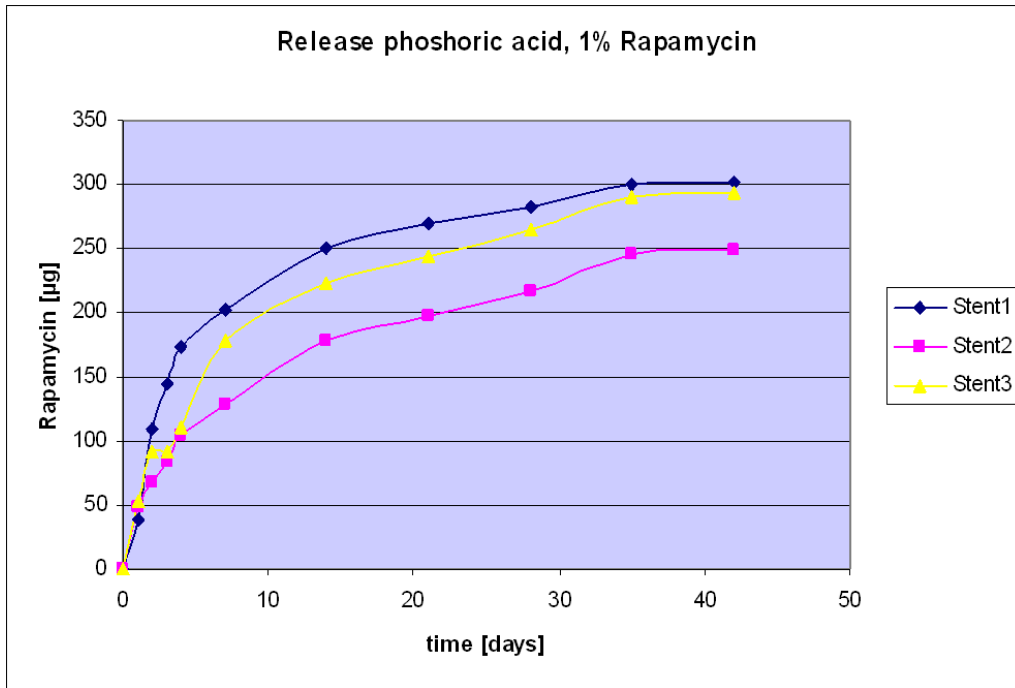
Figure 8.15: _Drug release of phosphoric acid combination etching._
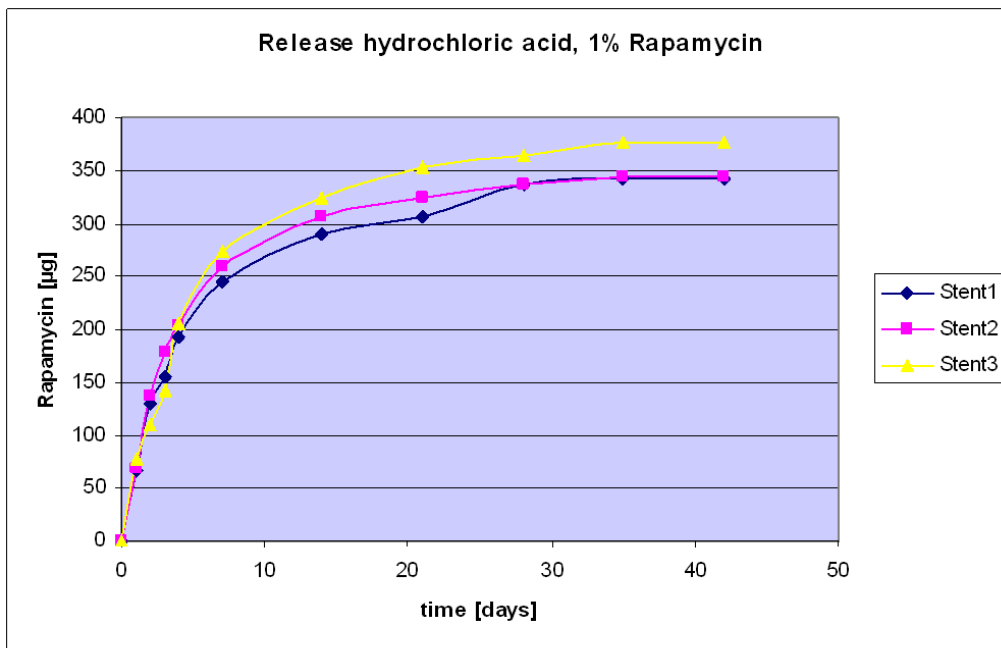
Figure 8.16: _Drug release of hydrochloric acid combination etching._
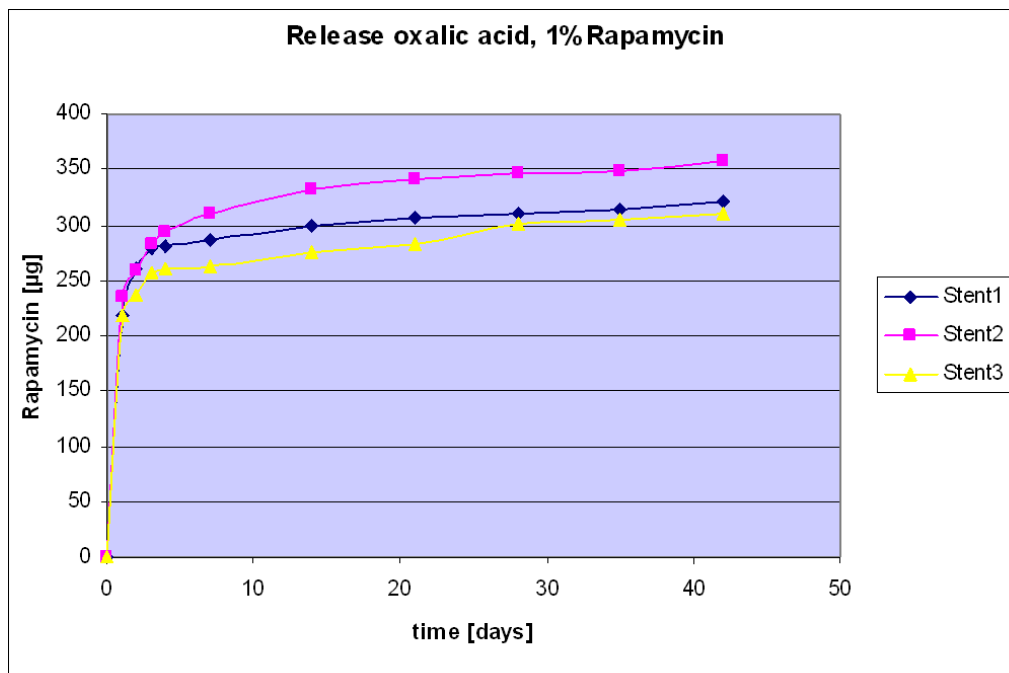
Figure 8.17: *Drug release of oxalic acid combination etching.*

9 Summary and Outlook

9.1 Summary

In this work different electrochemical etching methods for stainless steel surfaces have been investigated in respect to their applicability as surface modifications for drug coatings. The modification techniques are illustrated on 316L coronary stents. The basic aim was to provide a surface with sufficient adhesion of the drug. It was found that, beyond this, it is possible to create microdepots on the surfaces which have the capacity of storing a certain amount of substance. Through this the possibility is given to decelerate release of a drug. In contrast to other microstructuring methods where predefined structures are imposed onto the surface, the approach was to use the intrinsic material structures in order to create randomly distributed microstructures. The structures are worked out of the material by electrochemical etching. Two different etching principles were investigated in this work. One is based on the selective removal of crystal planes within the grain by hydrochloric acid etching. This method produces an increased roughness without creating microdepots. The other one bases on the selective material removal at grain boundaries by nitric acid etching. These etchings create a grid of microfurrows of different depth, depending on the etching strength. Both microstructures were found to be not suitable for the use on stents as single treatments. However it was found that promising microstructures can be generated when combining nitric acid etchings with a second etching step. For the second step of the combination etchings three acids were examined: phosphoric acid, hydrochloric acid and oxalic acid.

9.1.1 Microstructuring with Hydrochloric Acid

Etchings were performed using current densities from 0.36 to 2.86 mA/mm^2. In some cases at current densities between 0.72 and 1.08 mA/mm^2 evenly faceted surfaces could be generated with surface roughnesses between 0.22 and 0.71 (Ra) and between 0.87 and 3.29 (Rz), respectively. These surfaces, however, did only occur on

108

few specimens. It was found that the success rate for generating the microstructures could be considerably improved when the stent was not etched crimped on a pin, but hold directly into the etching solution by a platinum wire. This phenomenon is attributed to a black oxide layer generated by the etching process. This layer probably isolates the stent from the pin and leads to an adulteration of the actual current density by the pin. However, without the use of a pin still no sufficiently reproducible results could be obtained. In order to assess the reasons for the difficulties in reproducing the structures, the formation process was investigated, based on observations of the initial stage of the etching process. It is suggested that the formation of the structure is based on a form of atypical pitting corrosion that can develop in stirred etching solution when a high amount of initiation points is present.

Adhesion tests of hydrochloric acid etched stents revealed deteriorated adhesion properties in comparison with grit blasted and also in comparison with electropolished stents. This unexpected result is explained by the faceted microstructures probably acting as break initiators toward the drug layer. Following these results the etching process is regarded as unsuitable for a use on stents. Nevertheless a use in other application areas is imaginable, provided the reproductivity can be improved considerably. A possible use might be applications, where an increase of surface roughness is required and grit blasting or other strain inducing techniques cannot be used.

9.1.2 Microstructuring with Nitric Acid

The effect of electrochemical etching with nitric acid on 316L was examined at current densities between 0.1 and 9.8 mA/mm^2. A current voltage diagram was recorded and the selectivities at different current densities were determined on cross sectional micrographs of etched specimens. It was found that the selectivity of the etching process decreases gradually with increasing current densities, without having a distinct maximum within the measured range. Based on this observation it is assumed that the selectivity of the process may be rather dominated by differences in molecular structures (higher degree of disorder, voids etc.), than by differences in chemical composition. Supporting this assumption, observation on etched cross sections revealed that, besides grain boundaries, in some cases also twin boundaries or dislocations, respectively, were affected by the attacks.

The effect on the surface topography was investigated using 1.3 mA/mm^2 at etching times between 2 and 6 min. The generated surfaces and cross sectional micrographs of the specimens were investigated under SEM. The resulting structures ranged from small, crevice like furrows around the grains of 2 to 4 μm depth at 2 min to very rough (Rz = 15.8 μm), granulated surface resulting from detached grains at 6 min etching time. The surfaces cannot be used for stents directly. The slighter etched surfaces exhibit only small depot volumes. For the stronger etched surfaces a risk of particle detachment during implantation is present which can lead to clinical problems. However, the nitric acid etchings can be used as a basis for combination etchings as described in the following section.

9.1.3 Combination Etchings

Three types of acids were examined as second etching steps for a combination etching based on nitric acid etchings, namely phosphoric acid, hydrochloric acid and oxalic acid.

Phosphoric acid turned out to yield suitable depots when combined with nitric acid etching of 1.31 mA/mm^2 for 240 sec. The largest depots were obtained at phosphoric acid etching of 2.0 mA/mm^2 applied for 180 sec. Software analysis yielded a theoretical storage volume of $2.8 \cdot 10^{-3}$ mm^3/mm^2.

Hydrochloric acid was combined with nitric acid etchings at 1.3 mA/mm^2 for 180 sec. The largest depots with a theoretical storage volume of $3.1 \cdot 10^{-3}$ mm^3/mm^2 were obtained at a current of 1.9 mA/mm^2 applied for 30 sec. In contrast to the other etchings this etching step had to be carried out without a pin with the stent being etched on a platinum wire to improve the reproductivity.

Oxalic acid etchings were combined with 1.3 mA/mm^2 for 180 sec nitric acid etching. Best results were found for an etching of 2.0 mA/mm^2 for 120 sec with a theoretical storage volume of $2.7 \cdot 10^{-3}$ mm^3/mm^2. The oxalic acid etching was found to be better reproducible than the hydrochloric acid etching.

9.1.4 Performance

The corrosion behavior of the surfaces after treatment with the different acids was examined by electrochemical analysis performed in Ringers solution. It was found that nitric acid etched, phosphoric combination etched and hydrochloric combination etched stent surfaces show very similar behavior as electropolished and grit blasted reference stents. For oxalic acid combination etched stents an extended passivity area was recorded, indicating superior passivation behavior. In further investigations the long term ion release in Ringers solution was examined applying a potential of 150 mV above the break through potential. It was found that the mere nitric acid etched stents had the highest release of nickel ions. The hydrochloric acid combination etched stents had a slightly lower release than the nitric acid etched stents, whereas the release of all other stents were below or marginal above the detection limit. It is suggested that this findings can rather be attributed to the different surface areas as well as to an influence of possible acid remains within crevices than to chemical differences of the passivity layer. Results of auger electron spectroscopy which revealed almost identical composition of the passivity layers support this assumption.

In order to assess biocompatibility aspects, cell seeding experiments were performed with the combination etched surfaces. Cell seeding experiments with fibroblast cell lines revealed good proliferation for the oxalic acid combination etched, the hydrochloric combination etched and grit blasted reference surfaces. Phosphoric acid combination etched surfaces showed decreased proliferation most probably as a result of the smoother surface of the microstructures. Proliferation of primary endothelial cells or smooth muscle cells could not be accomplished on any surface.

For the oxalic and phosphoric combination etchings the radial strength and the fatigue properties were tested. The fatigue tests gave no evidences for material fatigue for any of the tested stents. The radial strength tests showed up to 30 % decreased collapse pressures for all etched stents. This result was expected since the tested stent design was not adjusted for the etching procedure. For medical use of the stents a specially modified design would be required in order to compensate the material loss and the slight notch effect caused by the etching process.

Oxalic acid and phosphoric acid combination etched stents were coated with 1% Rapamycin solution and the adhesion properties in an artificial blood circuit as well

as the release kinetics were tested. It was shown that the adhesion properties of oxalic acid etched stents are comparable to that of grit blasted reference stent while the phosphoric acid etched stents had slightly deteriorated properties.

All etched stents showed characteristic decelerated release curves with the phosphoric acid etched stents yielding the slowest release. With this etching method more than 30% of the coating still remains after the first week. For grit blasted stents, in comparison, 15% of the drug remained after one week. Oxalic acid etched stents showed a release which was only slightly superior than that of grit blasted stents with approx. 20% remaining after one week.

9.1.5 Conclusion

Two methods of a combined etching method, phosphoric combination etching and oxalic combination etching were found to be suitable to generate evenly distributed microdepots on stainless steel stent surfaces with which decelerated release kinetics can be obtained. Both were found to be equal or superior in terms of corrosion properties compared to grit blasted stents. The drug release could be significantly reduced.

9.2 Outlook

The experiments performed in this work suggest that, with certain types of combined etchings, microstructured stent surfaces can be generated with which the release kinetics can be considerably decelerated. The surfaces may be suitable for the use of drug coatings without a polymer. Chemical, biological and mechanical tests as well as in vitro experiments evaluating the coating behavior were carried out in order to evaluate the properties in comparison to conventional stents. In vivo tests are currently planed in order to validate the clinical applicability.

If the in vivo results will be positive the microstructures could be further optimized in order to yield an optimum release and an optimum distribution of the drug. This optimization could be rendered by a modulation of the etching parameters in terms of the release kinetics. The distribution, on the other hand could be adjusted to a certain degree by slight variations in the heat treatment of the stents, i.e. by

generating uniform grains of a certain size.

An aspect that may be subject of future research is the adaption of the inner (luminal) side of the stent in order to yield a targeted promotion of cell ingrowth. The inner side does not contain drugs, since in the initial stage it is in direct contact with the blood stream. However, after the initial stage this side is as well quickly covered with tissue, so that it is prone for a microstructuring specifically tailored for cell ingrowth. A future stent could receive two different surface treatments, a first one that comprises a microstructuring of the inner side, followed by a second step for the creation of microdepots for drug release on the three outer sides.

10 Appendix

10.1 Determination of Grain Size

Stents and raw material were electrically connected each with a thin wire and embedded upright in epoxy resin (Specifix-40, Struehrs, Willich, Germany) in a way that the wires sticks out of the resin. After hardening the specimens were polished with diamond suspension down to 1 μ particle size. The specimen was then hold into 40% nitric acid. The wires were connected with the positiv pole of a DC Transformator and a cathode was immersed into the acid. Etching was carried out at 0.9 V for approx. 2 min (required etching time may differ from stent to stent and has to be adjusted empirically). For the visualization of the dislocations a second etching step was performed using oxalic acid at 1.5 V for approx. 2 min. The images were taken using bright field mode of a light microscope (Axiovert 25, Carl Zeiss GmbH, Jena, Germany) at 200 X magnification. For the grain size determination 50 lines of 100 μm were drawn randomly on different cross sectional strut images of different stents and the number of intersected grain boundaries was counted. Accordingly 5000 μm devided by the sum counted for all struts yields the average intersectional grain size. It may be worth mentioning that this value is different from the actual three dimensional average size of the grains. However for the surface structuring the intersectional value is the most relevant.

10.2 Calculation of Polygon Line

The starting point was defined as the point of the outline with the largest x-coordinate. (The result is independent of the choice of the starting point as long as it is an extreme. So the smallest x-value or the y-value can also be used and will, independent of the orientation of the image, yield the same polygon). Firstly a straight line is calculated running through the starting point and a second point of the contour line, without sectioning the strut area. (There are two possibilities both of which lead to the same result.) A second straight line is drawn from this second point to the next touching point on the contour line, without sectioning the

strut area. This process is repeated until the starting point is reached again. The areas between the polygon line and the stent are defined as depot areas.

10.3 Cell Cultures

Reagents

- WST-measurement: Cell proliferation reagent WST-1 (Cat# 1 644 807, ready to use, Roche Diagnostics GmbH, Mannheim, Germany)

- cell tracking: CellTracker CM-Dil (Cat# C-7001, Molecular Probes, Karlsruhe, Germany), diluted 1:1000

- cell detachment agent: Trypsin/EDTA (Cat# L 2143, Biochrom AG, Berlin, Germany)

- Phosphate buffer saline (Cat# L 1825, Biochrom AG, Berlin, Germany)

- fixing of cells: 3 % glutardialdehyde (Cat# 1.04239.0250, Merck, Darmstadt, Germany)

Culture Media, Additions

- DMEM/phen: Dulbecco's Modified Eagle Medium hg with phenolred and stable L-glutamine (Cat# FG 0435, Biochrom AG, Berlin, Germany)

- ECGM: Endothelial Cell Growth Medium (Cat# C-22010, PromoCell, Heidelberg, Germany)

- FCS: fetal calf serum (HyClone von Perbio, Cat# CH 30160.3, Lot# CMK 0190, for UCSC-Medium) (Cat# S 0115, Lot# 364B, Biochrom AG, Berlin, Germany, for HUVEC- and 3T3-Medium)

- Na-P: Na-Pyruvat (Cat# L 0473, Biochrom AG, Berlin, Germany)

- LAPh: L-Ascorbinsäure-2-phosphat (Cat# A-8960, Sigma Aldrich Co., Munich, Germany)

- SMix: SupplementMix (Cat# C-39215, PromoCell, Heidelberg, Germany)

- Pen/S: Penicillin/Streptomycin (Cat# A 2213, Biochrom AG, Berlin, Germany)

- PA: Partricin A (Cat# A 2812, Biochrom AG, Berlin, Germany)

The following compositions of the culture media were used:

cells	DMEM	ECGM	FCS	SMix	Na-P	LAPh	Pen/S	PA
USCS	X	/	10%	/	1 mM	50 μM	X	X
HUVEC	/	X	10%	X	/	/	X	X
3T3	X	/	10%	/	/	/	X	X

WST-Tests

10 %vol. of cell proliferation reagent WST-1 (Roche Diagnostics GmbH, Mannheim, Germany) was added directly into the medium. After 3 hours the behaviour of these monolayers were analysed. Control was the culture medium and 10% WST-1. The photometric measurement of the control took place in a 96-well-Platten with 450 nm (reference wavelength 620 nm) on an ELISA reader (Sunrise, Tecan GmbH, Crailsheim, Germany). The absorption of the control was subtracted from the measured samples. The photometric measurements of the samples were performed three times and with the same parameters as the control. An average optical density (OD) with standard deviation was calculated. The difference in OD percentage from the samples was compared to the control well, which was taken to be 100%.WST-1, is the standard assay used in cytotoxicity test and is recommended by EN ISO 10993-5.

10.4 Composition of Ringers Solution

component	mass concentration
NaCl	6,80
KCl	0,40
$CaCl_2$ x H_2O	0,27
$MgSO_4$ x H_2O	0,20
NaH_2PO4 x H_2O	0,14
$NaHCO_3$	2,20
α-D-Glucose (C6H12O6)	1,00

10.5 Approximation of Strain

During dilatation the stent is expanded to 2.2 times the original diameter (from
1.8 to 3.8 mm outer diameter). This expansion leads to an average angle increase
from 65° to approx. 140° on each bending. Given that the center point of the angle
movement is in the middle of the stent strut this expansion leads to an approx.
prolongation of the inner contour line of 110 μm. In order to estimate the strain for
the affected part of the inner contour line the length of the affected part must be
known. Assuming that the strain is constant over the evenly rounded part which
has a length of approx. 1.2 mm and almost zero at the straight part the strain can
be estimated to some 9%. This calculation can only be a rough estimation, however
it seems reasonable that the strain will be not considerably higher than 6% since
this is the fracture elongation of 316L and dilatated electropolished stents do not
show any crevices after dilatation.

Bibliography

[1] R. G. Richards. Surfaces to control implant tissue adhesion for osteosynthesis: In vitro and in vivo evaluations. *19th European Conference on Biomaterials, Sorrento*, 2005.

[2] K. Mustafa and A. Wennerberg et al. Determining optimal surface roughness of tio(2) blasted titanium implant material for attachment, proliferation and differentiation of cells derived from human mandibular alveolar bone. *Clinical Oral Implants Research*, 12(5):515–25, 2001.

[3] J. Lincks and BD. Boyan et al. Response of mg63 osteoblast-like cells to titanium and titanium alloy is dependent on surface roughness and composition. *Biomaterials*, 19(23):2219–32, 1998.

[4] K. Mustafa and J. Wroblewski et al. Effects of titanium surfaces blasted with tio2 particles on the initial attachment of cells derived from human mandibular bone. a scanning electron microscopic and histomorphometric analysis. *Clinical Oral Implants Research*, 11(2):116–28, 2000.

[5] M. S. Sader and A. Balduino et al. Effect of three distinct treatments of titanium surface on osteoblast attachment, proliferation, and differentiation. *Clinical Oral Implants Research*, 16(6):667–675, 2005.

[6] D. Buser and R.K. Schenk et al. Influence of surface characteristics on bone integration of titanium implants. a histomorphometric study in miniature pigs. *Journal of Biomedical Material Research*, 25:889–902, 1991.

[7] B. W. Darvell, N. Samman, W. K. Luk, R. K. F. Clark, and H. Tideman. Contamination of titanium castings by aluminium oxide blasting. *Journal of Dentistry*, 23(5):319–322, 1995. TY - JOUR.

[8] U. Gbureck, A. Masten, J. Probst, and R. Thull. Tribochemical structuring and coating of implant metal surfaces with titanium oxide and hydroxyapatite

layers. *Materials Science and Engineering: C*, 23(3):461–465, 2003. TY -
JOUR.

[9] M.A.M. Silva and A.E. Martinelli et al. Surface modification of ti implants by
plasma oxidation in hollow cathode discharge. *Surface and Coatings Technology*, 200(8):2618–2626, 2006.

[10] O. Zinger and G. Zhao et al. Differential regulation of osteoblasts by substrate
microstructural features. *Biomaterials*, 26(14):1837–1847, 2005.

[11] S. Ban, Y. Iwaya, H. Kono, and H. Sato. Surface modification of titanium by
etching in concentrated sulfuric acid. *Dental Materials*, in press, 2006.

[12] Cagiannos C. and O.R. Abul-Khoudoud et al. Rapamycin-coated expanded
polytetrafluoroethylene bypass grafts exhibit decreased anastomotic neointimal hyperplasia in a porcine model. *Journal of Vascular Surgery*, 42(5):980–
988, 2005.

[13] Kim D.D. and M.M. Takeno et al. Glow discharge plasma deposition (gdpd)
technique for the local controlled delivery of hirudin from biomaterials. *Pharmaceutical Research*, 15(5):783–786, 1998.

[14] R. Kassing and R. Käsmaier. Lithographie der nächsten generation. *Physikalische Blätter*, pages 31–36, 2000.

[15] P. R. Choudhury. *Handbook of Microlithography, Micromachining and Microfabrication*, volume 1,2. Optical Engineering Press, 1997.

[16] R.-M. Beck. *Untersuchung von Oberflächenbeschichtungen bei Gefässstützen
zur Reduktion der Restenoserate*. PhD thesis, Uni Tübingen, 2001.

[17] P. Kuukasjarvi and A. Malmivaara et al. Overview of systematic reviews on
invasive treatment of stable coronary artery disease. *International Journal of
Technology Assessment in Health Care*, 22(2):219–234, 2006.

[18] A. Machraoui, P. Grewe, and A. Fischer. *Koronarstenting*, page 49. Steinkopff,
Darmstadt, 2001.

[19] S. Sobotta and F. Hammersen. *Histologie, Farbatlas der Mikroskopischen
Anatomie*, page 126. Urban und Schwarzenberg, 1975.

[20] M. Gawaz. *Das Blutplättchen*, page 89. Georg Thieme Verlag, 1999.

[21] R. Ross and J. A. Glomset. The pathogenesis of atherosclerosis, part i and ii. *New England Journal of Medicine*, 295:369–377, 420–425, 1976.

[22] A. C. Newby. An overview of the vascular response to injury: a tribute to the late russell ross. *Toxicology letters*, 112-113:519–529, 2000.

[23] H. Itabe and M. Ueda et al. Measurement of oxidized ldl present in human plasma and atherosclerotic lesions. *International Congress Series*, 1262:87–90, 2004.

[24] M. Gawaz. *Das Blutplättchen*, page 94. Georg Thieme Verlag, 1999.

[25] D. R. Jr. Holmes. State of the art in coronary intervention. *The American Journal of Cardiology*, 91(3, Supplement 1):50–53, 2003. TY - JOUR.

[26] M. Gawaz. *Das Blutplättchen*, page 104. Georg Thieme Verlag, 1999.

[27] P. H. Grewe, T. Deneke, A. Machraoui, J. Barmeyer, and K.-M. Muller. Acute and chronic tissue response to coronary stent implantation: pathologic findings in human specimen. *Journal of the American College of Cardiology*, 35(1):162, 2000. TY - JOUR.

[28] S. Kinlay and A. U. Coskun et al. Endothelial shear stress identified in vivo within the stent is related to in-stent restenosis and remodeling of stented coronary arteries. *Journal of the American College of Cardiology*, 39(Supplement 1):5, 2002. TY - JOUR.

[29] N. Kipshidze and D. George et al. Role of the endothelium in modulating neointimal formation: Vasculoprotective approaches to attenuate restenosis after percutaneous coronary interventions. *Journal of the American College of Cardiology*, 44(4):733–739, 2004.

[30] P. W. Serruys. *Handbook of Drug-Eluting Stents*, page 15. Taylor and Francis, 2005.

[31] P. H. Grewe, T. Deneke, A. Machraoui, J. Barmeyer, and K.-M. Muller. Acute and chronic tissue response to coronary stent implantation: pathologic findings in human specimen. *Journal of the American College of Cardiology*, 35(1):159–160, 2000. TY - JOUR.

[32] J. C. Palmaz, S. Bailey, D. Marton, and E. Sprague. Influence of stent design and material composition on procedure outcome. *Journal of Vascular Surgery*, 36(5):1031–1039, 2002. TY - JOUR.

[33] C. Fuss, E.A. Sprague, S.R. Bailey, and Palmaz J.C. Surface micro grooves improve endothelialization rate in vitro and in vivo. *American Journal of Cardiology*, 37(2 Suppl A):70A, 2001.

[34] S. O. Marx and A. R. Marks. Bench to bedside the development of rapamycin and its application of stent restenosis. *Circulation*, 104:852–855, 2001.

[35] K. McKeage, D. Murdoch, and K. L. Goa. The sirolimus-eluting stent a review of its use in the treatment of coronary artery disease. *American Journal of Cardiovascular Drugs*, 31:211–230, 2003.

[36] B. C. Berk, J. B. Gordon, D. R. Holmes, and R. W. Alexander. Pharmacologic roles of heparin and glucocorticoids to prevent restenosis after coronary angioplasty. *Journal of the American College of Cardiology*, 17:111B–117B, 1991.

[37] D.I. Axel, W. Kunert, and C. Goggelmann et al. Paclitaxel inhibits arterial smooth muscle cell proliferation and migration in vitro and in vivo using local drug delivery. *Circulation*, 96:636–645, 1997.

[38] E. K. Rowinsky and R. C. Donehower. Paclitaxel (taxol). *New England Journal of Medicine*, 332:1004–1014, 1995.

[39] A. M. Salam, J. Al Suwaidi, and D. R. Holmes. Drug-eluting coronary stents. *Current Problems in Cardiology*, 31:8–119, 2006.

[40] R. Fattori and T. Piva. Drug-eluting stents in vascular intervention. *The Lancet*, 361(9353):247–249, 2003. TY - JOUR.

[41] M.-C. Morice, P. Serruys, C. Constantini, and K. Wuelfert. Three-year follow-up of the ravel study: A randomized study with the sirolimus-eluting bx velocity(tm) stent in the treatment of patients with de novo native coronary artery lesions. *Journal of the American College of Cardiology*, 43(5, Supplement 1):A87–A88, 2004. TY - JOUR.

[42] R. Wombacher. *Polymere als Beschichtungs-materialien für Stents*. PhD thesis, Philipps- Universität Marburg, 2003.

[43] Wessely R., Kastrati A., and Schoemig A. Late restenosis in patients receiving a polymer coated sirolimus-eluting stent. *Ann Intern Med*, in press, 2005.

[44] McFadden EP., Stabile E.C., Regar E., Cheneau E., and T. Kinnaird et al. Late thrombosis in drug-eluting coronary stents after discontinuation of antiplatelet therapy. *Lancet*, 364:1519–1521, 2004.

[45] R. Virmani and G. Guagliumi et al. Localized hypersensitivity and late coronary thrombosis secondary to a sirolimus-eluting stent: should we be cautious? *Circulation*, 109:701–706, 2004.

[46] R. Wessely, J. Hausleiter, and C. Michaelis. Inhibition of neointima formation by a novel drug-eluting stent system that allows for dose-adjustable, multiple, and on-site stent coating. *Arteriosclerosis, Thrombosis, and Vascular Biology*, 25(4):748–753, 2005.

[47] A. Dibra and A. Kastrati et al. Influence of stent surface topography on the outcomes of patients undergoing coronary stenting: A randomized double-blind controlled trial. *Catheterization and Cardiovascular Interventions*, 65:374–380, 2005.

[48] Brunette D.M. The effect of surface topography on cell migration and adhesion. *Surface Characterization of Biomaterials*, 1987.

[49] J. E. Sousa and M. A. Costa et al. Lack of neointimal proliferation after implantation of sirolimus-coated stents in human coronary arteries. a quantitative coronary angiography and three-dimensional intravascular ultrasound study. *Circulation*, 103:192, 2001.

[50] P. W. Serruys and G. Sianos et al. The effect of variable dose and release kinetics on neointimal hyperplasia using a novel paclitaxel-eluting stent platform: The paclitaxel in-stent controlled elution study (pisces). *Journal of the American College of Cardiology*, 46(2):253–260, 2005.

[51] H. Wieneke and A. Schmermund et al. Therapeutic potential of active stent coating. *Expert Opinion on Investigational Drugs*, 12(5):771–779, 2003.

[52] S. H. Duda and T. C. Poerner et al. Drug-eluting stents: Potential applications for peripheral arterial occlusive disease. *Journal of Vascular and Interventional Radiology*, 14:293, 2003.

[53] T. J. Parry and R. Brosius et al. Drug-eluting stents: Sirolimus and paclitaxel differentially affect cultured cells and injured arteries. *European Journal of Pharmacology*, 524(1-3):19–29, 2005.

[54] C. Momma, S. Nolte, B. N. Chichkov, F. v. Alvensleben, and A. Tunnermann. Precise laser ablation with ultrashort pulses. *Applied Surface Science*, 109-110:15–19, 1997. TY - JOUR.

[55] S. H. Duda and T. C. Poerner et al. Drug-eluting stents: Potential applications for peripheral arterial occlusive disease. *Journal of Vascular and Interventional Radiology*, 14:295, 2003.

[56] B. L. van der Hoeven and M. M. Nuno et al. Drug-eluting stents: results, promises and problems. *International Journal of Cardiology*, 99(1):9–17, 2004.

[57] J. Hausleiter, A. Kastrati, and R. Wessely et al. Prevention of restenosis by a novel drug-eluting stent system with a dose-adjustable, polymer-free, on-site stent coating. *European Heart Journal*, 26:1475–1481, 2005.

[58] Colombo A., Moses JW., Morice MC., and J. Ludwig et al. Randomized study to evaluate sirolimus-eluting stents implanted at coronary bifurcation lesions. *Circulation*, 109:1244–1249, 2004.

[59] R. Haak and T. Smith. Surface treatment of am355 stainless steel for adhesive bonding. *International Journal of Adhesion and Adhesives*, 3(1):15–23, 1983. TY - JOUR.

[60] M. Haidopoulos and S. Turgeon. Surface modifications of 316 stainless steel for the improvement of its interface properties with rfgd-deposited fluorocarbon coating. *Surface and Coatings Technology*, 197(2-3):278–287, 2005.

[61] E. J. Sutow. The influence of electropolishing on the corrosion resistance of 316l stainless steel. *Journal Of Biomedical Materials Research*, 14(5):587–595, 1980. TY - JOUR.

[62] J. S. Noh, N. J. Laycock, W. Gao, and D. B. Wells. Effects of nitric acid passivation on the pitting resistance of 316 stainless steel. *Corrosion Science*, 42(12):2069–2084, 2000. TY - JOUR.

[63] S.-J. Lee and J.-J. Lai. The effects of electropolishing (ep) process parameters on corrosion resistance of 316l stainless steel. *Journal of Materials Processing Technology*, 140(1-3):210, 2003. TY - JOUR.

[64] M. A. Barbosa. The pitting resistance of aisi 316 stainless steel passivated in diluted nitric acid. *Corrosion Science*, 23:1293–1305, 1983.

[65] Surtec GMBH. Elektrochemische grundlagen. script, 1997.

[66] H. Kaesche. *Korrosion der Metalle*, page 117. Urban und Schwarzenberg, 1990.

[67] V. Kirchner. *Mikrostrukturierung von Edelstahl mit ultrakurzen Spannungspulsen*, pages 10–11. Freie Universität Berlin, 2001.

[68] W. Schmickler. Models for the interface between a metal and electrolyte solution. In J. Lipkowsky and P. N. Ross, editors, *Structure of Electrified Interfaces*, pages 201–238. VCH Publ. Inc., New York, 1993.

[69] K. B. Oldham and J. C. Myland. *Fundamentals of Electrochemical Science*. Academic Press Incorporated, 1994.

[70] J. A. McGeough. *Principles of Electrochemical Machining*, pages 5–6. Chapman and Hall, 1974.

[71] G. Vander Voort. *Applied Metallography*, pages 27,28. Van Nostrand Reinhold Company, 1989.

[72] G. Vander Voort. *Applied Metallography*, pages 21–39. Van Nostrand Reinhold Company, 1989.

[73] M. Prazak, V. Cihal, and M. Holinka. Ueber die differenzierung der strukturphasen beim metallographischen Ätzen. *Collection of Czechoslovak Chemical Communications*, 24:9–15, 1959.

[74] N. Sridhar and P. Crook. Designing an alloy to resist corrosion and wear. *Journal of metals*, 41(3):22–26, 1989.

[75] Kim D.H. and H.H. Lee et al. Chemical depth profile of passive oxide on stainless steel. *Applied Physics Letters*, 85(26):6427–6429, 2004.

[76] S. Haupt and H.-H. Strehblow. A combined surface analytical and electrochemical study of the formation of passive layers on fe/cr alloys in 0.5 m h2so4. *Corrosion Science*, 37(1):43–54, 1995.

[77] J. Sedriks. *Corrosion of Stainless Steels*. John Wiley and Sons, New York, 2 edition, 1996.

[78] V. Vignal, J. M. Olive, and D. Desjardins. Effect of molybdenum on passivity of stainlesssteelsin chloride media using ex situ near fieldmicroscopyobservations. *Corrosion Science*, 41(5):869–884, 1999. TY - JOUR.

[79] J. M. Bastidas, C. L. Torres, E. Cano, and J. L. Polo. Influence of molybdenum on passivation of polarised stainless steels in a chloride environment. *Corrosion Science*, 44(3):625–633, 2002. TY - JOUR.

[80] L. Beaunier and F Salihi. Grain boundaries corrosion of ni-mo alloys by electrochemical etching. *Journal de Physique*, C1(1):429–434, 1990.

[81] K. Sugimoto and Y. Sawada. The role of molybdenum additions to austenitic stainless steels in the inhibition of pitting in acid chloride solutions. *Corrosion Science*, 17(5):425–445, 1977. TY - JOUR.

[82] Y. C. Lu, M. Ives, and C. R. B. Clayton. Synergism of alloying elements and pitting corrosion resistance of stainless steels. *Corrosion Science*, 35(1-4):89–96, 1993.

[83] H. Ogawa, H. Omata, I. Itoh, and H. Okada. *Corrosion*, 34:53, 1978.

[84] D. Lin and T. Chang. Influence of si content on the intergranular corrosion of sus 309l stainless steels. *Materials Science and Engineering A*, 359(1-2):396–401, 2003. TY - JOUR.

[85] V. Kirchner. *Mikrostrukturierung von Edelstahl mit ultrakurzen Spannungspulsen*, pages 55–56. Freie Universität Berlin, 2001.

[86] G. Vander Voort. *Applied Metallography*, page 26. Van Nostrand Reinhold Company, 1989.

[87] H. Kaesche. *Korrosion der Metalle*, page 201. Urban und Schwarzenberg, 1990.

[88] L. Gmelin. *Handbuch der anorganischen Chemie*, chapter Cr-A2, pages 458–459. Springer, 1978.

[89] C.-C. Shih and C.-M. Shih et al. Effect of surface oxide properties on corrosion resistance of 316l stainless steel for biomedical applications. *Corrosion Science*, 46(2):427–441, 2004. TY - JOUR.

[90] I. Olefjord and L. Wegrelius. Surface analysis of passive state. *Corrosion Science*, 31:89–98, 1990. TY - JOUR.

[91] P. Marcus and J. M. Grimal. The anodic dissolution and passivation of ni—cr—fe alloys studied by esca. *Corrosion Science*, 33(5):805–814, 1992. TY - JOUR.

[92] R. Goetz and D. Landolt. The influence of chromium content and potential on the surface composition of fe—cr—mo alloys studied by aes. *Electrochimica Acta*, 29(5):667–676, 1984. TY - JOUR.

[93] R.J. Galvele, J.B. Lumsden, and R.W. Staehle. *Electrochem. Soc.*, 125:1204, 1978.

[94] G. Okamoto and T. Shibata. Passivity and the breakdown of passivity of stainless steels. In *Corrosion Monograph Series*, pages 646–677. Electrochem. Soc., 1978.

[95] D. Lothongkum, S. Chaikittisilpa, and A. W. Lothongkumb. Xps investigation of surface films on high cr-ni ferritic and austenitic stainless steels. *Applied Surface Science*, 218(1-4):203–210, 2003.

[96] M. Kaneko and H. S. Isaacs. Effects of molybdenum on the pitting of ferritic- and austenitic-stainless steels in bromide and chloride solutions. *Corrosion Science*, 44(8):1825–1834, 2002. TY - JOUR.

[97] A. J. Sedriks. Role of sulphide inclusions in pitting and crevice corrosion of stainless steels. *International Metals Reviews*, 28(5):295–307, 1983. TY - JOUR.

[98] T. Suter and H. Boehni. A new microelectrochemical method to study pit initiation on stainless steels. *Electrochemica Acta*, 42(20-22):3275–3280, 1997. TY - JOUR.

[99] P. Schmuki, A. Hildebrand, Friedrich S., and S. Virtanen. The composition of the boundary region of mns inclusions in stainless steel and its relevance in triggering pitting corrosion. *Corrosion Science*, 47:1239–1250, 2005.

[100] H.J. Dundas and A.P. Bond. Effects of delta ferrite and nitrogen contents on the resistance of austenitic stainless steels to pitting corrosion. *NACE Conference/75*, 159, 1975.

[101] P. V. Shigolev. *Electrolytic and Chemical Polishing of Metalls*. Freud Publishing, 1974.

[102] Thompson J.G. *Chem met engg*, 614(6), 1926.

[103] S. Fujimoto. Growth and properties of cr-rich thick and porous oxide films on type 304 stainless steel formed by square wave potential pulse polarisation. *Electrochimica Acta*, 47(4):548, 2001.

126

[104] L. Gmelin. *Handbuch der anorganischen Chemie*, chapter Fe-A1, page 316 ff. Springer, 1978.

[105] L. Gmelin. *Handbuch der anorganischen Chemie*, chapter Ni-A2, page 146. Springer, 1978.

[106] W Degner. *Elektrochemische Metallbearbeitung*, pages 20–21. VEB Verlag Technik, 1984.

[107] F. Christien, R. Le Gall, and G. Saindrenan. Phosphorus grain boundary segregation in steel 17-4 ph. *Scripta Materialia*, 48(3):301–306, 2003. TY - JOUR.

[108] H. Sahlaoui, H. Sidhom, and J. Philibert. Prediction of chromium depleted-zone evolution during aging of ni-cr-fe alloys. *Acta Materialia*, 50(6):1383–1392, 2002. TY - JOUR.

[109] G. Furutani, N. Nakajima, T. Konishi, and M. Kodama. Stress corrosion cracking on irradiated 316 stainless steel. *Journal of Nuclear Materials*, 288(2-3):179–186, 2001. TY - JOUR.

[110] M. Matula, L. Hyspecka, M. Svoboda, V. Vodarek, C. Dagbert, J. Galland, Z. Stonawska, and L. Tuma. Intergranular corrosion of aisi 316l steel. *Materials Characterization*, 46(2-3):203–210, 2001. TY - JOUR.

[111] H. Sahlaoui, K. Makhlouf, H. Sidhom, and J. Philibert. Effects of ageing conditions on the precipitates evolution, chromium depletion and intergranular corrosion susceptibility of aisi 316l: experimental and modeling results. *Materials Science and Engineering A*, 372(1-2):98–108, 2004. TY - JOUR.

[112] S. Kannan, A. Balamurugan, and S. Rajeswari. Electrochemical characterization of hydroxyapatite coatings on hno3 passivated 316l ss for implant applications. *Electrochimica Acta*, 50:2065–2072, 2005.

[113] E. B. Borghi, S. P. Ali, P. J. Morando, and M. A. Blesa. Cleaning of stainless steel surfaces and oxide dissolution by malonic and oxalic acids. *Journal of Nuclear Materials*, 229:122, 1996. TY - JOUR.

[114] E. B. Borghi, S. P. Ali, P. J. Morando, and M. A. Blesa. Cleaning of stainless steel surfaces and oxide dissolution by malonic and oxalic acids. *Journal of Nuclear Materials*, 229:115, 1996. TY - JOUR.

[115] H. Jiang, X. Chen, L. Hong, and M. Textor. Mineral-acid-free chemical polishing solutions for ferrous alloys. *Applied Surface Science*, 218(1-4):306–310, 2003.

[116] I. Sekine, C. Okano, and M. Yuasa. The corrosion behaviour of ferritic stainless steel in oxalic acid solutions. *Corrosion Science*, 30(4-5):351–366, 1990. TY - JOUR.

[117] E. B. Borghi, S. P. Ali, P. J. Morando, and M. A. Blesa. Cleaning of stainless steel surfaces and oxide dissolution by malonic and oxalic acids. *Journal of Nuclear Materials*, 229:121, 1996. TY - JOUR.

[118] G. L. Kehl. *The Principles of Metallographic Laboratory Practice*, page 434. McGraw-Hill Book Company, 1949.

[119] H. Schumann. *Metallographie*. Wiley Verlag, 2004.

[120] T. R. Giles. Pretreatment of various substrates prior to electrocoating. *Metal Finishing*, 99(9):10–12, 2001.

[121] S.-J. Lee and J.-J. Lai. The effects of electropolishing (ep) process parameters on corrosion resistance of 316l stainless steel. *Journal of Materials Processing Technology*, 140(1-3):206, 2003. TY - JOUR.

[122] J. D. Bronzino. *Biomedical Engineering Handbook, Ed.2*, volume 1, page 539. CRC Press and IEEE Press, 2000.

[123] A. J. Carter, M. Aggarwal, and Kopia G. A. Long-term effects of polymer-based, slow-release, sirolimus-eluting stents in a porcine coronary model. *Cardiovascular Research*, 63(4):622, 2004.

[124] M. Renke-Gluszko. *Drug Release of Coated Coronary Stents*. PhD thesis, TU München, 2006.

[125] P. Emschermann. Lymphe. In *Lexikon der Biologie*, page 304. Herder Verlag, 1994.

[126] R. Rettig, J. Kunze, and M. Stoever et al. Electrochemical behavior of surface etched 316l. *Journal of Materials Science, Materials in Medicine*, in press, 2006.

[127] R. Iijima, Y. Ikari, and E. Amiya et al. The impact of metallic allergy on stent implantation. metal allergy and recurrence of in-stent restenosis. *International Journal of Cardiology*, 104(3):319–325, 2005.

[128] R. Koester, D. Vieluf, and M. Kiehn et al. Nickel and molybdenum contact allergies in patients with coronary in-stent restenosis. *The Lancet*, 356(9245):1895–1897, 2000.

[129] M. Eblenkamp, J. Aigner, and J. Hintermair et al. Umbilical cord stromal cells (ucsc). cells featuring osteogenic differentiation potential. *Der Orthopäde*, 33:1338–1345, 2004.

[130] S. Silbernagl and A. Despopoulos. *Atlas der Physiologie*. dtv Taschenbücher, 2001.

[131] G. Vander Voort. *Metallography, Principles and Practice*, page 194. Materials Science and Engineering Series. MacGraw-Hill Book Company, 1984.

[132] V. Kirchner. *Mikrostrukturierung von Edelstahl mit ultrakurzen Spannungspulsen*, page 57. Freie Universität Berlin, 2001.

[133] M. Stoever, M. Renke-Gluszko, and T. Schratzenstaller et al. Microstructuring of stainless steel implants by electrochemical etching. *Journal of Materials Science, Materials in Medicine*, in press, 2006.

[134] F. C. Bell and D. E. Sonon. Improved metallographic etching techniques for stainless steel and for stainless steel to carbon steel weldments. *Metallography*, 9(2):105–106, 1976. TY - JOUR.

[135] J. A. McGeough. *Principles of Electrochemical Machining*, page 93. Chapman and Hall, 1974.

[136] K. Varga and P. Baradlai et al. Corrosion behaviour of stainless steel surfaces formed upon chemical decontamination. *Electrochimica Acta*, 46(24,25):3783–3790, 2001.

[137] P. H. Grewe, T. Deneke, A. Machraoui, J. Barmeyer, and K.-M. Muller. Rasterelektronenmikroskopische analyse der reaktiven und reparativen veränderungen humaner koronararterien nach stentimplantation. *Zeitschrift für Kardiologie*, 89(1):21 – 27, 2000.

[138] T. Schratzenstaller. *Entwicklung eines Trauma Reduzierenden Stentsystems*. PhD thesis, TU München, 2006.